Liposomal nanotherapy for treatment of atherosclerosis : passive versus active targeting

Darwitan, Anastasia

2020

Darwitan, A. (2020). Liposomal nanotherapy for treatment of atherosclerosis : passive versus active targeting. Doctoral thesis, Nanyang Technological University, Singapore.

https://hdl.handle.net/10356/137197

https://doi.org/10.32657/10356/137197

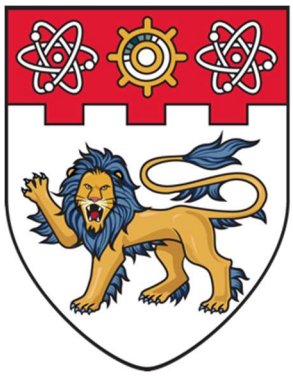

NANYANG TECHNOLOGICAL UNIVERSITY
SINGAPORE

LIPOSOMAL NANOTHERAPY FOR TREATMENT OF ATHEROSCLEROSIS: PASSIVE VERSUS ACTIVE TARGETING

ANASTASIA DARWITAN
Interdisciplinary Graduate School
NTU-Northwestern Institute for Nanomedicine
2020

LIPOSOMAL NANOTHERAPY FOR TREATMENT OF ATHEROSCLEROSIS: PASSIVE VERSUS ACTIVE TARGETING

ANASTASIA DARWITAN

Interdisciplinary Graduate School
NTU-Northwestern Institute for Nanomedicine

A thesis submitted to the Nanyang Technological University
in partial fulfilment of the requirement for the degree of
Doctor of Philosophy

2020

Statement of Originality

I hereby certify that the work embodied in this thesis is the result of original research, is free of plagiarised materials, and has not been submitted for a higher degree to any other University or Institution.

5 Aug 2019

. . . . . .
Date

. . . . . .
Anastasia Darwitan

Supervisor Declaration Statement

I have reviewed the content and presentation style of this thesis and declare it is free of plagiarism and of sufficient grammatical clarity to be examined. To the best of my knowledge, the research and writing are those of the candidate except as acknowledged in the Author Attribution Statement. I confirm that the investigations were conducted in accord with the ethics policies and integrity standards of Nanyang Technological University and that the research data are presented honestly and without prejudice.

21 August 2019

. . . . . .

Date

. . . . . .

Prof. Subbu Venkatraman

Authorship Attribution Statement

This thesis contains material from 2 papers pending to be submitted for publication in which I am listed as an author.

Chapter 4 is intended to be published as Anastasia Darwitan, Yee Shan Wong, T.H. Nguyen Luong, Bertrand Czarny, Anita Vincent, Yang Fei Tan, Aristo Muktabar, Jin Kai Tang, Kee Woei Ng and Subbu Venkatraman. Liposomal Nanotherapy for Treatment of Atherosclerosis.

The contributions of the co-authors are as follows:

- Prof. Subbu provided the initial project direction and edited the manuscript drafts.
- I prepared the manuscript drafts on liposomal formulation part. Dr. Wong Yee Shan prepared the drafts for the *in vitro* cell work and *in vivo* study. The manuscript was revised after discussion with Dr Wong Yee Shan.
- I co-designed the liposomal formulation studies with Dr Jayaganesh Natarajan and Dr. Wong Yee Shan. I performed all the laboratory work at the Ocular Therapeutic Engineering Centre, School of Materials Science and Engineering. I also analyzed the data.
- Microscopy was conducted by Dr. Vikas Nandwana at Northwestern University.
- Dr. Luong, Aristo Muktabar and Tang Jin Kai from Prof. Ng Kee Woei's group assisted in the *in vitro* cell studies of the liposomal formulation (data is not included in this thesis)
- Prof. Bertrand Czarny, Anita Vincent and Dr. Tan Yang Fei assisted in the *in vivo* work of the liposomal formulation (data is not included in this thesis)

Chapter 5 and 6 is intended to be published as Anastasia Darwitan, Yang Fei Tan, Yee Shan Wong, Anu Maashaa Nedumaran, Bertrand Czarny, and Subbu Venkatraman. Targeting Efficiency of Nanoliposomes on Atherosclerotic Foam Cells: PEG-To-Ligand Ratio Effects

The contributions of the co-authors are as follows:

- Prof. Subbu provided the initial project direction and edited the manuscript drafts.
- I prepared the manuscript drafts. The manuscript was revised after discussion with Dr Wong Yee Shan and Dr. Tan Yang Fei.
- I co-designed the studies with Dr Tan Yang Fei and discussed ideas with Dr. Tan Yang Fei and Dr. Wong Yee Shan. I performed all the laboratory work at the Ocular Therapeutic Engineering Centre, School of Materials Science and Engineering. I also analyzed the data.
- Prof. Bertrand Czarny and Anu Maashaa Nedumaran assisted in the *in vivo* biodistribution study

5 Aug 2019

. . . .

Date Anastasia Darwitan

Acknowledgements

I would like to thank Nanyang Technological University, Interdisciplinary Graduate School (IGS) and School of Materials Science & Engineering (MSE) for giving me the opportunity and research scholarship to pursue my PhD study. I am also very grateful to NTU-Northwestern Institute for Nanomedicine for funding my research work.

I would like to express my sincere gratitude to Professor Subbu Venkatraman for his invaluable advice throughout my PhD study. I am grateful to Prof. Subbu for granting me freedom to carry out my research while providing talented mentors to discuss ideas with. I would also like to thank my co-supervisor, Prof. Vinayak Dravid, and IGS mentor, Dr. Shad Thaxton, for their invaluable advices given during my Qualifying Examination and TAC meeting.

I would like to extend my sincere gratitude to Dr. Wong Yee Shan and Dr. Tan Yang Fei for their tremendous generosity in providing guidance, invaluable advices, and encouragement throughout my studies. I have been very fortunate to learn many research, presentation and writing skills from these two very talented individuals.

I would also like to thank Dr. Jayaganesh Natarajan, Prof. Bertrand Czarny, Dr. Luong, Dr. Krishna, and Dr. Miguel, who have shared their knowledge, criticism and questions at a few points in the course of my research. I am also thankful to Dr. Vikas Nandwana and his group members from Northwestern University for the discussions, friendship, and the help with the microscopy images.

I would like to extend my appreciation to my friends and lab mates, Alice Ng Jie Ying, Tang Jin Kai, Shaun Lim Wen Zheng, Anita Vincent, Chaw Su Yin, Anjanei, and those who have worked with me or provided friendship and encouragement during tough times. I am thankful to all MSE technicians and staff from the research office, general office, consumable stores, e-space,

organics lab, FACTS and many others, for their dedication and continuous support.

Last but not least, I am of utmost gratitude towards my parents, Mr. Oei Kian Seng and Mrs. Melinda Tan, BEc, for their understanding, encouragement and support throughout my studies. This thesis is dedicated to them.

Table of Contents

Table Captions

Figure Captions

Figure 2.1 Schematic illustration of cardiovascular diseases (CVD) in the context of global causes of deaths. (A) Ischaemic heart disease and stroke (in the red box) are two types of CVD that contribute to top 2 global causes of death. (B) Stroke and ischaemic heart disease alone have contributed to an estimate of a quarter of global deaths. Images were adapted from World Health Organization webpage

Figure 2.2 Schematic illustration of atherosclerotic plaque development. Entrapment of low-density lipoprotein (LDL) subendothelially and its oxidation initiates the process which culminates in the formation of fibrous plaque. Rupture of plaque leads to thrombotic occlusion of blood vessel

Figure 2.3 Schematic illustration of (A) liposome structure made up of phospholipid components; (B) individual phospholipid molecule composed of polar headgroup and a pair of nonpolar tails; (C) general structure of phosphatidylcholine

Figure 2.4 Structural change of bilayer can be tuned by altering the ambient temperature (T). When $T > T_c$, the liquid crystalline phase occurs. At this state, the bilayer is fluid and the drug can permeate through the bilayer easily. When $T < T_c$, the gel phase occurs. At this state, the bilayer is more tightly packed due to increased van der Waal's forces between lipid tails

Figure 2.5 Structure of various phospholipids with different acyl chain lengths. Lipids with longer chains have higher T_c due to increased intermolecular van der Waal's forces

Figure 2.6 Various PEG conformation on particle surface. (A) Low PEG surface density leads to mushroom conformation. (B) High surface PEG density leads to brush conformation with restricted PEG mobility. Rf = Flory radius

(average dimension of PEG in aqueous solution). D = Mean distance between PEG grafting sites

Figure 2.7 Structure of commercially available PEG-conjugated lipid (1,2-distearoyl-sn-glycero-3-phosphoethanolamine-N-[methoxy(polyethylene glycol)-2000] (ammonium salt), DSPE-PEG 2000)

Figure 2.8 Structure of commercially available folate-conjugated lipid (1,2-distearoyl-sn-glycero-3-phosphoethanolamine-N-[folate(polyethylene glycol)-2000] (ammonium salt), DSPE-PEG (2000)-Folate)

Figure 2.9 Illustration of filtration membranes in kidney. The pores of glomerular endothelial cells are capable of filtering particles < 15 nm

Figure 2.10 Illustration of venous sinuses in the red pulp of spleen. The endothelial cells are arranged in a barrel-like fashion, making narrow slits that enables red blood cells and particles < 200 nm to pass through to return into the venous circulation. Particles of >200 nm will be retained and phagocytosed by splenic macrophages

Figure 2.11 Schematic illustration of three general mechanisms of actions of glucocorticoids in anti-inflammation: nongenomic activation, DNA-dependent regulation, and protein interference mechanisms

Figure 2.12 (A & B) Accumulation of LN-PLP in macrophages of iliofemoral plaque (DAPI cell nuclei; CD68 macrophages; PEG liposome coating). (C - H) Arterial wall inflammation after LN-PLP administration in patients with region of interest shown in green (CT computed tomography; PET positron emission tomography). (E – H) Changes in TBR_{max} and TBR_{mean} in the left and right carotid artery (TBR target to background ratio)

Figure 2.13 (A) Monocyte recruitment and atherosclerotic plaque size on aortic arches and roots of LDL receptor knockout mice after 6 weeks high fat diet and

2 weeks treatment. (B) Plaque size, plaque stage, macrophage content, smooth muscle cells (SMC) content, and necrotic core size on atherosclerotic plaque of LDL receptor knockout mice after 6 weeks high fat diet and 6 weeks treatment. (C) Left: NF-κB activity in RAW267.4 NFκB-*luc* cells as the relative fold change to control without lipopolysaccharide (LPS) stimulation. Right: Cholesterol efflux in bone marrow-derived macrophages isolated from C57BL/6 mice

Figure 2.14 (A) Time-courses of DXM (i) and liposome (ii) serum concentration after DXM-liposome administration to atherogenic mice (L500 circle; L200 triangle; L70 square; free DXM diamond). (B) Aorta concentration 1 hour after administration. DXM in normal mice (i); Liposome in normal mice (ii); DXM in atherosclerotic mice (iii); Liposome in atherosclerotic mice (iv). (C) Effects of DXM-liposomes and free DXM on atherosclerotic mice (CE = cholesterol ester; TC = total cholesterol)

Figure 2.15 (A) Schematic of nanoemulsions with various DSPE-PEG 2000 concentrations. (B) Contents of nanoemulsions. (C) Flow cytometry histograms of cell uptake with various nanoemulsions. (D) Normalized cell uptake as the median fluorescence intensity divided by median cellular autofluorescence (CTRL white bars; RGD black bars). (E) Cellular uptake ratio between RGD and CTRL nanoemulsions

Figure 3.1 Schematic of electrical double layer interface of a particle in dispersion. The ionic concentration and electrical potential are a function of distance from the surface of the charged particle

Figure 3.2 General layout of a TEM, depicting basic operating components of TEM and the path of electron beam

Figure 3.3 (A) Schematic of working principle of xCELLigence® RTCA system. (B) Generic real-time impedance graph in cell apoptosis assay. The explanation of each phase is shown

over time at 4 °C storage

Figure 4.6 Cryo-TEM images of nanoliposomal formulation after extrusion. (A) Blank nanoliposomes composed of DPPC. (B) FA-loaded nanoliposomes composed of DPPC (drug/lipid molar ratio of 0.10 ± 0.01). (C) FA-loaded nanoliposomes composed of DPPC and DSPE-PEG 2000 (95:5 molar ratio) (drug/lipid molar ratio of 0.11 ± 0.003)

Figure 5.1 (A) Molecular structure of folate-FITC treated to the cells for cell surface folate receptor (FR) measurement. Relevant details such as excitation and emission wavelengths as well as molecular weight are inserted. (B) FR measurement represented by amount of folate-FITC attached on cell surface. HeLa and healthy human foreskin fibroblasts (HFF) were positive and negative control respectively. * $p < 0.05$; $n = 3$

Figure 5.2 Structure of commercially available folate-conjugated lipid (1,2-distearoyl-sn-glycero-3-phosphoethanolamine-N-[folate(polyethylene glycol)-2000] (ammonium salt), DSPE-PEG (2000)-Folate)

Figure 5.3 Measurement of folate molecule concentration in the active targeting liposome formulation composed of DPPC/DSPE-PEG 2000-Folate (99.1: 0.9 molar ratio) during storage at room temperature and 4 °C

Figure 5.4 xCELLigence cell viability and proliferation assay of foam cells in response to nanoliposomes (DPPC/DPPE-Rhodamine/DSPE-PEG 2000-Folate 99/0.1/0.9 molar ratio) of various concentrations. THP-1 cells were seeded and differentiated into macrophages (with PMA for 3 days) and foam cells (with oxidized LDL for 2 days) in xCELLigence E-plates. Current impedance due to cell proliferation (cell index) was monitored real-time

Figure 5.5 (A) Illustration of nanoliposomes with various ligand concentration. (B) Normalized cellular uptake as the mean fluorescence intensity (MFI) of rhodamine-positive cells after subtraction of untreated cells autofluorescence

MFI and normalized to MFI of bare liposomes (0% ligand concentration). (C) Dot plot from flow cytometry with gating of cells shown and logarithmic flow cytometry histograms for liposomes with various folate (FOL) content. Histograms for PEG 2000 and PEG 5000 spacer are shown

Figure 5.6 MTT assay measuring foam cell viability after treatment with bare DPPC liposomes and DPPC liposomes with DSPE-PEG 2000-Folate (0.5 mol%) labelled as 0% and PEG 2000 (0.5% FOL) respectively. Percentage of cell viability was normalized to the value of foam cells without liposome treatment labelled as untreated cells

Figure 6.1 Normalized cellular uptake as mean fluorescence intensity (MFI) of rhodamine-positive cells divided by MFI of cellular autofluorescence. The effect of particle-serum incubation time on cellular uptake was compared for various liposome concentration.
* p-value <0.05 vs. 30 mins; # p-value < 0.05 vs. 60 mins

Figure 6.2 Normalized cellular uptake as the mean fluorescence intensity (MFI) of rhodamine-positive cells after subtraction of untreated cells autofluorescence MFI and normalized to MFI of bare liposomes. * p-value <0.05 among the 3 PEG sizes of the same concentration; # p-value < 0.05 vs. bare LPS (Ctrl). LPS = liposomes. Ctrl = control

Figure 6.3 Evaluation of cellular uptake using confocal microscopy. Nuclei were visualized by staining with Hoechst 33342

Figure 6.4 MTT assay measuring foam cell viability after treatment with active targeting DPPC liposomes containing combination of 0.5 mol% DSPE-PEG 2000-Folate and DSPE-PEG of various concentrations. Treatment was done after incubation of liposomes in 80% human serum for 90 minutes at 37 °C. Percentage of cell viability was normalized to the value of foam cells without liposome treatment, labelled as untreated cells

Abstract

In spite of the success of current therapies and preventive strategies in reducing cardiovascular risk, cardiovascular diseases (CVD) continue to be the leading cause of death globally. Inflammation is the underlying pathological process of atherosclerosis, the major cause of most CVD, but has not been adequately addressed. Additionally, the increasing age trend of general population will present increasing incidence with individual's unique and complex coronary anatomy with high-risk comorbidities. Thus, there is a need for novel therapies that are effective.

Anti-inflammatory agents, such as glucocorticoids (GC), when administered systemically for long duration, are associated with systemic adverse effect. One strategy to circumvent this is by utilizing a nanocarrier to encapsulate the active agents, thereby preventing off-target interaction and enabling targeted and sustained delivery of the active compounds at the diseased site; hence, enhancement of benefit/risk ratio of the therapeutic agents.

In this report, both passive and active targeting strategies were explored using nanoliposomes as the nanocarrier. In passive strategy, nanoliposomes circulate in the bloodstream and preferentially accumulate at the sites of inflammation, which are characterized by dysfunctional endothelium and enhanced vascular leakiness, through 'Enhanced Permeability and Retention' (EPR) effect. Passive liposomes encapsulating fluocinolone acetonide (FA) were developed and reported in this thesis. Encapsulation efficiency of around 90% was achieved with final drug/lipid molar ratio of around 0.11. Release was sustained up to 30 days *in vitro* and the formulation was stable for at least 3 months.

In active strategy, active ligands were decorated on nanoliposomal surface for enhancement of cell internalization. In this report, it was demonstrated that foam cells expressed high number of targetable cell surface folate receptors. Optimum cell uptake enhancement was achieved with 0.5 mol% folate (FOL) with polyethylene glycol (PEG) 2000 spacer. Subsequently, ligand-free PEG was

incorporated on active liposomes with PEG 2000 (0.5% FOL) and cell uptake was evaluated after pre-incubation of liposomes in 80% serum in order to mimic the presence of high level of serum *in vivo*. It was demonstrated that the active targeting effect of active targeting nanoliposomes progressively decreased and eventually be lost as PEG-to-ligand ratio is increased. However, the value of PEG-to-ligand ratio at which the targeting effect was lost depended on PEG length (>2 for PEG 750; >0.5 for PEG 2000; <0.5 for PEG 5000).

The novel anti-inflammatory therapy developed in this PhD work could be envisioned for treatment after an acute clinical event or as adjunct therapy for prevention of in-stent restenosis in patients receiving bare metal stents. Individually, the passive liposomal formulation developed represents novel anti-inflammatory therapeutic option for atherosclerosis. It can also be considered for other inflammatory conditions, such as diabetic macular edema. The active liposome formulation developed could potentially enhance therapeutic efficacy of liposomal anti-inflammatory nanotherapy. The knowledge from active liposome studies could contribute in development of other active nanocarriers utilizing PEG and ligand-PEG.

Lay Summary

Current therapies and preventive strategies for artery blockage have successfully reduced the risk of fatal events. However, this disease remains the leading cause of death worldwide. Studies have shown that inflammation is the main cause of this disease, but it has not been addressed by current therapies. This is due to the side effects, such as high blood pressure and reduction of bone mass, associated with long-term injection of anti-inflammatory drug. One of the strategies to circumvent this is by packing the drug into nanoliposomes, which are millions of tiny capsules, that could protect the drug from interacting with healthy cells while circulating in the bloodstream and perform slow drug release at the diseased site.

In passive delivery strategy, the capsules circulate in the bloodstream and preferentially accumulate at the diseased sites due to leaky blood vessel around the sites. Passive drug-containing capsules were developed in this work and the drug encapsulation efficiency was found to be high at around 90%. The evaluation of drug release was also performed and was found to have the capability for sustained release for up to around 30 days.

In active delivery strategy, the capsules were furnished with targeting molecules on the surface to enhance their interaction with the diseased cells in order to increase the therapeutic effect of the drug. The availability of recipient molecules on the diseased cell surface was evaluated in this work and was found to be abundant. The quantity of targeting molecules required on the capsules were optimized.

Both passive and active capsules require polymer film coating to mask the capsules from the immune system in the body. The extent of coating needs to be optimized so that it does not counteract against the effect from the targeting molecules. In this work, the extent of polymer coating with respect to the targeting molecules, the number of which had been optimized earlier, was evaluated by examining the capability of the cells to internalize each type of

capsules. The capsules were pre-coated with human serum in order to mimic body condition.

The novel anti-inflammatory nanotherapy developed in this PhD work could be envisioned for treatment after an acute clinical event or as adjunct anti-inflammatory therapy in patients receiving bare metal stents. The knowledge derived from the study of active targeting could contribute in development of other type of active nanometer-sized capsules. The passive formulation developed can also be considered for other inflammatory conditions, such as diabetic macular edema.

Abbreviations

ACE	Angiotensin Converting Enzyme
Apoe$^{-/-}$	Apolipoprotein E-knockout
CTRL	Control
CVD	Cardiovascular Diseases
D/L	Drug-to-Lipid Ratio
DES	Drug Eluting Stents
Dex	Dexamethasone
DLS	Dynamic Light Scattering
DMPC	1,2-Dimyristoyl-sn-glycero-3-phosphocholine
DPPC	1,2-Dipalmitoyl-sn-glycero-3-phosphocholine
DPPE-Rhodamine	1,2-dipalmitoyl-sn-glycero-3-phosphoethanolamine-N-(lissamine rhodamine B sulfonyl) (ammonium salt)
DSPC	1,2-Distearoyl-sn-glycero-3-phosphocholine
DSPE-PEG 2000 N-	1,2-distearoyl-sn-glycero-3-phosphoethanolamine-[methoxy(polyethylene glycol)-2000] (ammonium salt)
DSPE-PEG 2000-Folate	1,2-distearoyl-sn-glycero-3-phosphoethanolamine-N-[folate(polyethylene glycol)-2000] (ammonium salt)
DSPE-PEG 5000	1,2-distearoyl-sn-glycero-3-phosphoethanolamine-N-[methoxy(polyethylene glycol)-5000] (ammonium salt)
DSPE-PEG 5000-Folate	1,2-distearoyl-sn-glycero-3-phosphoethanolamine-N-[folate(polyethylene glycol)-5000] (ammonium salt)
DSPE-PEG 750	1,2-distearoyl-sn-glycero-3-phosphoethanolamine-N-[methoxy(polyethylene glycol)-750] (ammonium salt)
DXM	Dexamethasone
EE%	Encapsulation Efficiency
Egg SM	Egg-Sphingomyelin

EPC	L-α-phosphatidylcholine (Egg, Chicken)
EPR	Enhanced Permeability and Retention
ePTFE	Expanded Polytetrafluoroethylene
FA	Fluocinolone Acetonide
FBS	Fetal Bovine Serum
FOL	Folate
Folate-FITC	Folic acid PEG Fluorescein PG2-FAFC-2k
FR	Folate Receptors
FSC	Forward Scatter
GC	Glucocorticoids
HFF	Human Foreskin Fibroblasts
HUVEC	Human Umbilical Vein Endothelial Cells
IPA	Isopropyl Alcohol
LDL	Low-density Lipoprotein
LDL-C	Low-density Lipoprotein Cholesterol
LN-PLP	Prednisolone Phosphate-loaded Nanoliposome
LPS	Liposomes
MFI	Mean Fluorescence Intensity
MLV	Multilamellar Vesicles
MTT	(3-(4,5-dimethylthiazol-2-yl)-2,5-diphenyltetrazolium bromide) tetrazolium salt
NADPH	Nicotinamide Adenine Dinucleotide Hydrogen
NO	Nitric Oxide
OxLDL	Oxidized Low-density Lipoprotein
PBS	Phosphate Buffered Saline
PCI	Percutaneous Intervention
PDI	Polydispersity Index
PEG	Polyethylene Glycol
PMA	Phorbol 12-myristate 13- acetate
RGD	Arginylglycylaspartic Acid
RPMI	Roswell Park Memorial Institute
SSC	Side Scatter
TEM	Transmission Electron Microscopy
UV	Ultraviolet

Chapter 1

Introduction

This chapter introduces the background and motivation of the research. The problem statement and the significance of the work are elaborated. The hypothesis is discussed with its specific objectives and scopes. Additionally. a brief introduction of each chapter is highlighted, and the novelty of overall research is listed.

1.1 Background

Cardiovascular diseases (CVD) represents the leading cause of death worldwide, contributing to about 17.9 million deaths in 2016 [1]. Despite the success of current preventive strategies, such as lifestyle changes and statin treatment, in reducing cardiovascular risk, the deaths from cardiovascular diseases continue to increase [2, 3]. Recent evidence has shown that inflammation is the underlying process of atherosclerosis [4, 5]. However, it has not been adequately addressed by current therapies, which are limited to mitigation of CVD risk factors such as dyslipidemia, hypertension and thrombotic complications.

Glucocorticoids (GC) are clinically-applied and the most widely used anti-inflammatory drugs that are effective for many inflammatory diseases [6, 7]. However, long-term systemic administration of GC has pro-atherogenic and systemic adverse effects such as hypertension, glucose intolerance, osteoporosis, and susceptibility to infection [7-9]. Encapsulating GC in nanocarriers, such as liposomes, is one appealing strategy to attain localized GC treatment on the atherosclerotic plaque, thereby enhancing the benefit/risk ratio of the drug.

Liposomes are biocompatible vesicles and widely utilized in cosmetic and pharmaceutical industries as delivery carriers of active compounds. Numerous liposomal formulations have been approved for clinical use in cancer therapy, fungal, viral infection and pain management [10]. GC encapsulation in liposomes have been largely studied in the application of asthma and rheumatoid arthritis, and have been shown to enhance the anti-inflammatory activity of GC at the targeted area [11]. Liposomes by themselves may serve as cholesterol acceptor, capable of mobilizing cholesterol deposits from atherosclerotic arteries to the liver for excretion [12].

Generally, delivery of active agent-encapsulated nanocarriers can be achieved by either passive or active targeting method. In passive method, active agents are protected by the nanocarrier, bypassing the mononuclear phagocyte system during circulation [13] and preferentially accumulate at the sites of inflammation characterized by dysfunctional endothelium and enhanced vascular leakiness

through EPR effect [14, 15]. In active method, ligands were incorporated on nanocarrier surface for enhancement of cellular internalization. In both passive and active methods, incorporation of polyethylene glycol (PEG) on the nanocarrier surface is crucial to improve pharmacokinetics of encapsulated drugs in systemic administration [16, 17]. However, PEG molecules are known to exert steric barrier, hindering particle-cell interaction [18]. Thus, their presence on nanocarrier surface could counteract the active targeting effect in active nanocarriers.

In this thesis, passive and active targeting liposomes as strategies for delivering encapsulated GC to atherosclerotic lesions will be explored. The hypothesis is discussed in Section 1.3 and the characteristics of the nanoliposomal formulations as well as the effect of PEG-to-ligand ratio effects are analyzed and discussed in-depth in Chapter 4 – 6.

1.2 Significance and Problem Statement

This research project aims to assist in the development of the next generation of CVD therapeutic treatments. CVD is the number one cause of death worldwide, with an estimate of 17.9 million people died from this disease in 2016, contributing to around a quarter of total global deaths [19]. Current therapeutic methods have not adequately addressed the issue of inflammation, which is the underlying process of this disease. This thesis will attempt to address this issue by investigating both passive and active nanoliposomes as nanocarriers for GC. As such, this project will contribute in the development of novel anti-inflammatory nanotherapies for CVD.

1.3 Hypothesis

In both passive and active liposomes, incorporation of polyethylene glycol (PEG) on the liposomal surface is crucial to improve pharmacokinetics of encapsulated drugs in systemic administration. However, PEG molecules are known to exert steric barrier, hindering particle-cell interaction. Thus, their presence could counteract the active targeting effect in active liposomes. As the

nanoparticle surface coverage by PEG is more extensive at high PEG surface density, we expect the active targeting effect to decrease as PEG surface density is increased. Thus, we hypothesize that targeting effect of active targeting nanoliposomes will progressively decrease and eventually be lost as PEG-to-ligand ratio is increased.

1.4 Objectives and Scope

The aim of this project is to study the interplay between ligand and neighbouring PEG and its effect on foam cell uptake. In order to prove the hypothesis, the study will be broken down into 3 milestones:

1. Evaluation of liposomes as GC carrier (study of passive targeting nanocarrier). Evaluation of loading and release of GC from liposomes will be done. PEGylation of liposomes will also be performed to investigate its effect on GC loading and release.

2. Determination of active ligand for foam cell targeting (study of active targeting nanocarrier). Evaluation of foam cell surface receptor numbers and cell uptake of ligand-incorporating liposomes will be done.

3. Evaluation of PEG-to-ligand ratio on foam cell uptake (study of passive versus active targeting nanocarrier). Effect of PEG density and PEG chain lengths variation on foam cell uptake will be investigated

Hydrophobic GC will be the type of drug used in this study. This study will only consider single drug encapsulation. Foam cell will be the type of cell studied. Ligand used will be a small molecule conjugated at the distal end of PEG. The parameters studied in optimization of nanoliposomal loading capacity and release of GC will be lipid chain lengths and PEGylation. Foam cell uptake will be the method used for assessing the targeting ability of the active ligand molecules

1.5 Dissertation Overview

This thesis is arranged into seven chapters as follows:

Chapter 1 provides research overview, hypothesis, objectives, outcomes and thesis overview

Chapter 2 reviews literature concerning fundamental pathology of atherosclerosis, contemporary therapeutic solution, opportunities for nanomedicine in development of novel therapeutic solution, and current research progress in novel nanotherapies.

Chapter 3 presents materials and methods used in the studies. The underlying principles of characterization techniques as well as rationale for selection of these techniques were elaborated.

Chapter 4 provides results and discussion with regards to passive liposomes. The effect of lipid chain length and PEGylation on GC loading, release, and liposome stability are discussed.

Chapter 5 provides results and discussion with regards to active liposomes. Synthesis and characterization of active liposomes are elaborated. Effect of active ligand content and spacer length on the targeting efficiency are investigated.

Chapter 6 provides investigation of active versus passive liposomes. The extent of active targeting effect when the liposomal surface PEGylation density is increased in active liposomes is compared to passive liposomes. This chapter provides experimental results that prove the hypothesis of this thesis.

Chapter 7 draws a thread linking the results from the various studies in this thesis. Opportunities and future development pertaining to novel nanotherapies for atherosclerosis are discussed.

1.6 Findings and Outcomes/Originality

Novel outcomes from this research includes:

1. Establishment of a novel anti-inflammatory nanotherapy for atherosclerosis treatment
2. Knowledge of lipid chain length and PEGylation effect on lipophilic small molecular drug loading and release
3. A method for optimization of liposomal surface PEGylation and ligand density in the condition that better mimic *in vivo* condition by pre-incubating nanoparticle in serum
4. Insight of how nanoparticle surface PEGylation affect the targeting efficiency of active ligands.

References

[1] Organization, W.H. *Cardiovascular disease*. 2019 [cited 2019 25 Mar 2019]; Available from: https://www.who.int/cardiovascular_diseases/en/.

[2] Libby, P., *The forgotten majority - Unfinished business in cardiovascular risk reduction.* Journal of the American College of Cardiology, 2005. **46**(7): p. 1225-1228.

[3] Roth, G.A., et al., *Demographic and epidemiologic drivers of global cardiovascular mortality.* N Engl J Med, 2015. **372**(14): p. 1333-41.

[4] Libby, P., P.M. Ridker, and A. Maseri, *Inflammation and atherosclerosis.* Circulation, 2002. **105**(9): p. 1135-1143.

[5] Ross, R., *Mechanisms of disease - Atherosclerosis - An inflammatory disease.* New England Journal of Medicine, 1999. **340**(2): p. 115-126.

[6] Barnes, P.J., *How corticosteroids control inflammation: Quintiles prize lecture 2005.* British Journal of Pharmacology, 2006. **148**(3): p. 245-254.

[7] Czock, D., et al., *Pharmacokinetics and pharmacodynamics of systemically administered glucocorticoids.* Clinical Pharmacokinetics, 2005. **44**(1): p. 61-98.

[8] Wei, L., T.M. MacDonald, and B.R. Walker, *Taking glucocorticoids by prescription is associated with subsequent cardiovascular disease.* Annals of Internal Medicine, 2004. **141**(10): p. 764-770.

[9] Schacke, H., W.D. Docke, and K. Asadullah, *Mechanisms involved in the side effects of glucocorticoids.* Pharmacology & Therapeutics, 2002. **96**(1): p. 23-43.

[10] Bulbake, U., et al., *Liposomal Formulations in Clinical Use: An Updated Review.* Pharmaceutics, 2017. **9**(2).

[11] Ozbakir, B., et al., *Liposomal corticosteroids for the treatment of inflammatory disorders and cancer.* Journal of Controlled Release, 2014. **190**: p. 624-636.

[12] Rodrigueza, W.V., M.C. Phillips, and K.J. Williams, *Structural and metabolic consequences of liposome-lipoprotein interactions.* Advanced Drug Delivery Reviews, 1998. **32**(1-2): p. 31-43.

[13] Bozzuto, G. and A. Molinari, *Liposomes as nanomedical devices.* International Journal of Nanomedicine, 2015. **10**: p. 975-999.

[14] Barkhausen, J., et al., *Detection of atherosclerotic plaque with gadofluorine-enhanced magnetic resonance imaging.* Circulation, 2003. **108**(5): p. 605-609.

[15] Colangelo, S., et al., *Alterations in endothelial F-actin microfilaments in rabbit aorta in hypercholesterolemia.* Arteriosclerosis Thrombosis and Vascular Biology, 1998. **18**(1): p. 52-56.

[16] Torchilin, V.P., *Recent advances with liposomes as pharmaceutical carriers.* Nature Reviews Drug Discovery, 2005. **4**(2): p. 145-160.

[17] Klibanov, A.L., et al., *Amphipathic Polyethyleneglycols Effectively Prolong the Circulation Time of Liposomes.* Febs Letters, 1990. **268**(1): p. 235-237.

[18] Gabizon, A., et al., *Targeting folate receptor with folate linked to extremities of poly(ethylene glycol)-grafted liposomes: in vitro studies.* Bioconjug Chem, 1999. **10**(2): p. 289-98.

[19] Organization, W.H. *The Top 10 Causes of Death*. 2018 [cited 2019 May]; Available from: http://www.who.int/mediacentre/factsheets/fs310/en/.

Chapter 2

Literature Review

This chapter summarizes pathology of atherosclerosis, current established therapies, potential novel nanotherapies, and current research progress in atherosclerosis nanotherapies. This chapter provides the landscape of atherosclerosis and its therapeutic tools today. Additionally, the importance of the development of novel therapies and how nanomedicine can contribute to this area are also highlighted. Finally, the landscape of current research progress in atherosclerosis nanotherapies is provided and how the results supported the design of this PhD study is described.

2.1 Background of Atherosclerosis

Cardiovascular diseases (CVD) are number one causes of death globally, dubbed as "the world's number one killer" by World Health Organization. In 2016, it was associated with about 17.9 million deaths, contributing to 31% of total global deaths [1]. Atherosclerosis is the major cause of most CVD such as acute myocardial infarction and stroke, and thus represents the leading cause of death worldwide.

For over 50 years, efforts have been made to treat CVD. Despite the success of preventive strategies, such as lifestyle changes and statin treatment, and advances in pharmacological and revascularization interventions in reducing cardiovascular risks, the morbidity and mortality rates caused by this disease remain high [2, 3].

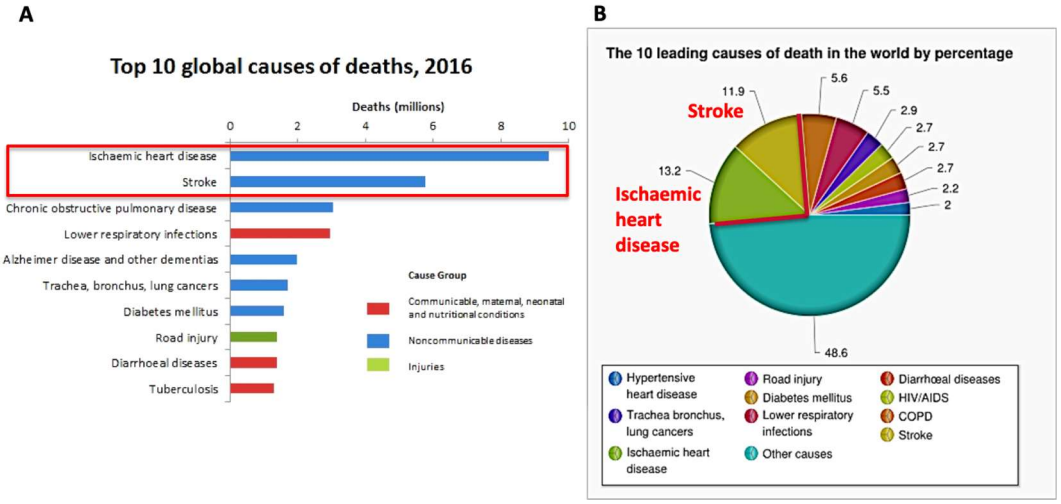

Figure 2.1 Schematic illustration of cardiovascular diseases (CVD) in the context of global causes of deaths. (A) Ischaemic heart disease and stroke (in the red box) are two types of CVD that contribute to top 2 global causes of death. (B) Stroke and ischaemic heart disease alone have contributed to an estimate of a quarter of global deaths. Images were adapted from World Health Organization webpage [1]

Recently, evidence has shown that inflammation is the underlying process of atherosclerosis [4, 5], beginning with endothelial dysfunction, a condition deemed to be caused by cardiovascular risk factors such as hypertension and

chronic smoking [6, 7]. This condition leads to increased permeation of lipoproteins and other macromolecules, enhanced expression of chemotactic and adhesion molecules, such as VCAM1, ICAM 1, monocyte chemotactic protein 1, E-selectin and P-selectin, and increased recruitment and accumulation of monocytes at the lesion area [7, 8]. The monocytes were then transformed into macrophages and finally foam cells after taking up apolipoprotein B-containing low-density lipoprotein (LDL). Subsequent downstream signaling events occur, with production of inflammatory cytokines and chemokines such as IL-1ß, TNF, IL-6, CCL5, CXCL1, CCL3, and activation of transcription factors, such as NF-κB [9]. With prolonged endoplasmic reticulum stress, apoptosis of macrophages and foam cells occur. The apoptotic cells cannot be effectively cleared in advanced atherosclerosis due to impaired efferocytosis, leading to secondary necrosis. The buildup of necrotic core over time drives plaque destabilization. At the same time, weakening of fibrous cap shielding the plaque from the bloodstream by continuous production of matrix-degrading proteases from activated macrophages, causes the plaque to be vulnerable and prone to rupture. In the event of fibrous cap rupture, thrombogenic material is exposed to the bloodstream, prompting activation of platelet and occurrence of blood clotting, leading to conditions such as stroke and myocardial infarction [9].

Despite the evidence of inflammation being the underlying process of atherosclerosis, the use of systemic anti-inflammatory therapies as a treatment is not feasible as many molecular targets of these agents have important roles in host defense. Therefore, there is a need to develop a targeted therapy that delivers localized anti-inflammatory treatment.

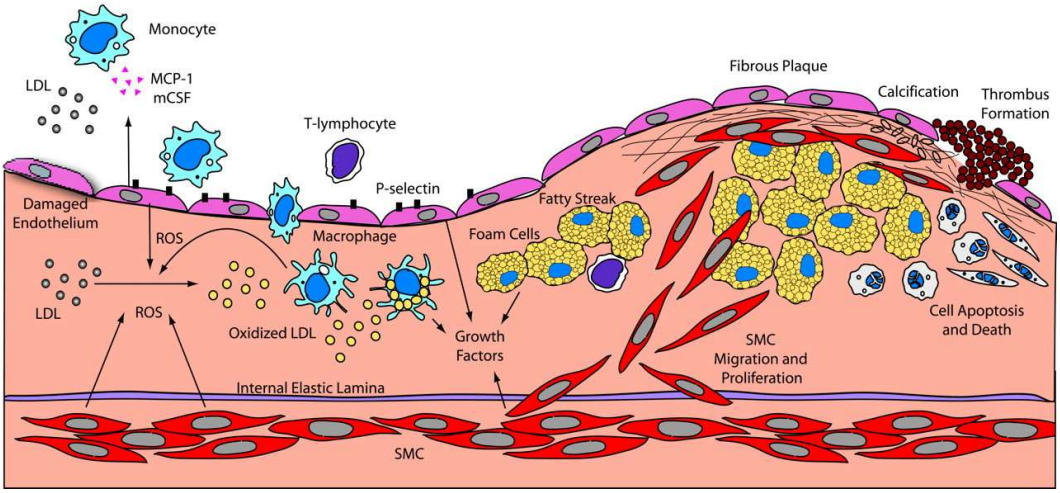

Figure 2.2 Schematic illustration of atherosclerotic plaque development. Entrapment of low-density lipoprotein (LDL) subendothelially and its oxidation initiates the process which culminates in the formation of fibrous plaque. Rupture of plaque leads to thrombotic occlusion of blood vessel [10]

2.2 Established Atherosclerosis Therapies

Dyslipidemia, diabetes, smoking, and hypertension are major risk factors for CVD. Current therapies for clinical use are prescribed to overcome some of these risk factors to reduce CVD risks, but they do not directly address the underlying inflammation mechanism of atherosclerosis. Current therapies are limited to mitigation of dyslipidemia, hypertension and thrombotic complications.

Statin is clinically prescribed for its serum cholesterol-reducing activity and upregulation ability of LDL receptor expression in hepatocytes [11]. As secondary prevention for patients with prior coronary artery disease, statin treatment shows marked risk reduction associated to lowering of LDL cholesterol (LDL-C) [12]. However, for patients with high initial LDL value, achieving acceptable LDL level is often not possible with statins alone, even at maximally tolerated dose [13]. Since 2015, FDA has approved a few PCSK9 inhibitors for patients with persistently high LDL-C level after high-intensity statin treatment [14]. Recently, various studies have reported pleiotropic effects of statin, which include anti-inflammatory actions, endothelial function improvement, and modulation of thrombosis and coagulation [15-18]. However, anti-inflammatory effect of statin has been demonstrated only at very high dose

[15], which is currently not feasible in clinical practice due to increased risk of adverse effect that is present with high oral dose of statin [19].

Angiotensin-converting-enzyme (ACE) inhibitors are antihypertensive agents, commonly prescribed for management of CVD. ACE inhibitors block the activation of the renin-angiotensin system, which greatly contributes to CVD risks [20]. A meta-analysis of 3 clinical studies with low left ventricular ejection fraction reported reduction of myocardial infarction risk by 23% with treatment of ACE inhibitors [20]. ACE inhibitors were also reported to significantly reduce the rates of myocardial infarction, stroke, and death in high-risk patients without known left ventricular dysfunction [21]. However, recently it was reported that long-term use of ACE inhibitors could cause aldosterone breakthrough, whereby aldosterone level may not remain suppressed after prolonged treatment of ACE inhibitors, but instead potentially increase above pretreatment levels, limiting the beneficial effect of the therapy [22, 23]. This limitation is currently widely investigated.

Aspirin is the most widely prescribed anti-platelet drug for secondary prevention of ischemic events, followed by adenosine diphosphate $P2Y_{12}$ receptor blockers, such as thienopyridine derivatives. Aspirin was found to be effective as secondary prevention, as reported in meta-analyses study to cause a reduction in atherothrombotic outcomes by about 20% in high-risk patients [24]. However, the benefit/risk ratio of aspirin for primary prevention in low-risk patients were found to be very small [25]. Dual therapy of aspirin with thienopyridine derivatives, such as ticlopidine and clopidogrel, was found to substantially reduce myocardial infarction and death compared to aspirin alone [26]. Despite the advances in antiplatelet therapies, atherothrombotic events still impair the prognosis of CVD patients. Thus, this area remains a subject of intense research.

2.3 Percutaneous Intervention (PCI) and Bypass Graft Surgery

PCI is currently the most common way of myocardial revascularization for patients with less complex conditions as well as those with acute coronary syndrome [27].

Balloon angioplasty is commonly used in combination with stenting. It is an effective treatment for coronary stenoses, through compression of the plaque on the atherosclerotic vessel wall. Nowadays, drug-coated balloon angioplasty is being developed, with clinical success being constrained to paclitaxel-based systems [28], which has very high transfer rate into the vessel wall as well as high binding capabilities compared to sirolimus and its analogues [29]. Drug-coated balloon angioplasty is more frequently used in peripheral vasculature rather than in coronary circulation, where drug-eluting stents (DES) are more commonly used and have superior efficacy and safety [27]. Both platforms are applied clinically for the treatment of in-stent restenosis. DES usually provide the best clinical outcomes, while drug-coated balloon is able to provide fairly good outcomes without additional layer of stent [27]. Future investigations on the possibility to identify which procedure would benefit an individual will be helpful.

Stent implantation prevents vessel recoil, which could occur with standalone balloon angioplasty, and affixes dissected plaque and tissue, thereby providing better acute gain and stability compared to standalone balloon angioplasty. Early stent thrombosis is usually overcome by antiplatelet therapies ticlopidine and aspirin. Stents are usually made of cobalt or platinum chromium alloys. Thin struts are usually preferred as they were shown to provide lower restenosis rates [30], possibly owing to reduced vessel wall trauma induced with thin struts and the ability to be re-endothelialized more rapidly.

Drug-eluting stents (DES), with sirolimus or one of its analogues, were developed to overcome neointimal hyperplasia issue present with bare metal stents. Contemporary DES are classified in terms of the polymer coating utilized to load the drug, whether it is permanent, biodegradable, or polymer-free. Two types of widely used permanent polymer DES are fluoropolymer everolimus DES and the Biolinx zotarolimus DES. Most large scale randomized trials found similar clinical outcomes with both platforms [31-34]. Biodegradable polymeric DES are usually made of either polylactic or polylactic-co-glycolic acid. Depending on the molecular weight and crystallinity of the polymer, they are degraded to carbon dioxide and water, typically within 1.5 to 24 months.

Biodegradable DES are speculated to have reduced adverse effects from polymer residue after stenting. However, there is yet to be any concrete evidence on its superiority compared to current permanent polymer DES [35, 36]. Polymer-free DES aim to prevent adverse effects from polymer hypersensitivity. Moreover, they could eliminate the issue of cracking or webbing of polymer coating during stent expansion. The challenge with polymer-free DES lies in the control of drug elution. Early generation of polymer-free DES had very rapid drug elution that was inadequate to inhibit neointimal hyperplasia effectively, resulting in inferior antirestenotic efficacy [37]. Several solutions are proposed and being developed, including surface modification, the use of more hydrophobic drugs, and the loading of a second type of drug that targets the additional element of restenotic response cascade. A novel hollow stent design with drugs loaded within the hollow frame and released through abluminal holes were reported to show encouraging results [38]. In a study with polymer-free DES with biolimus A9, superiority were shown compared to bare metal stents for the composite of cardiac death, myocardial infarction or stent thrombosis at 12 months, with lower rate of repeat revascularization [39]. However, there is a shortage of efficacy and safety data comparing polymer-free DES and the new generation of polymeric DES.

The need for PCI will remain and continue to increase with the increasing age of the general population. With this trend, many will have complex coronary anatomy with high-risk comorbidities, such that advancements in PCI technology will be required. Additionally, the use of adjunctive secondary prevention therapies could be beneficial to further improve cardiac event-free survival.

Although PCI is currently the most frequently used revascularization procedure, coronary bypass surgery remains essential especially in the management of advanced and complex obstructive coronary disease. For example, coronary bypass surgery showed more superior outcomes in predominantly stable patients with three-vessel disease in randomized trials, compared to PCI [40, 41]. The grafts of choice are usually left internal mammary artery and veins (especially the great saphenous vein) as most commonly used conduits due to their length and availability [42]. Vessel wall remodeling, moderate intimal hyperplasia and

arterialization after graft surgery are expected as the grafts adapt to the new arterial environment [43]. However, in some cases graft remodeling continues such that clinical stenosis occurs. Loss of patency in vein grafts by more than 20% was reported to occur within first month post-surgery due to acute thrombosis [42]. Overall patency rates further diminish to approximately 60% after 10 years due to intimal hyperplasia and atherosclerosis [44-46]. Novel therapies, including *ex vivo* gene therapy, are being studied and developed in effort to prevent graft failure [47].

Prosthetic polymeric grafts, made of woven polyethylene terephthalate (Dacron) or expanded polytetrafluoroethylene (ePTFE), have been utilized in patients with limited suitable autologous grafts due to pre-existing vascular disease or prior vein harvesting [48]. However, prosthetic grafts often fail with those less than 6 mm diameter due to thrombogenicity of internal graft surface and lack of compliance between the graft and native blood vessel [49]. A substantial effort is underway to develop compliant and functional blood vessel substitutes [50, 51].

Despite the success of current therapies and procedures in mitigating cardiovascular risk, CVD remains to be the leading cause of death globally [1]. Additionally, with the trend of increasing age of the general population, with individual's unique and complex pathophysiology, there will be a demand for advancement in therapeutic methods for CVD. Nanomedicine has a potential to contribute to the development of novel therapies that could target vulnerable plaque or underlying inflammation process of atherosclerosis. Thus, this area is worth exploring in an effort to add another effective tool to the arsenal of methods for the treatment of atherosclerosis.

2.4 Nanomedicine-based Strategies for Atherosclerosis Treatment

Nanomedicine has a promising future for atherosclerosis treatment, because of the capability of nanoparticles to improve bioavailability of drugs and the customization of nanoparticle structure to target molecules involved in atherosclerotic progression. Types of nanocarriers most frequently studied for drug delivery are lipid-based, such as solid lipid nanoparticles, lipid micelles,

nanoemulsions, nanosuspensions, and liposomes. Other materials used for nanocarriers include virus-like, carbon- or organometallic-based, as well as inorganic particles, such as gold, silver, and metal oxide.

2.4.1 Nanoliposomes as Drug Delivery System

In this thesis, liposomes were selected as the nanocarriers for delivery of anti-inflammatory drug. Liposome is a spherical structure made of phospholipid bilayer, with aqueous core and hydrophobic bilayer compartment (**Figure 2.3**). Each phospholipid molecule is composed of a polar phosphate headgroup and a pair of fatty acid chains, linked by a glycerol backbone.

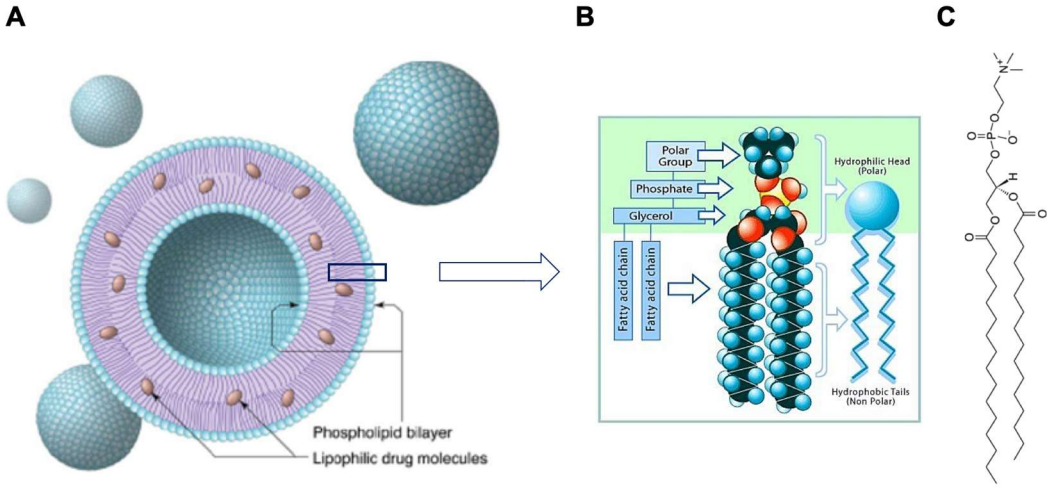

Figure 2.3 Schematic illustration of (A) liposome structure made up of phospholipid components; (B) individual phospholipid molecule composed of polar headgroup and a pair of nonpolar tails; (C) general structure of phosphatidylcholine [52, 53]

Liposomes have numerous advantages, which include biocompatibility, capability of encapsulating pharmaceutical agent and delivering it to the targeted site, as well as easy modification of surface to obtain stealth and active targeting capabilities [54]. Furthermore, liposomes can serve as cholesterol acceptors, capable of mobilizing cholesterol deposits from atherosclerotic arteries to the liver for excretion [55]. Liposomes have been widely utilized in cosmetic and pharmaceutical industries as delivery carriers for active compounds. Numerous liposomal formulations have been approved for clinical use in cancer therapy,

fungal, viral infection and pain management [56]. The primary challenges of using liposomes as drug delivery system are the difficulties in loading adequate amount of drugs and achieving sustained release with low initial drug burst release. In this thesis, the design of liposomal system was optimized to achieve high encapsulation of hydrophobic drug, and the factors affecting the drug release rate are discussed.

2.4.1.1 Thermal Properties of Liposomes

In a liposome composed of a single type of phospholipid, its physical state is dependent on the degree of molecular interactions between acyl chains and can be tuned by the change in temperature. At low temperature, the van der Waal's forces and hydrophobic interactions between acyl chains are increased, leading to constrained motion and ordered packing of lipid tails (gel phase) (**Figure 2.4**). Permeability of drug across the bilayer membrane is low at gel phase. When the temperature is sufficiently high, the van der Waal's forces and hydrophobic interactions between acyl chains are weaker, resulting in increased motion of acyl chains, increased fluidity and disordered packing (liquid crystalline phase) (**Figure 2.4**). The temperature at which the structure changes between ordered and disordered states is known as lipid transition temperature, T_c. At T_c, the permeability of cargo across lipid bilayer increases rapidly [57].

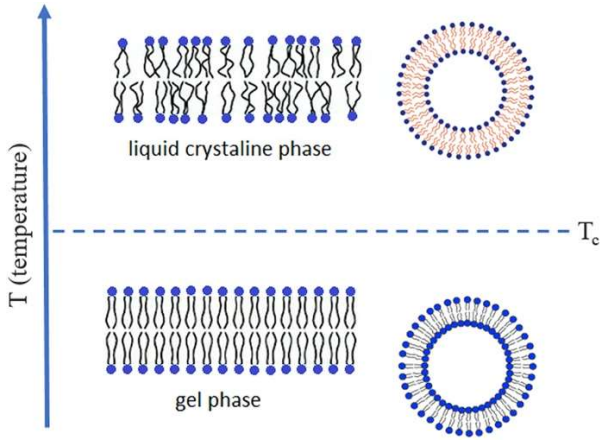

Figure 2.4 Structural change of bilayer can be tuned by altering the ambient temperature (T). When $T > T_c$, the liquid crystalline phase occurs. At this state, the bilayer is fluid and the drug can permeate through the bilayer easily. When $T < T_c$, the gel phase occurs. At this state, the bilayer is more tightly packed due to increased van der Waal's forces between lipid tails [58].

Various parameters, such as pH, ionic strength, additives, lipid headgroup and fatty acid chains, can affect the T_c of bilayer [59, 60]. Bilayers composed of lipids with longer fatty acid chains have higher T_c due to increased intermolecular van der Waal's forces on the lipid tails (**Figure 2.5**).

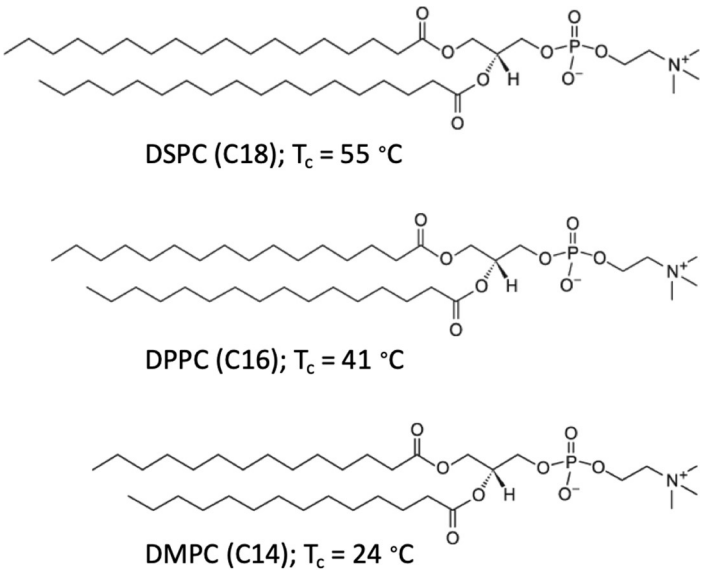

Figure 2.5 Structure of various phospholipids with different acyl chain lengths. Lipids with longer chains have higher T_c due to increased intermolecular van der Waal's forces [61, 62]

2.4.1.2 Surface Functionalization of Nanoliposomes

2.4.1.2.1 Polyethylene Glycol (PEG)

Surface properties of nanoparticles affect, to a large extent, the pharmacokinetics and the biodistribution of the nanoparticles. Therefore, nanoparticles designed for intravenous injection have been modified to obtain a hydrophilic and compatible surface. Among the molecules used for surface coating were polysaccharides [63], poly (amino acids) [64], and synthetic polymers [65]. Within the class of synthetic polymers, PEG has been identified to be highly suitable for this purpose and is currently the most extensively used surface coating for nanoparticles [66, 67]. Favorable PEG properties include its high hydrophilicity, nontoxicity, and its low level of protein or cellular adsorption. To date, numerous PEG therapeutics has been approved by FDA [66, 68].

PEGylated nanoliposomes, known as stealth liposomes, can efficiently bypass mononuclear phagocyte system, thereby enabling prolonged blood circulation of approximately 8 – 10 times longer than that of unPEGylated liposomes [69, 70]. The hydrophilic surface of PEGylated liposomes prevents opsonin from binding to the liposomal surface and marking the particle as a foreign substance, thereby avoiding recognition by mononuclear phagocyte and hence avoidance of blood clearance [71-73]. The nanoparticle circulation time is dependent on the particle size, PEG length, PEG surface density, and the overall particle surface charge [74-76]. Stealth liposomes have been utilized for passive drug targeting in antitumor therapies, by making use of malformed and leaky vasculature in tumor tissue, favoring accumulation of particles in the size range of about 20 to 200 nm [77-80]. A similar pathological condition is observed in atherosclerosis at late stages, whereby new microvessels are formed, infiltrating the atherosclerotic lesion [81, 82]. These microvessels are found to be leaky [83] and likewise, able to accumulate particles larger than 20 nm, such as contrast agents [84, 85] and drug-loaded nanocarriers such as reconstituted high-density lipoprotein [86] and liposomes [87].

On the surface of a nanoparticle, PEG is known to arrange themselves in various conformation, depending on their surface density. At low PEG density, mushroom conformation is formed, whereby the nanoparticle surface is not completely covered by PEG and there is no lateral interaction between individual PEG chains (**Figure 2.6 A**). At high PEG density, brush conformation is formed, whereby the lateral interactions between PEG chains are present, inducing the chains to stretch outwards (**Figure 2.6 B**) [88].

PEG conformation on the surface of a nanoparticle can be estimated by comparing the Flory radius (Rf) of the PEG and the mean distance between the PEG grafting sites (D). It is generally accepted that when $D > Rf$, the PEG chains are expected to be present in mushroom regime, and when $D < Rf$, PEG chains are present in brush regime [89-91]. When D is similar to Rf, the PEG chains undergo a so-called mushroom-to-brush transition, whereby the beginning of brush-like behavior is observed [92, 93].

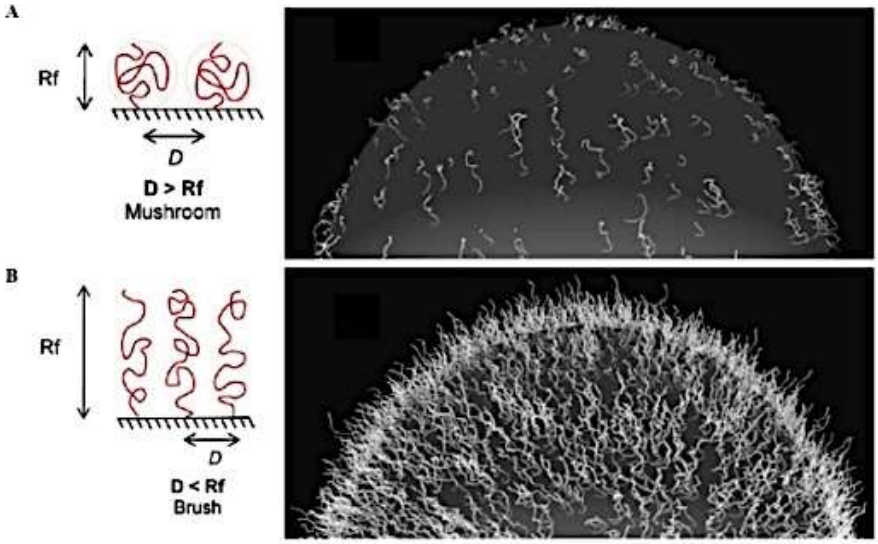

Figure 2.6 Various PEG conformation on particle surface. (A) Low PEG surface density leads to mushroom conformation. (B) High surface PEG density leads to brush conformation with restricted PEG mobility. Rf = Flory radius (average dimension of PEG in aqueous solution). D = Mean distance between PEG grafting sites [91].

The Flory radius of a PEG can be calculated with the following equation:

$$Rf = aN^{3/5}$$

N is the degree of polymerization, which can be represented as $N = M_w/44$, where M_w is the weight-average molecular weight and 44 Da is the molecular weight of (CH2-CH2-O) monomer. Thus, for PEG 2K, $N = 2000/44 \approx 45$, while a is the monomer length (0.35 nm [92]) [89, 94]. Therefore, Rf for PEG 2K equals 3.44 nm [93].

To calculate D, the number of lipid molecules between two PEG grafting sites has to be considered. This can be estimated by considering the molar percentages of lipids added into the system. Subsequently, the total surface area between the PEG grafting sites can be computed by taking into account the surface area of the hydrophilic head group of individual lipid molecules. The head group of phosphatidylcholine is around 0.71 nm^2 [95]. Assuming the surface area covered by one PEG chain as a circle, D can be considered as the diameter of the circle. By using the classical formula for area of circle, D can then be calculated [93].

PEGylation can be achieved in nanoliposomes by incorporating commercially available PEG-conjugated lipid, DSPE-PEG. In this lipid, PEG is conjugated via carbamate linkage on the lipid head of the phosphoethanolamine which contains NH_2 group (**Figure 2.7**).

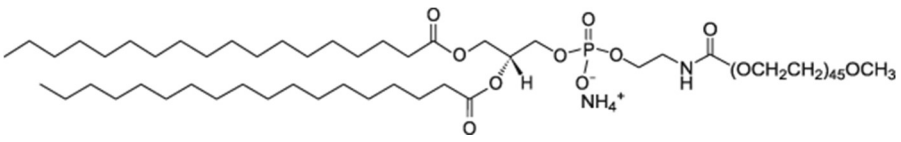

Figure 2.7 Structure of commercially available PEG-conjugated lipid (DSPE-PEG 2000) [96].

2.4.1.2.2 Active Ligand

In general, active targeting for atherosclerosis is aimed towards interaction with inflammatory biomarkers expressed in either activated endothelial cells (EC), macrophages or platelets.

For EC, the overexpression of adhesion receptors (such as E-selectin, ICAM-1 and VCAM-1) are targeted. These receptors function to help in the recruitment of monocytes into the plaque. Common ligands studied include Sialyl Lewis^a (a tetrasaccharide which is usually attached to O-glycans on the surface of cells), anti-VCAM-1 antibody, anti-ICAM-1 antibody and peptides specific to ICAM-1 receptor. The advantage of targeting EC is the accessibility of the cells from the bloodstream. The main challenge is the shear stress from the blood flow affecting the binding force of the ligand to the receptor.

For macrophages, scavenger receptors (such as SR-A and CD36), which are receptors function in uptaking oxidized lipids, are commonly targeted. Ligands used include dextran sulfate, oxidized phosphatidylcholine and HDL. Macrophage is a potential target for detection and treatment of atherosclerosis.

For platelet, expression of P-selectin receptor on its surface is commonly targeted. Ligands used include anti-P-selectin antibody and fuciodan (a sulfated

polysaccharide that binds P-selectin). However, this method might only be useful in the situation where the extracellular material is exposed.

Researchers are also exploring on the possibility of using multiple ligands in a single nanocarrier to improve the therapeutic performance. This aims to achieve either tighter binding of target cells or the ability to bind different cells involved in the lesion. The challenge is the possible steric / spatial limitations, as specific markers could be expressed too close or too far away from one another for the multi-targeting nanocarriers to make a significant difference.
Folate receptors (FR) on foam cells are potential targets worth exploring. It was recently reported in a study with apoE-deficient mice at 21 weeks of age, that 91.2 ± 2.4% of foam cells expressed FR-β, whereas only 4.6 ± 1.2% of non-lipid-loaded macrophages expressed FR-β in the aortic sinus lesion [97]. Another study showed that FR-β is expressed by 60% to 70% of CD68-positive lesional macrophages but not by T cells, endothelial cells, or smooth muscle cells [98]. FR are expressed only by limited types of cells, such as hematopoetic cells of the myelomonocytic lineage and myelocytic leukemia, and epithelial cells from the kidney and placenta, while most other healthy tissues express either low or negligible FR levels [99]. FR has also been reported to be overexpressed in activated macrophages, but either lacking or not expressed in nonactivated macrophages [100-102].

FR is a 38000 Da glycosyl-phosphatidylinositol-anchored protein, which has high affinity to the vitamin folic acid (KD < 1 nM) [103, 104]. Upon binding, the receptor-ligand complex is endocytosed and delivered to a low pH environment where the dissociation of the ligand from the receptor takes place [105]. With its high ligand-receptor binding affinity and capability for delivering associated active molecules specifically to activated macrophages without affecting other normal cells which express negligible quantity of FR, folate targeting is a method that is worth further investigation.

Fabrication of active targeting liposomes with folate ligand can be simply done by incorporation of commercially available folate-conjugated lipid. Folate is

commonly conjugated at the end of a PEG spacer of a specific length via amide bond (**Figure 2.8**).

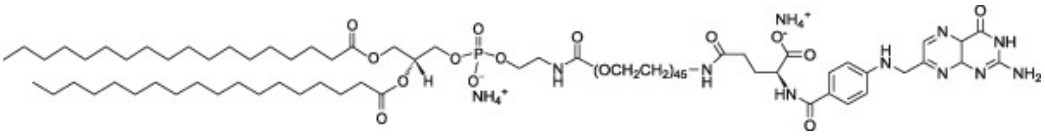

Figure 2.8 Structure of commercially available folate-conjugated lipid (DSPE-PEG (2000)-Folate) [96]

2.4.2 Size Effect of Nanoliposomes for Drug Delivery

The size of nanoparticles will affect the circulation time as well as the extravasation through leaky vasculature. Nanoparticles of smaller than ~15 nm will be cleared by renal filtration. Nanoparticles of bigger than ~200 nm will be trapped in the spleen, and eventually be engulfed by the splenic macrophages. Thus, nanoparticle size has to be kept small, typically ~ 100 – 200 nm and be masked from recognition by macrophages from reticuloendothelial system (RES).

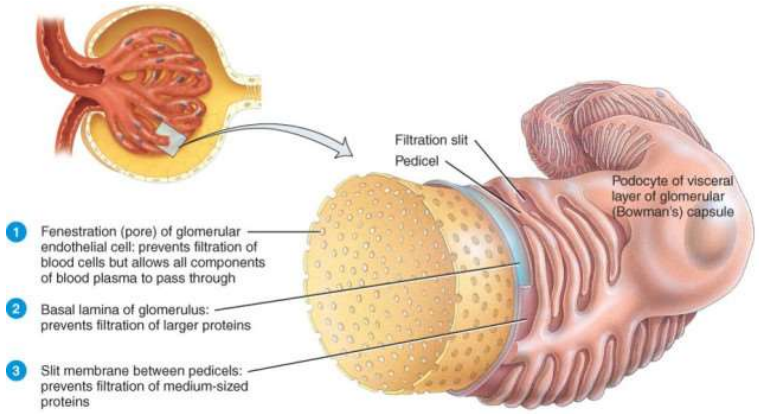

Figure 2.9 Illustration of filtration membranes in kidney. The pores of glomerular endothelial cells are capable of filtering particles < 15 nm [106].

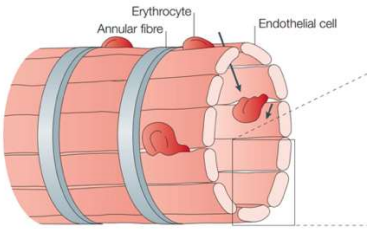

Figure 2.10 Illustration of venous sinuses in the red pulp of spleen. The endothelial cells are arranged in a barrel-like fashion, making narrow slits that enables red blood cells and particles < 200 nm to pass through to return into the venous circulation. Particles of >200 nm will be retained and phagocytosed by splenic macrophages [107].

Leaky vasculature is present in a certain pathological area, such as in tumor tissue, which has been shown to favor accumulation of particles in the size range of about 20 to 200 nm [77-80]. A similar pathological condition is observed in atherosclerosis at late stages, whereby new microvessels are formed, infiltrating the atherosclerotic lesion [81, 82]. These microvessels are found to be leaky [83] and likewise, able to accumulate particles larger than 20 nm, such as contrast agents [84, 85] and drug-loaded nanocarriers such as reconstituted high-density lipoprotein [86] and liposomes [87]

2.5 Glucocorticoids (GC) as Anti-inflammatory Drugs

Among the anti-inflammatory compounds investigated for atherosclerosis therapy, GC are clinically applied, the most extensively used anti-inflammatory drugs that are effective for many inflammatory diseases [6, 108]. Of all types of GC, dexamethasone (Dex) has been the most intensively studied for treatment of atherosclerosis and in-stent restenosis [109-112]. Dex has been demonstrated to suppress the development of atherosclerosis *in vivo* [113-117] as well as accumulation of cholesterol ester in foam cells and macrophages in vitro [118, 119]. Besides Dex, fluocinolone acetonide (FA) has recently been reported to show antiatherogenic effect. FA was shown to reduce lipid accumulation and inflammatory cytokine secretion of human THP-1 derived atherosclerotic foam cells either as well or better than Dex [120]. However, long-term systemic administration of GC has pro-atherogenic and systemic adverse effects such as

hypertension, glucose intolerance, osteoporosis, and susceptibility to infection [6, 7, 121]. Encapsulating GC in nanocarriers is one appealing strategy to attain localized GC treatment on the atherosclerotic plaque, thereby enhancing the benefit/risk ratio of the drug.

Table 2.1 Adverse effects resulted from prolonged exposure or high dose of corticosteroids [122, 123]

Tissue	Side Effects
Adrenal gland	Adrenal atrophy, Cushing's syndrome
Cardiovascular system	Dyslipidemia, hypertension, thrombosis, vasculitis
Central nervous system	Changes in behavior, cognition, memory, and mood, cerebral atrophy
Gastrointestinal tract	Gastrointestinal bleeding, pancreatitis, peptic ulcer
Immune system	Broad immunosuppression, activation of latent viruses
Integument	Atrophy, delayed wound healing, erythema, hypertrichosis, perioral dermatitis, petechiae, glucocorticoid-induced acne, striae rubrae, distensae, telangiectasia
Musculoskeletal system	Bone necrosis, muscle atrophy, osteoporosis, retardation of longitudinal bone growth
Eyes	Cataracts, glaucoma
Kidney	Increased sodium retention and potassium excretion
Reproductive system	Delayed puberty, fetal growth retardation, hypogonadism

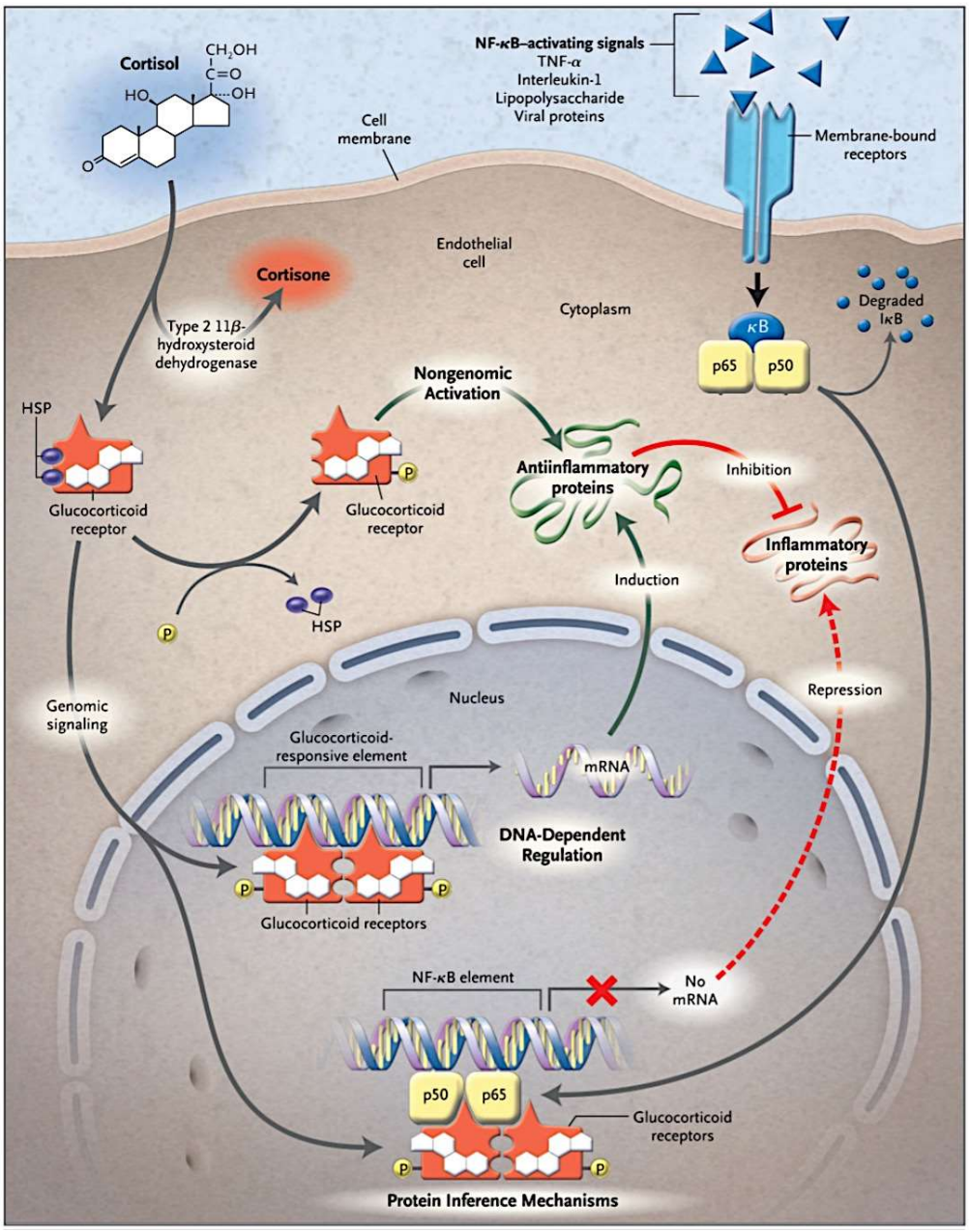

Figure 2.11 Schematic illustration of three general mechanisms of actions of glucocorticoids in anti-inflammation: nongenomic activation, DNA-dependent regulation, and protein interference mechanisms [123]

The mechanisms of action of GC are illustrated in **Figure 2.11**. GC affect cells by binding to GC receptors present in the cell cytoplasm. The activated glucocorticoid receptor interacts with transcription factors that mediate the expression of inflammatory genes, such as nuclear factor-kappa B (NF-κB) and activator protein-1 (AP-1), resulting in anti-inflammatory effects. Subsequently, the receptor complex translocates to the nucleus where it initiates the

transcription of glucocorticoid-responsive genes such as lipocortins, which leads to inhibition of phospholipase A2. This condition leads to inhibition of the release of arachidonic acid from membrane phospholipids and eventually prevents the synthesis of prostaglandins and leukotrienes, which are both potent mediators of inflammation [48]. GC has also been shown to produce anti-inflammatory effects through non-transcriptional activation of membrane-associated receptors and second messengers, such as endothelial nitric oxide synthase [123, 124]. Several transcriptional effects regulated by activated glucocorticoid receptors are listed in **Table 2.2**.

Table 2.2 Transcriptional effects regulated by activated glucocorticoid receptor [125]

Decreased transcription	Increased transcription
•Chemokines IL-8, RANTES, macrophage Inflammatory protein-1α, monocyte chemoattractant protein (MCP)-1, MCP-3, MCP-4, eotaxin •Cytokines Interleukins-1, 2, 3, 4, 5, 6, 9, 11, 12, 13, 16, 17, 18, TNF-α, granulocyte macrophage colony-stimulating factor, stem cell factor •Inducible enzymes Inducible nitric oxide synthase, cyclooxygenase-2, cytoplasmic phospholipase A_2 •Endothelin-1 receptors Neurokinin NK_1-receptors, NK_2-receptors •Adhesion molecules Intercellular cell adhesion molecule-1, E-selectin	•Lipocortin-1/annexin-1 (phospholipase A_2 inhibitor) •Clara cell protein (CC10, phospholipase A_2 inhibitor) •β_2-adrenoceptor •Secretory leukocyte inhibitory protein (SLPI) •IL-1 receptor antagonist •IL-1R2 (decoy receptor) •IκBα (inhibitor of NF-κB) •CD163 (scavenger receptor) •MAP Kinase phosphatase 1 (MKP-1)

2.6 Current Research on Passive and Active Targeting Nanotherapies

In this section, selected relevant literature examples are summarized and key points are highlighted.

2.6.1 Glucocorticoids (GC)-loaded Passive Nanoliposomes

2.6.1.1 Prednisolone Phosphate-loaded Nanoliposomes (LN-PLP) [87, 126]

This literature work reported the first clinical study of nanoliposomes (DPPC/cholesterol/DSPE-PEG 2000 62/33/5 molar ratio) encapsulating a type of GC, prednisolone phosphate, for atherosclerosis treatment. Studies conducted include LN-PLP pharmacokinetics, accumulation in the iliofemoral atherosclerotic plaque, and therapeutic efficacy on carotid atherosclerotic plaque.

Briefly, pharmacokinetics was conducted by intravenous injection of LN-PLP (dose of 0.375, 0.75, and 1.5 mg/kg) and measurement of the serum concentrations of prednisolone phosphate pro-drug as well as prednisolone on day 1, 3, 7 and weekly up to 12 weeks. LN-PLP plaque accumulation was conducted by fluorescent microscopy observation of antibody-tagged tissue macrophages and liposomes on cells harvested from iliofemoral plaque on day 10 after antecubital vein injection of LN-PLP (dose 1.5 mg/kg) or saline on day 0 and 7. Therapeutic efficacy was assessed by dynamic contrast enhanced-magnetic resonance imaging (DCE-MRI) and 18fluorodeoxyglucose positron emission tomography/computed tomography (FDG-PET/CT) imaging of carotid arteries of patients with existing arterial wall inflammation on day 10 after intravenous injections of LN-PLP (dose 1.5 mg/kg) or saline on days 0 and 7.

The pharmacokinetics result showed prolonged circulation of LN-PLP with drug half-life of 45 – 63 hours. Plaque accumulation study showed co-localization of PEG (LN-PLP coating) and macrophages (around 77% of positively-stained macrophages had PEG). However, a decrease in arterial wall inflammation was not detected. Possible reasons for the lack of efficacy discussed in the report were inadequate dose of prednisolone reaching the plaque, short time span of the study (10 days versus 12 weeks of majority of the studies assessing the effect of anti-inflammatory compounds in human CVD), and the pathobiological differences of the acute injury rabbit atherosclerosis model versus chronic inflammatory, lipid-rich atherosclerosis in humans, rendering discrepant results

between clinical and pre-clinical studies. The formulation was reported to be well-tolerated with no serious adverse events.

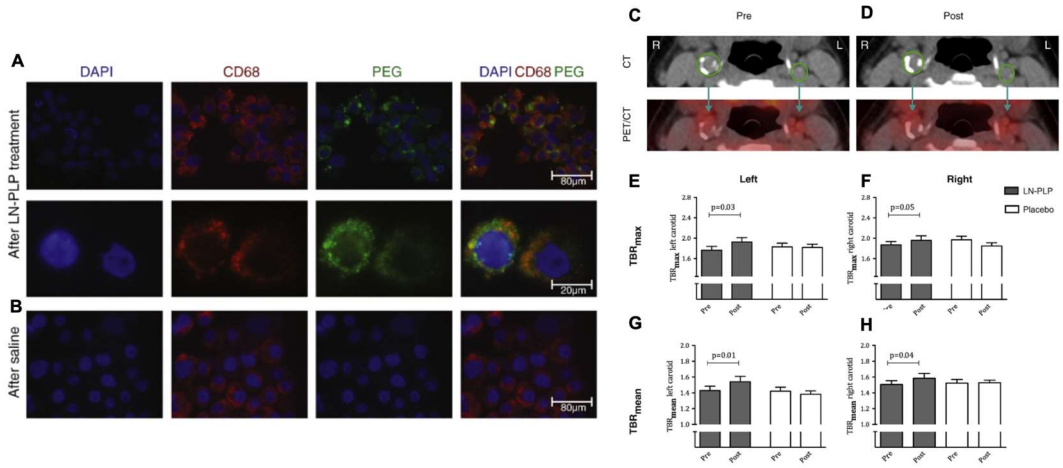

Figure 2.12 (A & B) Accumulation of LN-PLP in macrophages of iliofemoral plaque (DAPI cell nuclei; CD68 macrophages; PEG liposome coating). (C - H) Arterial wall inflammation after LN-PLP administration in patients with region of interest shown in green (CT computed tomography; PET positron emission tomography). (E – H) Changes in TBR_{max} and TBR_{mean} in the left and right carotid artery (TBR target to background ratio) [87]

In the following year, the same group reported increased recruitment of pro-inflammatory monocytes into the plaque on aortic arches and roots of LDL receptor knockout mice 2 weeks after treatment with LN-PLP. This increment was not observed in blank liposomes. Additionally, they reported more advanced plaque stage, with lower smooth muscle cell content, less collagen, enlarged necrotic core areas and higher expression of mRNA chemokines MCP-1 and Sdf-1α in LN-PLP treated plaque compared to those of bare drug and blank liposomes after 6 weeks treatment. *In vitro* study with macrophages showed decreased NF-κB-associated inflammation after treatment with LN-PLP and bare drug, but not blank liposomes. The cholesterol efflux capacity of macrophages reduced after all treatments compared to control. Further investigation showed increased expression of the intracellular lipid chaperone Fabp4 and decreased expression of the major cholesterol efflux transporter Abca1 in LN-PLP treated macrophages. This suggested heightened vulnerability for lipid stress and decreased capability for lipid efflux, which led to an increased number of macrophages undergoing late apoptosis and necrosis.

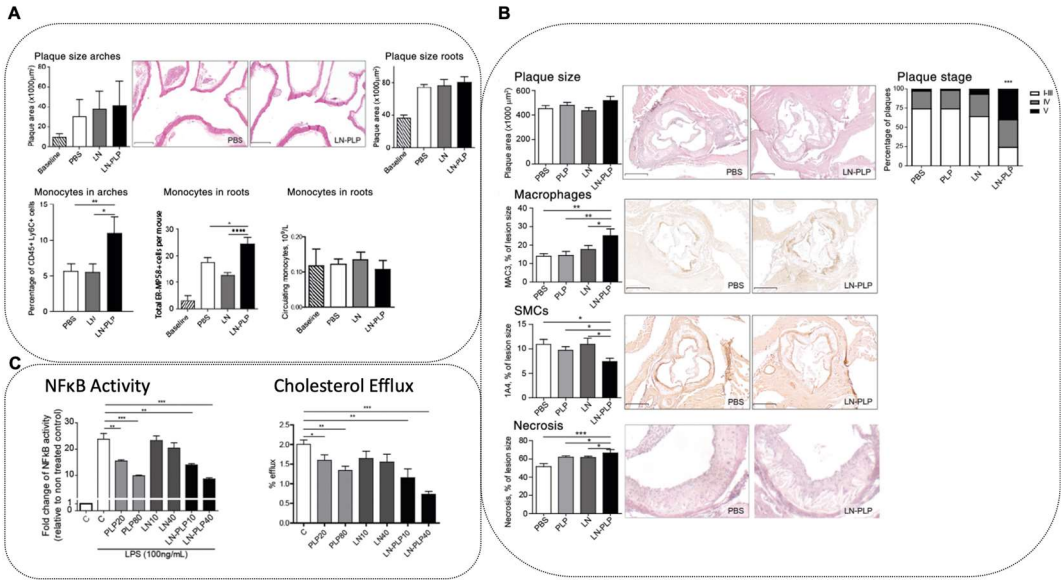

Figure 2.13 (A) Monocyte recruitment and atherosclerotic plaque size on aortic arches and roots of LDL receptor knockout mice after 6 weeks high fat diet and 2 weeks treatment. (B) Plaque size, plaque stage, macrophage content, smooth muscle cells (SMC) content, and necrotic core size on atherosclerotic plaque of LDL receptor knockout mice after 6 weeks high fat diet and 6 weeks treatment. (C) Left: NF-κB activity in RAW267.4 NFκB-*luc* cells as the relative fold change to control without lipopolysaccharide (LPS) stimulation. Right: Cholesterol efflux in bone marrow-derived macrophages isolated from C57BL/6 mice [126]

From the two studies, it is noteworthy that new anti-inflammatory nanotherapy candidates need to undergo screening with lipid-rich atherosclerotic environment, assessing the inflammation as well as cholesterol efflux capability.

LN-PLP was demonstrated to have long drug half-life, as reported in the first work. This set a reference for PEG concentration for passive liposomes to be used in our study. DSPE-PEG 2000 of 5 mol% concentration was also used in FDA-approved cancer nanotherapy, Doxil®, which demonstrated doxorubicin circulation half-life of about 90 hours in humans and more than 350 hours presence in human circulation [127]. Blood circulation time is affected by the liposomal composition, thus the presence of cholesterol in LN-PLP might affect the circulation time as well. However, the occupancy of cholesterol in the liposomal bilayer could reduce the ability of liposomes to pick up cholesterol

from the plaque [8], thereby decreasing its cholesterol efflux capability. Thus, inclusion of cholesterol was not considered in our liposomal formulation.

It was demonstrated in the LN-PLP study that it is feasible to deliver passive liposomes to atherosclerotic plaque in human. It is interesting to investigate if active ligand decoration on the liposomal surface will yield even better liposomal accumulation on atherosclerotic plaque. Finally, the safety assessment from the LN-PLP clinical study was relatively favorable, with no serious adverse effect. This encourages the use of nanoliposomes as carriers for anti-inflammatory drugs.

2.6.1.2 Dexamethasone-loaded Nanoliposomes [128]

This literature reported an *in vivo* study of dexamethasone (DXM)-loaded liposomes (EPC/cholesterol/dicetylphosphate 70/20/10 molar ratio; drug/lipid molar ratio 0.134; DXM concentration 1 mg/mL), comparing the effect of various particle sizes (519 nm L500, 202 nm L200, and 68.6 nm L70) on pharmacokinetics, liposomal accumulation in the aorta, and anti-atherogenic efficacy in both normal and atherogenic mice fed with cholesterol diet for 14 weeks.

The pharmacokinetics study was conducted by tail vein injection of [^{3}H]DXM-loaded liposomes or [^{3}H]CHE-labelled liposome containing DXM to both normal and atherogenic mice. At indicated timepoints, blood and subsequently aorta were collected. The radioactivity of [^{3}H]DXM and [^{3}H]CHE in serum and aorta were then measured with a scintillation counter. For the *in vivo* efficacy study, DXM-liposomes or free DXM were injected intravenously via tail vein to atherogenic mice weekly for 8 – 14 weeks. Serum and aorta were collected one day after final treatment. Serum total cholesterol level as well as aortic cholesterol level were assayed.

The elimination rates of both DXM and liposomes from the serum were found to increase as the particle size increased. DXM serum concentration of L70 and L200 were found to be higher than that of free DXM for both normal and atherogenic mice. In the aorta of atherogenic mice, there was about 5-fold increment in accumulation of DXM-loaded L200 compared to that of normal

mice. L200 also showed significantly greater accumulation than free DXM, L70, and L500 in atherogenic mice. The *in vitro* cell uptake study with macrophages and foam cells showed decreasing uptake as particle sizes decreased, with L70 showed significantly lower uptake than L500 and L200. These results, therefore, implied that L200 was able to cross through the endothelial cell junction on the atherosclerotic vessel wall and be taken up by the atherosclerotic macrophages and foam cells; whereas L500 could not cross the endothelial cell junction due to its large particle size although it could be taken up by the macrophages and foam cells theoretically. L70 was able to cross through the junction but could not be taken up by the atherosclerotic macrophages and foam cells. The cholesterol level in the aorta was found to be significantly lower in atherogenic mice treated with L200, even when the free DXM dose was increased to 10 times higher than the dose of DXM in L200.

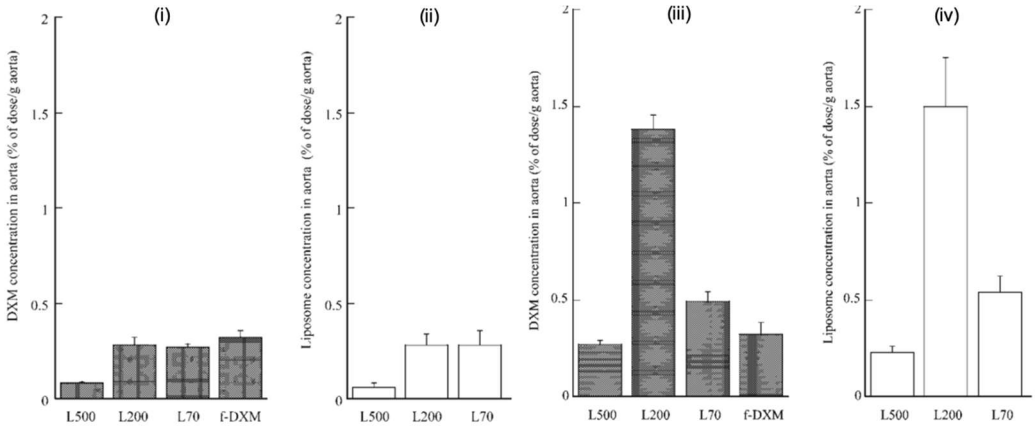

Figure 2.14 Aorta concentration 1 hour after administration of DXM-liposomes. DXM in normal mice (i); Liposome in normal mice (ii); DXM in atherosclerotic mice (iii); Liposome in atherosclerotic mice (iv) (L500 nm = 519 nm particle size; L200 = 202 nm; L70 = 68.6 nm) [128]

Notable in this study is the anti-atherogenic efficacy of dexamethasone-loaded nanoliposomes in atherosclerotic mice, in terms of cholesterol level reduction in the aorta. Additionally, the biodistribution study clearly showed that it is feasible for liposomes of size 200 nm or less to accumulate in the atherosclerotic lesion.

2.6.2 Active Targeting Nanoliposomes: Effect of PEG Surface Density on Ligand Targeting Efficiency

Hak et al. synthesized nanoemulsions with various DSPE-PEG 2000 content (5, 10, 20, 30, 40, and 50 mol% assigned as P5, P10, P20, P30, P40, and P50 respectively). As nanoparticle size can affect cell uptake, the sizes of the nanoemulsions were maintained by increasing soybean oil content within the nanoemulsions as PEG content increased. The hydrodynamic size was maintained to be about 100 nm with PDI well below 0.2. The targeting ligand used was $\alpha_v\beta_3$-integrin specific RGD (arginine-glycine-aspartic acid) peptide on human umbilical vein endothelial cells (HUVEC). The cells were incubated with medium without nanoemulsions (blank), passive nontargeted version of the formulations listed earlier (CTRL), or the active targeting nanoemulsions. Cell uptake was measured by flow cytometry. It was found that increased cellular uptake with RGD functionalization compared to CTRL were only observed in the case of P5 and P10. For P20 and higher PEG densities, negligible targeting effect was found.

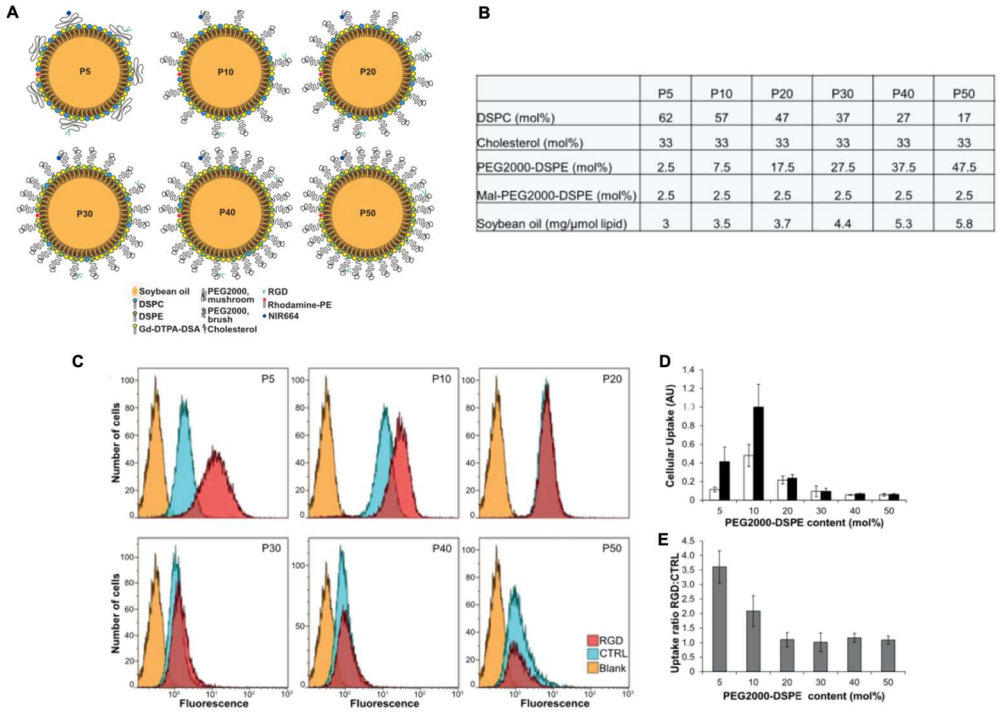

	P5	P10	P20	P30	P40	P50
DSPC (mol%)	62	57	47	37	27	17
Cholesterol (mol%)	33	33	33	33	33	33
PEG2000-DSPE (mol%)	2.5	7.5	17.5	27.5	37.5	47.5
Mal-PEG2000-DSPE (mol%)	2.5	2.5	2.5	2.5	2.5	2.5
Soybean oil (mg/μmol lipid)	3	3.5	3.7	4.4	5.3	5.8

Figure 2.15 (A) Schematic of nanoemulsions with various DSPE-PEG 2000 concentrations. (B) Contents of nanoemulsions. (C) Flow cytometry histograms of cell uptake with various nanoemulsions. (D) Normalized cell uptake as the

median fluorescence intensity divided by median cellular autofluorescence (CTRL white bars; RGD black bars). (E) Cellular uptake ratio between RGD and CTRL nanoemulsions

In other literature, a longer PEG spacer has been used in an effort to present the ligand above the cloud of PEG coating. For example, studies reported by Gabizon et al [129] and Yamada et al [130] demonstrated enhanced tumor cellular uptake with PEG 3350 and PEG 5000 spacer respectively. Altogether, these results highlight the importance of optimizing liposomal design parameters, such as ligand spacer length, PEG coating length, and PEG-to-ligand ratio for each ligand-receptor system and cell type.

References

[1] Organization, W.H. *Cardiovascular disease*. 2019 [cited 2019 25 Mar 2019]; Available from: https://www.who.int/cardiovascular_diseases/en/.

[2] Roth, G.A., et al., *Demographic and epidemiologic drivers of global cardiovascular mortality.* N Engl J Med, 2015. **372**(14): p. 1333-41.

[3] Benjamin, E.J., et al., *Heart Disease and Stroke Statistics-2019 Update: A Report From the American Heart Association.* Circulation, 2019. **139**(10): p. e56-e528.

[4] Libby, P., P.M. Ridker, and A. Maseri, *Inflammation and atherosclerosis.* Circulation, 2002. **105**(9): p. 1135-1143.

[5] Ross, R., *Mechanisms of disease - Atherosclerosis - An inflammatory disease.* New England Journal of Medicine, 1999. **340**(2): p. 115-126.

[6] Falk, E., *Pathogenesis of atherosclerosis.* J Am Coll Cardiol, 2006. **47**(8 Suppl): p. C7-12.

[7] Chiu, J.J. and S. Chien, *Effects of disturbed flow on vascular endothelium: pathophysiological basis and clinical perspectives.* Physiol Rev, 2011. **91**(1): p. 327-87.

[8] Lobatto, M.E., et al., *Perspectives and opportunities for nanomedicine in the management of atherosclerosis.* Nat Rev Drug Discov, 2011. **10**(11): p. 835-52.

[9] Schiener, M., et al., *Nanomedicine-based strategies for treatment of atherosclerosis.* Trends Mol Med, 2014. **20**(5): p. 271-81.

[10] Madamanchi, N.R., A. Vendrov, and M.S. Runge, *Oxidative stress and vascular disease.* Arterioscler Thromb Vasc Biol, 2005. **25**(1): p. 29-38.

[11] Goldstein, J.L. and M.S. Brown, *Regulation of the mevalonate pathway.* Nature, 1990. **343**(6257): p. 425-30.

[12] Weber, C. and H. Noels, *Atherosclerosis: current pathogenesis and therapeutic options.* Nat Med, 2011. **17**(11): p. 1410-22.

[13] Steinberg, D. and J.L. Witztum, *Inhibition of PCSK9: a powerful weapon for achieving ideal LDL cholesterol levels.* Proc Natl Acad Sci U S A, 2009. **106**(24): p. 9546-7.

[14] Hess, P.L., et al., *Implications of the FDA approval of PCSK9 inhibitors and FOURIER results for contemporary cardiovascular practice: An*

NCDR Research to Practice (R2P) project. Am Heart J, 2018. **195**: p. 151-152.

[15] Sparrow, C.P., et al., *Simvastatin has anti-inflammatory and antiatherosclerotic activities independent of plasma cholesterol lowering.* Arterioscler Thromb Vasc Biol, 2001. **21**(1): p. 115-21.

[16] Walter, D.H., et al., *Statin therapy, inflammation and recurrent coronary events in patients following coronary stent implantation.* J Am Coll Cardiol, 2001. **38**(7): p. 2006-12.

[17] Wilson, S.H., et al., *Simvastatin preserves coronary endothelial function in hypercholesterolemia in the absence of lipid lowering.* Arterioscler Thromb Vasc Biol, 2001. **21**(1): p. 122-8.

[18] Ray, K.K. and C.P. Cannon, *The potential relevance of the multiple lipid-independent (pleiotropic) effects of statins in the management of acute coronary syndromes.* J Am Coll Cardiol, 2005. **46**(8): p. 1425-33.

[19] Armitage, J., *The safety of statins in clinical practice.* Lancet, 2007. **370**(9601): p. 1781-90.

[20] Lonn, E.M., et al., *Emerging role of angiotensin-converting enzyme inhibitors in cardiac and vascular protection.* Circulation, 1994. **90**(4): p. 2056-69.

[21] Heart Outcomes Prevention Evaluation Study, I., et al., *Effects of an angiotensin-converting-enzyme inhibitor, ramipril, on cardiovascular events in high-risk patients.* N Engl J Med, 2000. **342**(3): p. 145-53.

[22] Bomback, A.S. and P.J. Klemmer, *The incidence and implications of aldosterone breakthrough.* Nat Clin Pract Nephrol, 2007. **3**(9): p. 486-92.

[23] Sato, A. and T. Saruta, *Aldosterone breakthrough during angiotensin-converting enzyme inhibitor therapy.* Am J Hypertens, 2003. **16**(9 Pt 1): p. 781-8.

[24] Antithrombotic Trialists, C., *Collaborative meta-analysis of randomised trials of antiplatelet therapy for prevention of death, myocardial infarction, and stroke in high risk patients.* BMJ, 2002. **324**(7329): p. 71-86.

[25] Antithrombotic Trialists, C., et al., *Aspirin in the primary and secondary prevention of vascular disease: collaborative meta-analysis of individual*

participant data from randomised trials. Lancet, 2009. **373**(9678): p. 1849-60.

[26] Mehta, S.R., S. Yusuf, and I. Clopidogrel in Unstable angina to prevent Recurrent Events Study, *The Clopidogrel in Unstable angina to prevent Recurrent Events (CURE) trial programme; rationale, design and baseline characteristics including a meta-analysis of the effects of thienopyridines in vascular disease.* Eur Heart J, 2000. **21**(24): p. 2033-41.

[27] Byrne, R.A., et al., *Coronary balloon angioplasty, stents, and scaffolds.* Lancet, 2017. **390**(10096): p. 781-792.

[28] Byrne, R.A., et al., *Drug-coated balloon therapy in coronary and peripheral artery disease.* Nat Rev Cardiol, 2014. **11**(1): p. 13-23.

[29] Levin, A.D., et al., *Specific binding to intracellular proteins determines arterial transport properties for rapamycin and paclitaxel.* Proc Natl Acad Sci U S A, 2004. **101**(25): p. 9463-7.

[30] Kastrati, A., et al., *Intracoronary stenting and angiographic results: strut thickness effect on restenosis outcome (ISAR-STEREO) trial.* Circulation, 2001. **103**(23): p. 2816-21.

[31] von Birgelen, C., et al., *Third-generation zotarolimus-eluting and everolimus-eluting stents in all-comer patients requiring a percutaneous coronary intervention (DUTCH PEERS): a randomised, single-blind, multicentre, non-inferiority trial.* Lancet, 2014. **383**(9915): p. 413-23.

[32] Park, K.W., et al., *A randomized comparison of platinum chromium-based everolimus-eluting stents versus cobalt chromium-based Zotarolimus-Eluting stents in all-comers receiving percutaneous coronary intervention: HOST-ASSURE (harmonizing optimal strategy for treatment of coronary artery stenosis-safety & effectiveness of drug-eluting stents & anti-platelet regimen), a randomized, controlled, noninferiority trial.* J Am Coll Cardiol, 2014. **63**(25 Pt A): p. 2805-16.

[33] von Birgelen, C., et al., *A randomized controlled trial in second-generation zotarolimus-eluting Resolute stents versus everolimus-eluting Xience V stents in real-world patients: the TWENTE trial.* J Am Coll Cardiol, 2012. **59**(15): p. 1350-61.

[34] Serruys, P.W., et al., *Comparison of zotarolimus-eluting and everolimus-eluting coronary stents.* N Engl J Med, 2010. **363**(2): p. 136-46.

[35] Vlachojannis, G.J., et al., *Biodegradable Polymer Biolimus-Eluting Stents Versus Durable Polymer Everolimus-Eluting Stents in Patients With Coronary Artery Disease: Final 5-Year Report From the COMPARE II Trial (Abluminal Biodegradable Polymer Biolimus-Eluting Stent Versus Durable Polymer Everolimus-Eluting Stent).* JACC Cardiovasc Interv, 2017. **10**(12): p. 1215-1221.

[36] Kufner, S., et al., *Five-year outcomes from a trial of three limus-eluting stents with different polymer coatings in patients with coronary artery disease: final results from the ISAR-TEST 4 randomised trial.* EuroIntervention, 2016. **11**(12): p. 1372-9.

[37] Genereux, P., et al., *Dedicated Bifurcation Stent for the Treatment of Bifurcation Lesions Involving Large Side Branches: Outcomes From the Tryton Confirmatory Study.* JACC Cardiovasc Interv, 2016. **9**(13): p. 1338-46.

[38] Worthley, S.G., et al., *First-in-Human Evaluation of a Novel Polymer-Free Drug-Filled Stent: Angiographic, IVUS, OCT, and Clinical Outcomes From the RevElution Study.* JACC Cardiovasc Interv, 2017. **10**(2): p. 147-156.

[39] Urban, P., et al., *Polymer-free Drug-Coated Coronary Stents in Patients at High Bleeding Risk.* N Engl J Med, 2015. **373**(21): p. 2038-47.

[40] Giacoppo, D., et al., *Percutaneous Coronary Intervention vs Coronary Artery Bypass Grafting in Patients With Left Main Coronary Artery Stenosis: A Systematic Review and Meta-analysis.* JAMA Cardiol, 2017. **2**(10): p. 1079-1088.

[41] Mohr, F.W., et al., *Coronary artery bypass graft surgery versus percutaneous coronary intervention in patients with three-vessel disease and left main coronary disease: 5-year follow-up of the randomised, clinical SYNTAX trial.* Lancet, 2013. **381**(9867): p. 629-38.

[42] Goldman, S., et al., *Long-term patency of saphenous vein and left internal mammary artery grafts after coronary artery bypass surgery: results from a Department of Veterans Affairs Cooperative Study.* J Am Coll Cardiol, 2004. **44**(11): p. 2149-56.

[43] de Vries, M.R., et al., *Vein graft failure: from pathophysiology to clinical outcomes.* Nat Rev Cardiol, 2016. **13**(8): p. 451-70.

[44] Owens, C.D., *Adaptive changes in autogenous vein grafts for arterial reconstruction: clinical implications.* J Vasc Surg, 2010. **51**(3): p. 736-46.

[45] Walts, A.E., M.C. Fishbein, and J.M. Matloff, *Thrombosed, ruptured atheromatous plaques in saphenous vein coronary artery bypass grafts: ten years' experience.* Am Heart J, 1987. **114**(4 Pt 1): p. 718-23.

[46] Motwani, J.G. and E.J. Topol, *Aortocoronary saphenous vein graft disease: pathogenesis, predisposition, and prevention.* Circulation, 1998. **97**(9): p. 916-31.

[47] Wan, S., et al., *Vein graft failure: current clinical practice and potential for gene therapeutics.* Gene Ther, 2012. **19**(6): p. 630-6.

[48] Bergan, J.J., et al., *Randomization of autogenous vein and polytetrafluorethylene grafts in femoral-distal reconstruction.* Surgery, 1982. **92**(6): p. 921-30.

[49] Abbott, W.M., et al., *Effect of compliance mismatch on vascular graft patency.* J Vasc Surg, 1987. **5**(2): p. 376-82.

[50] Xue, L. and H.P. Greisler, *Biomaterials in the development and future of vascular grafts.* J Vasc Surg, 2003. **37**(2): p. 472-80.

[51] Wang, X., et al., *Development of small-diameter vascular grafts.* World J Surg, 2007. **31**(4): p. 682-9.

[52] *16:0 PC (DPPC)*. 2020 [cited 2020 5 Feb]; Available from: https://avantilipids.com.

[53] *Liposome Production*. 2005-2020 [cited 2020 5 Feb]; Available from: https://www.creative-biostructure.com.

[54] Torchilin, V.P., *Recent advances with liposomes as pharmaceutical carriers.* Nature Reviews Drug Discovery, 2005. **4**(2): p. 145-160.

[55] Rodrigueza, W.V., M.C. Phillips, and K.J. Williams, *Structural and metabolic consequences of liposome-lipoprotein interactions.* Advanced Drug Delivery Reviews, 1998. **32**(1-2): p. 31-43.

[56] Bulbake, U., et al., *Liposomal Formulations in Clinical Use: An Updated Review.* Pharmaceutics, 2017. **9**(2).

[57] Demetzos, C., *Differential Scanning Calorimetry (DSC): a tool to study the thermal behavior of lipid bilayers and liposomal stability.* J Liposome Res, 2008. **18**(3): p. 159-73.

[58] Wang, N., M. Chen, and T. Wang, *Liposomes used as a vaccine adjuvant-delivery system: From basics to clinical immunization.* J Control Release, 2019. **303**: p. 130-150.

[59] Gennis, R.B., *Biomembranes : molecular structure and function*. Springer advanced texts in chemistry. 1989, New York: Springer-Verlag. xvii, 533 p.

[60] New, R.R.C., *Liposomes : a practical approach*. Practical approach series. 1990, Oxford: IRL ;

IRL. xvi, 301 p.

[61] Silvius, J.R., *Thermotropic phase transitions of pure lipids in model membranes and their modifications by membrane proteins.* Lipid-protein interactions, 1982. **2**: p. 239-281.

[62] *Phase Transition Temperatures for Glycerophospholipids*. [cited 2020 5 Feb]; Available from: https://avantilipids.com/wp-content/uploads/2015/11/Phase_Transition_Temps_for_Glycerophospholipids_Table.pdf.

[63] Dias, A.M., et al., *A biotechnological perspective on the application of iron oxide magnetic colloids modified with polysaccharides.* Biotechnol Adv, 2011. **29**(1): p. 142-55.

[64] Metselaar, J.M., et al., *A novel family of L-amino acid-based biodegradable polymer-lipid conjugates for the development of long-circulating liposomes with effective drug-targeting capacity.* Bioconjug Chem, 2003. **14**(6): p. 1156-64.

[65] Zhang, F., et al., *Polymer-coated nanoparticles: a universal tool for biolabelling experiments.* Small, 2011. **7**(22): p. 3113-27.

[66] Ryan, S.M., et al., *Advances in PEGylation of important biotech molecules: delivery aspects.* Expert Opin Drug Deliv, 2008. **5**(4): p. 371-83.

[67] Bhadra, D., et al., *Pegnology: a review of PEG-ylated systems.* Pharmazie, 2002. **57**(1): p. 5-29.

[68] Wagner, V., et al., *The emerging nanomedicine landscape.* Nat Biotechnol, 2006. **24**(10): p. 1211-7.

[69] Klibanov, A.L., et al., *Amphipathic Polyethyleneglycols Effectively Prolong the Circulation Time of Liposomes.* Febs Letters, 1990. **268**(1): p. 235-237.

[70] Torchilin, V.P., *Recent advances with liposomes as pharmaceutical carriers.* Nat Rev Drug Discov, 2005. **4**(2): p. 145-60.

[71] Moghimi, S.M. and H.M. Patel, *Tissue specific opsonins for phagocytic cells and their different affinity for cholesterol-rich liposomes.* FEBS Lett, 1988. **233**(1): p. 143-7.

[72] Moghimi, S.M. and H.M. Patel, *Differential properties of organ-specific serum opsonins for liver and spleen macrophages.* Biochim Biophys Acta, 1989. **984**(3): p. 379-83.

[73] Senior, J.H., *Fate and behavior of liposomes in vivo: a review of controlling factors.* Crit Rev Ther Drug Carrier Syst, 1987. **3**(2): p. 123-93.

[74] Blume, G. and G. Cevc, *Molecular mechanism of the lipid vesicle longevity in vivo.* Biochim Biophys Acta, 1993. **1146**(2): p. 157-68.

[75] Fang, C., et al., *In vivo tumor targeting of tumor necrosis factor-alpha-loaded stealth nanoparticles: effect of MePEG molecular weight and particle size.* Eur J Pharm Sci, 2006. **27**(1): p. 27-36.

[76] Maldiney, T., et al., *Effect of core diameter, surface coating, and PEG chain length on the biodistribution of persistent luminescence nanoparticles in mice.* ACS Nano, 2011. **5**(2): p. 854-62.

[77] Underwood, J.C. and I. Carr, *The ultrastructure and permeability characteristics of the blood vessels of a transplantable rat sarcoma.* J Pathol, 1972. **107**(3): p. 157-66.

[78] Peterson, H.I. and K.L. Appelgren, *Experimental studies on the uptake and rentention of labelled proteins in a rat tumour.* Eur J Cancer, 1973. **9**(8): p. 543-7.

[79] Ackerman, N.B. and P.A. Hechmer, *Studies on the capillary permeability of experimental liver metastases.* Surg Gynecol Obstet, 1978. **146**(6): p. 884-8.

[80] Taurin, S., H. Nehoff, and K. Greish, *Anticancer nanomedicine and tumor vascular permeability; Where is the missing link?* J Control Release, 2012. **164**(3): p. 265-75.

[81] Staub, D., et al., *Vasa vasorum and plaque neovascularization on contrast-enhanced carotid ultrasound imaging correlates with cardiovascular disease and past cardiovascular events.* Stroke, 2010. **41**(1): p. 41-7.

[82] de Boer, O.J., et al., *Leucocyte recruitment in rupture prone regions of lipid-rich plaques: a prominent role for neovascularization?* Cardiovasc Res, 1999. **41**(2): p. 443-9.

[83] Sluimer, J.C., et al., *Thin-walled microvessels in human coronary atherosclerotic plaques show incomplete endothelial junctions relevance of compromised structural integrity for intraplaque microvascular leakage.* J Am Coll Cardiol, 2009. **53**(17): p. 1517-27.

[84] Phinikaridou, A., et al., *Noninvasive magnetic resonance imaging evaluation of endothelial permeability in murine atherosclerosis using an albumin-binding contrast agent.* Circulation, 2012. **126**(6): p. 707-19.

[85] Barkhausen, J., et al., *Detection of atherosclerotic plaque with gadofluorine-enhanced magnetic resonance imaging.* Circulation, 2003. **108**(5): p. 605-609.

[86] Duivenvoorden, R., et al., *A statin-loaded reconstituted high-density lipoprotein nanoparticle inhibits atherosclerotic plaque inflammation.* Nat Commun, 2014. **5**: p. 3065.

[87] van der Valk, F.M., et al., *Prednisolone-containing liposomes accumulate in human atherosclerotic macrophages upon intravenous administration.* Nanomedicine, 2015. **11**(5): p. 1039-46.

[88] Georgiev, G.A., et al., *Effects of poly (ethylene glycol) chains conformational transition on the properties of mixed DMPC/DMPE-PEG thin liquid films and monolayers.* Colloids Surf B Biointerfaces, 2007. **59**(2): p. 184-93.

[89] de Gennes, P.G., *Polymers at an interface; a simplified view.* Advances in Colloid and Interface Science, 1987. **27**(3-4): p. 189-209.

[90] Howard, M.D.J., M.; Dziubla, T. D.; Lu, X., *PEGylation of nanocarrier drug delivery systems: state of the art.* J Biomed Nanotechnol, 2008(4): p. 133 - 148.

[91] Yu, M.K., J. Park, and S. Jon, *Targeting strategies for multifunctional nanoparticles in cancer imaging and therapy.* Theranostics, 2012. **2**(1): p. 3-44.

[92] Hansen, P.L., et al., *Osmotic properties of poly(ethylene glycols): quantitative features of brush and bulk scaling laws.* Biophys J, 2003. **84**(1): p. 350-5.

[93] Hak, S., et al., *The effect of nanoparticle polyethylene glycol surface density on ligand-directed tumor targeting studied in vivo by dual modality imaging.* ACS Nano, 2012. **6**(6): p. 5648-58.

[94] Kenworthy, A.K., et al., *Range and magnitude of the steric pressure between bilayers containing phospholipids with covalently attached poly(ethylene glycol).* Biophys J, 1995. **68**(5): p. 1921-36.

[95] Radovic-Moreno, A.F., et al., *Immunomodulatory spherical nucleic acids.* Proc Natl Acad Sci U S A, 2015. **112**(13): p. 3892-7.

[96] 2020 [cited 2020 5 Feb]; Available from: https://avantilipids.com.

[97] Furusho, Y., et al., *Novel Therapy for Atherosclerosis Using Recombinant Immunotoxin Against Folate Receptor beta-Expressing Macrophages.* J Am Heart Assoc, 2012. **1**(4): p. e003079.

[98] Hilgendorf, I. and F.K. Swirski, *Folate receptor: a macrophage "achilles' heel"?* J Am Heart Assoc, 2012. **1**(4): p. e004036.

[99] Antony, A.C., *Folate receptors.* Annu Rev Nutr, 1996. **16**: p. 501-21.

[100] Xia, W., et al., *A functional folate receptor is induced during macrophage activation and can be used to target drugs to activated macrophages.* Blood, 2009. **113**(2): p. 438-46.

[101] Varghese, B., et al., *Folate receptor-beta in activated macrophages: ligand binding and receptor recycling kinetics.* Mol Pharm, 2014. **11**(10): p. 3609-16.

[102] Antohe, F., *Endothelial cells and macrophages, partners in atherosclerotic plaque progression.* Arch Physiol Biochem, 2006. **112**(4-5): p. 245-53.

[103] Salter, D.N., et al., *The preparation and properties of folate-binding protein from cow's milk.* Biochem J, 1981. **193**(2): p. 469-76.

[104] Selhub, J., O. Ahmad, and I.H. Rosenberg, *Preparation and use of affinity columns with bovine milk folate-binding protein (FBP) covalently linked to Sepharose 4B.* Methods Enzymol, 1980. **66**: p. 686-90.

[105] Kamen, B.A., A.K. Smith, and R.G. Anderson, *The folate receptor works in tandem with a probenecid-sensitive carrier in MA104 cells in vitro.* J Clin Invest, 1991. **87**(4): p. 1442-9.

[106] *Physiological base of Human Movement*. [cited 2020 5 Feb]; Available from: https://utssportandsociety.wordpress.com/physiological-base-of-human-movement-lecture-9/.

[107] Cataldi, M., et al., *Emerging Role of the Spleen in the Pharmacokinetics of Monoclonal Antibodies, Nanoparticles and Exosomes.* Int J Mol Sci, 2017. **18**(6).

[108] Naghavi, M., et al., *From vulnerable plaque to vulnerable patient: a call for new definitions and risk assessment strategies: Part I.* Circulation, 2003. **108**(14): p. 1664-72.

[109] Poon, M., et al., *Dexamethasone inhibits macrophage accumulation after balloon arterial injury in cholesterol fed rabbits.* Atherosclerosis, 2001. **155**(2): p. 371-80.

[110] Asai, K., et al., *Dexamethasone-Induced Suppression of Aortic Atherosclerosis in Cholesterol-Fed Rabbits - Possible Mechanisms.* Arteriosclerosis and Thrombosis, 1993. **13**(6): p. 892-899.

[111] Hoffmann, R., et al., *Evaluation of a high-dose Dexamethasone-eluting stent.* American Journal of Cardiology, 2004. **94**(2): p. 193-195.

[112] Liu, X.S., et al., *Study of antirestenosis with the BiodivYsio dexamethasone-eluting stent (STRIDE): A first-in-human multicenter pilot trial.* Catheterization and Cardiovascular Interventions, 2003. **60**(2): p. 172-178.

[113] Makheja, A.N., et al., *Anti-inflammatory drugs in experimental atherosclerosis. 7. Spontaneous atherosclerosis in WHHL rabbits and inhibition by cortisone acetate.* Atherosclerosis, 1989. **76**(2-3): p. 155-61.

[114] Naito, M., et al., *Effects of dexamethasone on experimental atherosclerosis in cholesterol-fed rabbits.* J Nutr Sci Vitaminol (Tokyo), 1992. **38**(3): p. 255-64.

[115] Asai, K., et al., *Dexamethasone-induced suppression of aortic atherosclerosis in cholesterol-fed rabbits. Possible mechanisms.* Arterioscler Thromb, 1993. **13**(6): p. 892-9.

[116] Van Put, D.J., et al., *Dexamethasone influences intimal thickening and vascular reactivity in the rabbit collared carotid artery.* Eur J Pharmacol, 1995. **294**(2-3): p. 753-61.

[117] Tauchi, Y., et al., *Effect of dexamethasone palmitate-low density lipoprotein complex on cholesterol ester accumulation in aorta of atherogenic model mice.* Biol Pharm Bull, 2001. **24**(8): p. 925-9.

[118] Tauchi, Y., et al., *Preparation of a complex of dexamethasone palmitate-low density lipoprotein and its effect on foam cell formation of murine peritoneal macrophages.* J Pharm Sci, 1999. **88**(7): p. 709-14.

[119] Tauchi, Y., et al., *Inhibitory effect of dexamethasone palmitate-low density lipoprotein complex on low density lipoprotein-induced macrophage foam cell formation.* Biol Pharm Bull, 2000. **23**(4): p. 466-71.

[120] Nguyen, L.T.H., et al., *The Potential of Fluocinolone Acetonide to Mitigate Inflammation and Lipid Accumulation in 2D and 3D Foam Cell Cultures.* Biomed Res Int, 2018. **2018**: p. 3739251.

[121] Kolodgie, F.D., et al., *Elimination of neoangiogenesis for plaque stabilization: is there a role for local drug therapy?* J Am Coll Cardiol, 2007. **49**(21): p. 2093-101.

[122] Schacke, H., W.D. Docke, and K. Asadullah, *Mechanisms involved in the side effects of glucocorticoids.* Pharmacology & Therapeutics, 2002. **96**(1): p. 23-43.

[123] Rhen, T. and J.A. Cidlowski, *Antiinflammatory action of glucocorticoids--new mechanisms for old drugs.* N Engl J Med, 2005. **353**(16): p. 1711-23.

[124] Hafezi-Moghadam, A., et al., *Acute cardiovascular protective effects of corticosteroids are mediated by non-transcriptional activation of endothelial nitric oxide synthase.* Nat Med, 2002. **8**(5): p. 473-9.

[125] Hayashi, R., et al., *Effects of glucocorticoids on gene transcription.* Eur J Pharmacol, 2004. **500**(1-3): p. 51-62.

[126] van der Valk, F.M., et al., *Liposomal prednisolone promotes macrophage lipotoxicity in experimental atherosclerosis.* Nanomedicine, 2016. **12**(6): p. 1463-70.

[127] Barenholz, Y., *Doxil(R)--the first FDA-approved nano-drug: lessons learned.* J Control Release, 2012. **160**(2): p. 117-34.

[128] Chono, S., et al., *Efficient drug delivery to atherosclerotic lesions and the antiatherosclerotic effect by dexamethasone incorporated into liposomes in atherogenic mice.* J Drug Target, 2005. **13**(4): p. 267-76.

[129] Gabizon, A., et al., *Targeting folate receptor with folate linked to extremities of poly(ethylene glycol)-grafted liposomes: in vitro studies.* Bioconjug Chem, 1999. **10**(2): p. 289-98.

[130] Yamada, A., et al., *Design of folate-linked liposomal doxorubicin to its antitumor effect in mice.* Clin Cancer Res, 2008. **14**(24): p. 8161-8.

Chapter 3

Experimental Methodology

This chapter describes the materials and experimental methods used in the studies. The nanoliposomes fabrication as well as its characterization methods were described, together with various in vitro test experiments conducted to measure the properties and cellular uptake of both passive and active liposomes. Additionally, the working principles of characterization tools, their advantages and limitations, as well as the rationale for selection of these tools for the studies are discussed, as well.

3.1 Materials

3.1.1 Liposome Formulations

1,2-Dimyristoyl-sn-glycero-3-phosphocholine (DMPC), 1,2-Dipalmitoyl-sn-glycero-3-phosphocholine (DPPC), 1,2-Distearoyl-sn-glycero-3-phosphocholine (DSPC), L-α-phosphatidylcholine (Egg, Chicken) (EPC), Egg-Sphingomyelin (Egg SM) were purchased from NOF Corporation, Japan. 1,2-distearoyl-sn-glycero-3-phosphoethanolamine-N-[methoxy(polyethylene glycol)-2000] (ammonium salt) (DSPE-PEG 2000), 1,2-distearoyl-sn-glycero-3-phosphoethanolamine-N-[methoxy(polyethylene glycol)-750] (ammonium salt) (DSPE-PEG 750), 1,2-distearoyl-sn-glycero-3-phosphoethanolamine-N-[methoxy(polyethylene glycol)-5000] (ammonium salt) (DSPE-PEG 5000), 1,2-distearoyl-sn-glycero-3-phosphoethanolamine-N-[folate(polyethylene glycol)-2000] (ammonium salt) (DSPE-PEG 2000-Folate), 1,2-distearoyl-sn-glycero-3-phosphoethanolamine-N-[folate(polyethylene glycol)-5000] (ammonium salt) (DSPE-PEG 5000-Folate), and 1,2-dipalmitoyl-sn-glycero-3-phosphoethanolamine-N-(lissamine rhodamine B sulfonyl) (ammonium salt) (DPPE-Rhodamine) were purchased from Avanti Polar Lipids, Inc., USA. Fluocinolone Acetonide (FA) was purchased from International Laboratory, USA. Extrusion materials such as drain discs as well as polycarbonate filter membranes of 0.08 and 0.2 μm in size were obtained from Northern Lipids Inc., Canada. Phosphate buffer salts such as sodium chloride (NaCl), sodium phosphate dibasic anhydrous (Na2HPO4), potassium chloride (KCl), and potassium phosphate monobasic anhydrous (KH2PO4) were acquired from Sigma-Aldrich and used without further purification. Chemicals used in lipid measurement such as ferric chloride hexahydrate and ammonium thiocyanate were obtained from Sigma-Aldrich. The water was from Milli-Q purification system with the resistivity maintained at 18.2 ± 0.2 mΩ cm.

3.1.2 Cell Studies

Human monocytic THP-1 cells were from ATCC® TIB202™, USA. Roswell Park Memorial Institute (RPMI) 1640 Medium (ATCC modification),

Penicillin-Streptomycin (PS) Solution, fetal bovine serum (FBS) and sterile phosphate buffered saline (PBS) were obtained from Pan Biotech, Germany. Phorbol 12-myristate 13- acetate (PMA) and 2-mercaptoethanol were purchased from Sigma Aldrich, USA. Oxidized low-density lipoprotein (OxLDL) was from Alfa Aesar, USA. Folic acid PEG Fluorescein PG2-FAFC-2k (Folate-FITC) was purchased from Nanocs Inc., USA. Trypsin-EDTA (0.25%) was from Gibco™ Life Technologies, USA. Human serum was obtained from Sigma Aldrich H4522, USA.

3.2 Experimental Methods

3.2.1 Preparation of Nanoliposomes

Nanoliposomes were synthesized by thin film hydration technique as elaborated elsewhere [1]. Briefly, known amount of drug and phospholipids, including folate-tagged, rhodamine-tagged (0.1 mol%) and PEGylated lipids, were taken in a round bottom flask. Subsequently, chloroform/methanol (2:1, vol/vol) solvent mixture was added to the flask to dissolve the lipid. Afterwards, the solvent mixture was removed at 40 °C using rotary evaporator (IKA® RV 10, Germany) linked to a water bath (IKA® MB10 basic, Germany). Flask rotation was set at 150 rpm, operating under low pressure condition for as long as 1 hour. Drug-contained thin film was formed and hydration with phosphate-buffered saline (PBS) (150 mM, pH 7.4) was performed in order to obtain multilamellar vesicles (MLV). In active liposomes, the MLVs solution was centrifuged (13,000 rpm; 20 minutes; 4 °C) (Sorvall™ ST 16R, Thermo Scientific™) in order to remove uninserted folate molecules. The supernatant was subsequently removed, and the pellet was reconstituted in PBS 7.4 at 60 °C. Vesicle sizing was performed by sequentially extruding the MLVs through polycarbonate filters (0.2 μm, 5 passes/0.08 μm, 7 passes) mounted on a bench top extruder (Transferra Nanosciences Inc., Canada).

3.2.2 Characterization of Liposomes

The mean particle size and zeta potential measurement were obtained using Zetasizer Nano ZS (Malvern Instruments Ltd., UK) at 25 °C. The storage stability (4 °C) of the particles was continuously monitored. Lipid concentration after extrusion was determined with a colorimetric method as previously described [2]. A calibration curve was prepared with lipid or lipid mixture of concern (absorbance wavelength 485 nm) and used for determination of final lipid concentration in liposomal formulation. To image the nanoliposomes with cryo-TEM (Hitachi H8100), 3-5 µL of nanoliposomal suspension was deposited on glow discharged lacey C TEM grid. The grid was blotted (Vitrobot™) and rapidly plunged in liquid ethane at freezing rate on the order of 106 K/s, avoiding formation of ice crystals. The grid was subsequently transferred into cryo holder and inserted into TEM. Imaging was performed at 100 kV and 2 µA.

3.2.3 Drug Encapsulation Efficiency and Active Ligand Insertion Efficiency

To determine the amount of drug encapsulation, the drug-loaded liposomes were ultra-centrifuged to remove the non-entrapped drugs within the liposomes and the amount of non-entrapped drugs was determined spectrophotometrically at 243nm using UV-Vis absorption spectroscopy (Tecan Infinite® M200, Switzerland). The total drug amount was obtained by incubation of drug-loaded liposomes with 80% isopropyl alcohol (IPA) (v/v) to rupture the lipid bilayer. The drug encapsulation efficiency (EE%) was calculated as (encapsulated drug amount/total drug amount) x 100.

To determine the total amount of inserted ligand, the liposomal structure was ruptured with 80% IPA and the insertion efficiency was calculated as (measured ligand amount/initial ligand amount) x 100. The number of folate molecules per liposomes was calculated with respect to the particle size measured using dynamic light scattering (**Appendix**).

3.2.4 *In vitro* Release Study

A dialysis method was used for evaluation of drug release from nanoliposomes. Briefly, a cellulose ester dialysis bag (100 KDa MWCO, 1.6 cm dia x 6 cm length) was filled with 1 mL drug-loaded nanoliposomal formulation and dialyzed against 40 mL PBS pH 7.4 while continuously agitated in an orbital shaker (Sartorius Certomat®, Sartorius Stedim North America Inc, Bohemia NY) maintained at 37 °C at 50 rpm. The dialysate was exchanged with fresh PBS pH 7.4 every 24 hours to maintain sink condition. The drug concentration in the release buffer was quantified using UV-vis spectrophotometer.

3.2.5 Cell Culture

THP-1 cells were cultured in RPMI supplemented with 10% FBS, 1% PS solution, and 0.05 mM 2-mercaptoethanol. The cells were maintained in a humidified incubator at 37 °C with 5% CO_2 and its medium was replaced every 2 – 3 days by centrifuging the cells at 125 g for 7 minutes. The cells were subcultured once the concentration reaches 8 x 10^5 cells/mL. The cells used in the experiment were at passage 8 to 15. To differentiate the monocytes into foam cells, THP-1 cells were seeded on tissue culture plates at appropriate density in differentiation medium, containing growth medium supplemented with 50 ng/mL PMA for 3 days to obtain macrophages. Subsequently, oxLDL (100 μg/mL) in differentiation medium was fed to the cells for 2 days to obtain foam cells.

3.2.6 Folate Receptor Measurement

THP-1 cells were seeded on 48-well plates at 1 x 10^5 cells/well. and transformed into foam cells. Folate-FITC (200 nM; 3 mL/well) was treated to the cells and the treated cells were subsequently incubated in humidified incubator (37 °C; 5% CO_2) for 1 hour. Following incubation, cells were washed 3 times with sterile PBS to remove the unbound FITC molecules. Subsequently, cells were trypsinized, counted, and placed on 96-well black plate (Nunc™, Thermo Scientific™) at 10,000 cells/well. The fluorescence intensity of the surface-

bound folate-FITC was measured using a microplate reader (Tecan Infinite® M200, Switzerland) with excitation/emission wavelengths of 490/520 nm, gain 100.

3.2.7 Cell Uptake of Liposomes

The uptake of rhodamine-tagged liposomes into foam cells were evaluated using confocal microscopy and flow cytometry. For confocal microscopy, the foam cells were cultured on a 4-well chambered coverglass (Lab-Tek® 155383 Nunc™, USA) at 5000 cells/well and then incubated with liposomes at 200 μM lipid concentration (2×10^{-12} mol/cell) in the differentiation medium for 6 hours at 37ºC. After incubation, the cells were rinsed with PBS and subsequently stained with 10 μg/mL Hoechst 33342, Trihydrochloride, Trihydrate (Molecular Probes®, Life Technologies, USA) for 15 minutes at room temperature. Subsequently, the samples were imaged using a confocal laser scanning microscope (Leica TCS SP5, Leica Microsystems). Imaging settings where control cells without particle treatment showed no red rhodamine signal were fixed and used for all samples.

For flow cytometry, the foam cells were cultured in 24-well plates at 2×10^5 cells/well and then treated with liposomes (200 μM) with inclusion of DPPE-Rhodamine lipids (0.1 mol%) and incubated for 6 hours at 37°C. After that, the cells were trypsinized and collected by centrifugation at 450 ×g for 5 min. The cell pellets were then re-suspended in PBS and their uptake of liposomes were quantified using Guava easyCyte system. The data was analyzed using GuavaExpress Pro software (EMD Millipore, USA). The fluorescent signal of all samples was compared with that of control cells without liposome treatment. Only when the signal of the sample is higher than the control will it be considered as positive signal. For opsonin binding tests, nanoliposomal solution was first diluted in PBS 7.4 to desired concentration and then incubated in 80% human serum at 37°C for 30, 60, and 90 minutes prior to performing procedures for flow cytometry described above.

3.3 Characterization Techniques

3.3.1 Dynamic Light Scattering (DLS)

Malvern Zetasizer Nano ZS (UK) was used to determine the average size of the liposomal vesicles, their size distribution/polydispersity index (PdI) as well as their zeta potential. Briefly, the liposomal solution was diluted in deionized water (final particle concentration ~ 0.18 mM) and 1 mL was placed into cuvette (Malvern, UK). Any air bubbles were removed in order to avoid undesired interference in the measurement. Vesicle sizes, PdI, and the zeta potential (for charged liposomes) were measured after extrusion, after drug release study, and monitored while in storage at 4 ^{o}C.

The vesicle sizes and their PdI were measured by using DLS technique. Essentially, this technique measures the diffusion of particles, assuming they are spherical in shape, under Brownian motion; and subsequently correlates the diffusion coefficient values with the particle size and size distribution by using the Stokes-Einstein equation. This method measures the hydrodynamic diameter, which is diameter of a smooth, spherical particle diffusing at the same speed as the sample particles. This measure includes hydration layer surrounding the particle. Some limitations of this method include poor resolution (i.e. inability to measure two different populations of sizes unless their sizes differ by 50% or more), and inclusion of the size of large particles in the average size value even if they are present in small amount causing error from a little presence of dust. Multiple light scattering from multiple particles can cause inaccuracy, thus the particle concentration has to be optimized. The upper limit of DLS is ~ 8 μm.

Particle zeta potential was measured by applying electric field on particle suspension. As electric field is applied, the particles move in a certain direction with a certain velocity that is a related to the particle charge, the suspending medium, and the electric field strength. As a laser shines through the particle suspension, the mobility of the particles caused the shift in the frequency of scattered light, known as Doppler effect. This shift is proportional to the velocity

of the particle, and the particle velocity is proportional to the electrical potential at the shear/slipping plane of the particle, which is zeta potential. Zeta potential is a measure of the electric potential at the shear/slipping plane of the particle relative to a point in the bulk of dispersion medium. To put it simply, it is a measure of the potential difference between the surface of the stationary fluid attached to the particle and the dispersion medium. It is not equal to the particle surface potential, however currently it is the only available method to measure the properties of the particle double layer interface.

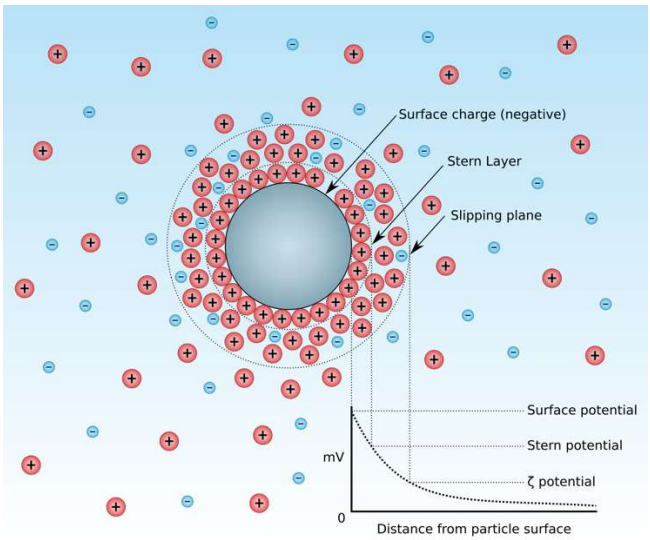

Figure 3.1 Schematic of electrical double layer interface of a particle in dispersion. The ionic concentration and electrical potential are a function of distance from the surface of the charged particle [3].

There are several parameters that could affect the accuracy of particle zeta potential measurement. Particle concentration should be optimized to avoid light scattering interference that could cause low signal-to-noise ratio. Aggregation of nanoparticles will affect the electrophoretic mobility of the particles; thus, aggregated samples are not suitable for zeta potential measurement. Characteristics of dispersion medium, such as its viscosity, pH, and ionic concentration, affects the zeta potential. Temperature affects the mobility of the particles, and thus the zeta potential.

3.3.2 UV-Vis Spectroscopy and Fluorescence Characterization

UV-Vis absorption spectroscopy (Tecan Infinite® M200, Switzerland) was used to estimate the drug concentration after liposome fabrication for evaluation of encapsulation efficiency and final drug loading as well as during drug release study at every timepoint. It was also used for estimation of folate ligand insertion efficiency. Briefly, 150 µL of sample was aliquoted into a 96-wells UV plate (Corning, USA) and mounted into UV plate reader.

UV-Vis absorption spectroscopy is based on the principle that ultraviolet (UV) and visible light radiation can be absorbed by atoms and molecules of samples, to excite their electron from lower to higher energy levels. As the energy levels of matter are quantized, only light with a precise amount of energy and wavelength can be absorbed. For UV-vis spectrometer, the spectra covered is in the range of 200 – 800 nm. Briefly, in UV-vis spectrometer setup, a light source is used to shine through the sample solution after it is split into different wavelengths by passing it through diffraction grating. For each wavelength, the light intensity after it has passed through the sample is measured by the detector, which converts the light into electrical current. The light intensity passing through the sample cell (I) is then compared to the light intensity passing through the reference cell (I_0). If I is less than I_0, then the sample is considered to have absorbed some of the light. The relationship between the absorbance (A) and light intensity can be written as $A = \log_{10} (I / I_0)$. According to Beer-Lambert Law, the absorbance is related to the concentration of the sample (c), the optical path length (l) which is the dimension of cuvette cells in UV-vis spectrometer, and the molar extinction ($\mathcal{E}$) which is a constant for a particular substance at a particular wavelength. Beer-Lambert Law can be expressed as $A = \mathcal{E}cl$. As both $\mathcal{E}$ and c are constant in UV-vis spectrometer, a linear correlation between absorbance versus concentration can be plotted. Practically, a series of standards with known concentration can be plotted versus their respective absorbance to form a calibration graph. Only when the graph is linear is the Beer-Lambert Law obeyed and the graph can be used for determination of the unknown sample concentration in question. This technique is easy to use without the need to manipulate the sample. However, it cannot differentiate the molecule of interest from contaminants that have absorbance at the same wavelength. To maintain

accuracy, sample has to be prepared clear from other molecules/contaminants that absorb UV at similar wavelength as the molecule of interest, to avoid interference in absorbance. Another limitation of this technique is its low sensitivity. UV-vis spectrometer is inadequate for samples of very low concentration.

As both GC studied in this thesis (dexamethasone and FA) have their own characteristics maximum absorption wavelength, their amount in a solution can thus be easily determined by using this technique.

Fluorescence measurement is based on the principle that if photon of a specific wavelength is absorbed by a fluorophore, it would excite some of the electrons which would then return to the ground state almost instantaneously while emitting another photon of longer wavelength. As the wavelengths of exciting and emitted light differ, the intensity of the emitted light can be captured by the detector with minimum background noise from the exciting light. This technique is approximately 1000 times more sensitive than the absorption spectrophotometric method, allowing it to be used for sample containing low molecules of interest. Additionally, this technique provides more specificity, whereby it only detects molecules that fluoresce. However, this method often involves costly reagents, necessitating scientists to consider price per assay or even per data point. To maintain accuracy, sample impurities should be avoided as light scatter or absorption from these substances could interfere with the readings. Fluorimetry (Tecan Infinite® M200, Switzerland) was used to measure the amount of folate-FITC bound on cell surface folate receptor

3.3.3 Cryo Transmission Electron Microscopy (CryoTEM)

TEM produces images of a sample by shining a high-energy electron beam through a sample. The interactions between the electrons and the atoms in the sample produce information about the physical features of the sample. As electrons possess wavelength that is much smaller than that of photons, it is capable to interact with objects that are smaller than the wavelength of photons, thereby is capable of attaining images with resolution much greater than that

from a light microscope. Resolution of less than 1 nm and magnification of up to 1,000,000 times could be achieved with TEM.

Basic TEM components can be seen in Figure 3.2. The electron beam is produced from the electron gun and subsequently focused into a coherent beam by the condenser lens placed below the gun. The beam then hit the specimen and parts of it are transmitted through, depending on the thickness and the electron transparency of the specimen. The transmitted beam is then focused by the objective lens and passed down the column through intermediate and projector lenses by which the image formed is magnified and the contrast is enhanced. Eventually, the image falls on the phosphor screen and light is generated, enabling the user to see the image. The darker part in the image indicates the area with fewer transmitted electrons, whereas the brighter area indicates more transmitted electrons [4].

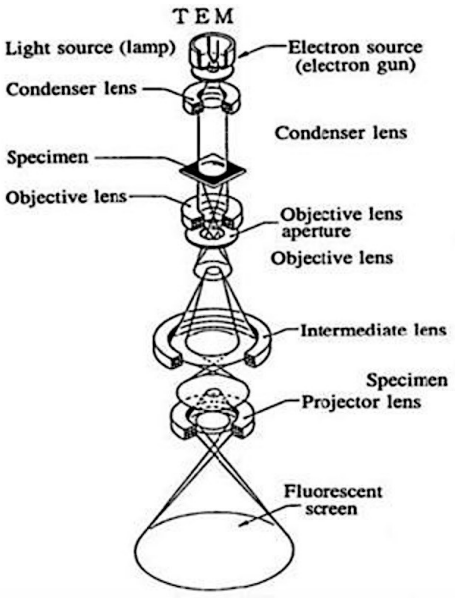

Figure 3.2 General layout of a TEM, depicting basic operating components of TEM and the path of electron beam [4]

In cryoTEM, sample is frozen such that the sample can be maintained in the aqueous environment and imaged in its natural state. This technique is, therefore, suitable for imaging of liposomes without disrupting its integrity, which would otherwise occur if imaged in dry state. A very thin specimen is rapidly plunged

into a liquid ethane bath to quickly freeze the specimen and avoid the formation of ice crystals, which could absorb the electron beam, rendering obscuration of the sample image.

Some limitations of cryo TEM include laborious and time-consuming sample preparation, high potential of artifacts induction during sample preparation, samples limited to electron transparent samples, and black and white images.

3.3.4 xCELLigence

XCELLigence® real-time cell analysis (ACEA Biosciences, Inc., USA) measures cell viability and proliferation based on current impedance due to cell adherence on microelectrodes embedded in the bottom of microtiter wells. When the microelectrodes are submerged in an electrically conductive solution such as buffer or cell growth medium and electric potential across electrodes is applied, the electrons will transfer from negative to positive terminal through the bulk solution. As the completion of the circuit is dependent on the microelectrode-bulk solution interaction, the adherence of the cells on the microelectrodes will impede the electron flow. The magnitude of the impedance is dependent on the cell number, size, shape of the cells as well as the cell-microelectrode attachment quality. It is important to note that, neither the microelectrode surface nor the electric potential affect the cell health or behavior. The current impedance is expressed as a unitless parameter called “Cell Index”, which increases rapidly after a few hours of cell seeding due to deposition of cells onto the microelectrodes (**Figure 3.3 B**). If the cells seeded are low and there is empty area on the electrode surface, the cells will proliferate and cause gradual and steady increase in the cell index. As cells approach 100% confluence, the cell index plateaus as the electrode surface area that is accessible to the bulk solution is no longer changing. Nanoparticles are subsequently treated to the cells. Nanoparticles by themselves will not cause changes in cell index due to its lack of adherence to the microelectrodes. If it causes apoptosis to the adhered cells, cell index will decrease as a result of cell rounding and detachment from the well.

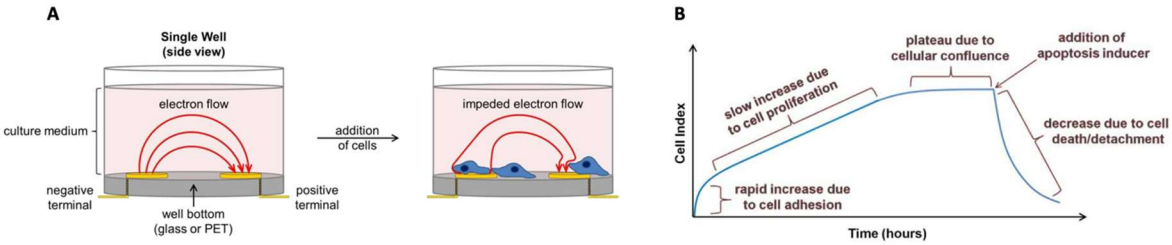

Figure 3.3 (A) Schematic of working principle of xCELLigence® RTCA system. (B) Generic real-time impedance graph in cell apoptosis assay. The explanation of each phase is shown [5].

The advantage of this system is its capability to track cell viability and proliferation in real-time manner, its simplicity to use without the need to use labeling or secondary assay, and its automatic data plotting feature. Some limitations include the high capital cost for acquiring the instrument as well as the microelectrode-embedded plate, and incapability of directly measuring the viability of poorly adherent or suspension cells.

3.3.5 MTT Assay

MTT assay has been regarded as gold standard for cytotoxicity assay, widely adopted and reported in numerous published articles. This assay is based on conversion of MTT (3-(4,5-dimethylthiazol-2-yl)-2,5-diphenyltetrazolium bromide) tetrazolium salt by viable cells with active metabolism into a purple colored formazan product with an absorbance maximum near 570 nm. The most widely believed mechanism is that, the MTT is reduced by NADH (nicotinamide adenine dinucleotide hydrogen) or NADPH (nicotinamide adenine dinucleotide phosphate hydrogen) generated by dehydrogenase enzymes from mitochondrial respiration process (**Figure 3.4**). Thus, the conversion of MTT to formazan is indirectly related to the cellular energy capacity. It is noteworthy that MTT reduction is not a direct indication of cell proliferation. Additionally, any agent that could affect the cell mitochondrial activity will affect the signal of this assay.

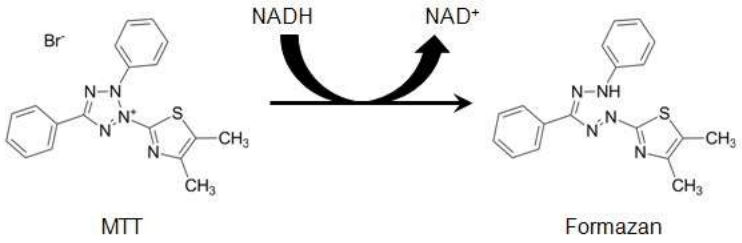

Figure 3.4 Schematic illustration of conversion of MTT to formazan by NADH reducing agent [6].

3.3.6 Confocal Microscopy and Flow Cytometry

Cellular uptake of nanoliposomes were detected qualitatively by confocal microscopy and quantitatively by flow cytometer. Confocal microscopy delivers enhanced resolution compared to conventional fluorescence microscope due to its usage of point illumination and a pinhole in front of the detector, rendering elimination of out-of-focus signal. This system also allows for 3D imaging by scanning the light beam across x-y plane as well as the depth of sample. In practice, the resolution in direction of z-axis is about 0.8 μm, which is 2 – 3 times worse than the lateral resolution [7]. The limitations of this technique include the slow point-by-point scanning rate relative to wide-field detection of conventional fluorescence microscope and its lower z-axis resolution.

Flow cytometer provides high sensitivity and high throughput for analyzing properties of individual cells in the size range of 1 – 40 μm in diameter [8] and thus, is a powerful instrument to measure fluorochrome-labelled nanoparticle cellular uptake. The instrument consists of 3 system components: fluidics, optics, and electronics. In fluidics system, the sample fluid is injected, and the cells are aligned in a single file through laser beam intercept. The optics system consists of the laser source, filters, and light detectors. As the laser beam shines onto the cell, it will excite any compatible fluorescent probes bound on the cells, causing it to fluoresce at a specific wavelength. A number of detectors are aimed to capture the light scattered / emitted by the cell. One of them is placed in line with the laser beam, aimed to capture forward scatter (FSC), which gives

information about the cell volume. Several detectors are placed perpendicular to the laser beam, aimed to detect side scatter (SSC), which contains information about the inner complexity of the cell, such as the nuclear shape, the amount and type of cytoplasmic granules, and the membrane roughness. Within flow cytometer, the scattered fluorescent signal will be split into defined wavelengths by a set of filters and mirrors and channeled into their respective detector for detection of a specified wavelength. The signal is then converted by the electronic system into data that can be interpreted by software.

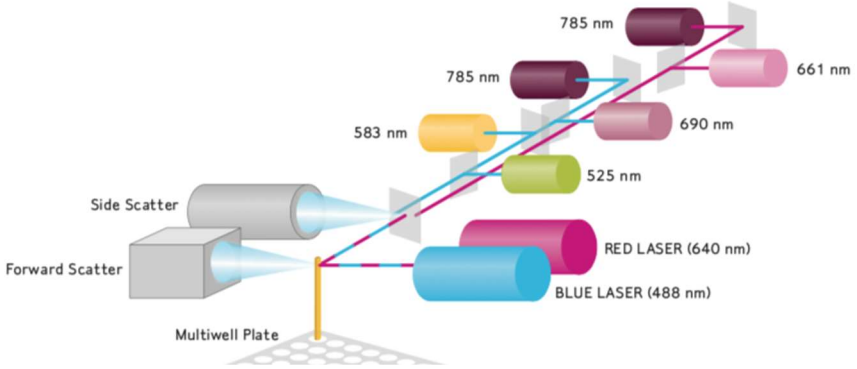

Figure 3.5 Schematic of system components within flow cytometer (Guava easyCyte 8 system). Cell sample is aspirated into a microcapillary flow cell. A red or blue diode laser shines through the cell and excites the fluorophore bound on the cells. The signals emitted by the cell are split and eventually detected by photomultipliers and a photo diode [9].

It is worth noted that the fluorescent signal obtained is not an absolute value, as the signal intensity is dependent on the condition of excitation source, the number of fluorophores per particle, quantum yield of fluorophores, and the condition of the detector. Thus, the signal intensity does not indicate neither mass nor number of nanoparticles per cell, but it is useful for comparison between different experimental conditions.

References

[1] Hironaka, K., et al., *Design and evaluation of a liposomal delivery system targeting the posterior segment of the eye.* Journal of Controlled Release, 2009. **136**(3): p. 247-253.

[2] Stewart, J.C.M., *Colorimetric Determination of Phospholipids with Ammonium Ferrothiocyanate.* Analytical Biochemistry, 1980. **104**(1): p. 10-14.

[3] *Zeta potential*. 2012 [cited 2019 May]; Available from: https://en.wikipedia.org/wiki/Zeta_potential.

[4] *Transmission Electron Microscopy (TEM)*. 2010 [cited 2019 May]; Available from: https://warwick.ac.uk/fac/sci/physics/current/postgraduate/regs/mpagswarwick/ex5/techniques/structural/tem/.

[5] *xCELLigence RTCA HT Real Time Cell Analyzer – High Throughput*. 2019 [cited 2019 May]; Available from: https://www.aceabio.com/products/rtca-ht/.

[6] Riss, T.L., et al., *Cell Viability Assays*, in *Assay Guidance Manual*, G.S. Sittampalam, et al., Editors. 2004: Bethesda (MD).

[7] *Resolution in a confocal system*. [cited 2019 May]; Available from: http://microscopy.berkeley.edu/courses/TLM/clsm/resolution.html.

[8] Ibuki, Y. and T. Toyooka, *Nanoparticle uptake measured by flow cytometry.* Methods Mol Biol, 2012. **926**: p. 157-66.

[9] *Flow Cytometry Solutions*. 2010, EMD Millipore: USA.

Chapter 4

Liposomal-based Anti-inflammatory Nanotherapy

In this chapter, anti-inflammatory drug-encapsulated liposomes (passive liposomes) were formulated. Our aim was to develop a stable, intravenously injectable glucocorticoids (GC)-loaded nanoliposomal formulation with high drug loading that exhibits a sustained release profile with low burst. This chapter contains results and discussion of characteristics of GC-loaded nanoliposomes, lipid selection and evaluation of GC loading and release from nanoliposomes. On the second part, PEGylation was incorporated to obtain long-circulating liposomes. The effect of PEGylation on GC loading, release, and particle stability are discussed.

4.1 Dexamethasone-loaded Nanoliposomes as Anti-inflammatory Therapy

Dexamethasone (Dex) was selected as this drug has been studied extensively for treatment of atherosclerosis and in-stent restenosis [1-4]. Nanoliposomes were formulated with various types of lipids to encapsulate this GC. However, the encapsulation efficiencies (EE%) were not very high (~ 55 – 70%) (**Table 4.1**). Using two of the formulations with the highest EE%, a release study was performed. With these formulations, it was observed that the majority of the drug was released in the first 48 hours (**Figure 4.1A**), indicating high drug leakage when the liposomes are in circulation. A PEGylated alternative formulation was fabricated to observe if there is any barrier effect from PEG that could slow down the release rate. However, the release rate was not significantly different (**Figure 4.1B**). These results indicate the incompatibility between the nanoliposomes and the drug. Relatively low EE% and high initial drug burst release could be related to low partitioning of drug in the liposomal bilayer. Thus, a more lipophilic GC was selected for the subsequent trials.

Table 4.1 Characteristics of dexamethasone-loaded nanoliposomes with various compositions

	Lipid composition	Encapsulation efficiency, EE (%)
Saturated Lipids	DMPC	61.3 ± 2.8
	DPPC	56.9 ± 9.4
	DSPC	62.8 ± 4.0
Unsaturated Lipids	EPC	65.3 ± 0.8
	Egg SM	66.4 ± 2.2

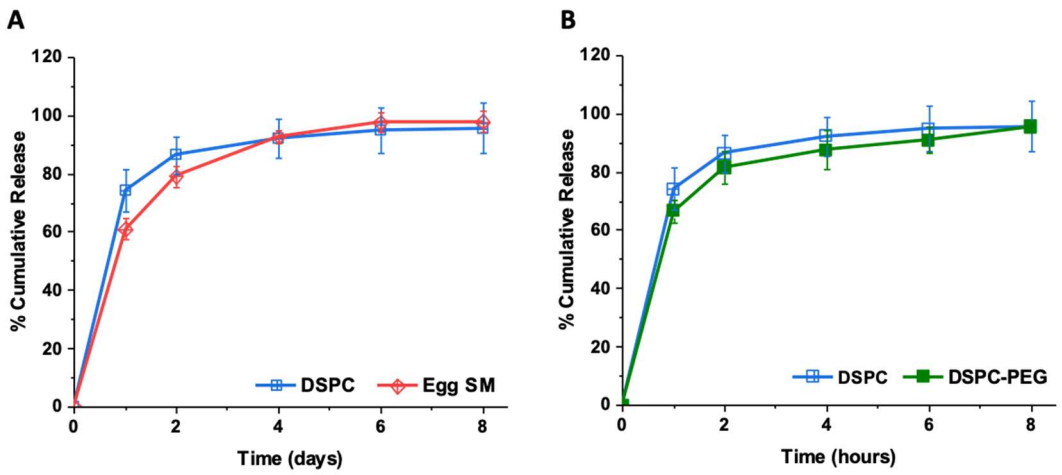

Figure 4.1 *In vitro* dialysis release profiles of dexamethasone-loaded nanoliposomes after extrusion. (A) Cumulative drug release profiles of dexamethasone-loaded nanoliposomes composed of DSPC and Egg SM. (B) Cumulative drug release profiles of dexamethasone-loaded nanoliposomes composed of DSPC and DSPC/DSPE-PEG 2000 (95: 5 molar ratio)

4.2 Fluocinolone Acetonide (FA)-loaded Nanoliposomes as Anti-inflammatory Therapy

Following the study with dexamethasone, a more lipophilic GC was selected for encapsulation in nanoliposomes. Fluocinolone acetonide (FA), having higher octanol/water partition coefficient (~ 2.56 (FA) vs. 1.96 (Dex) [5]) was selected. Besides its higher lipophilicity, FA was recently reported to reduce lipid accumulation and inflammatory cytokine secretion of human THP-1 derived atherosclerotic foam cells as well as, if not better than Dex *in vitro* [6]. Therefore, FA could be a potential agent for atherosclerosis therapy, and its encapsulation in nanoliposomes is worth exploring.

4.2.1 Effect of Lipid Acyl Chain Lengths on FA Loading and Release

FA-loaded nanoliposomes composed of phospholipids of various chain lengths DMPC (C_{14}), DPPC (C_{16}), and DSPC (C_{18}) were formulated.

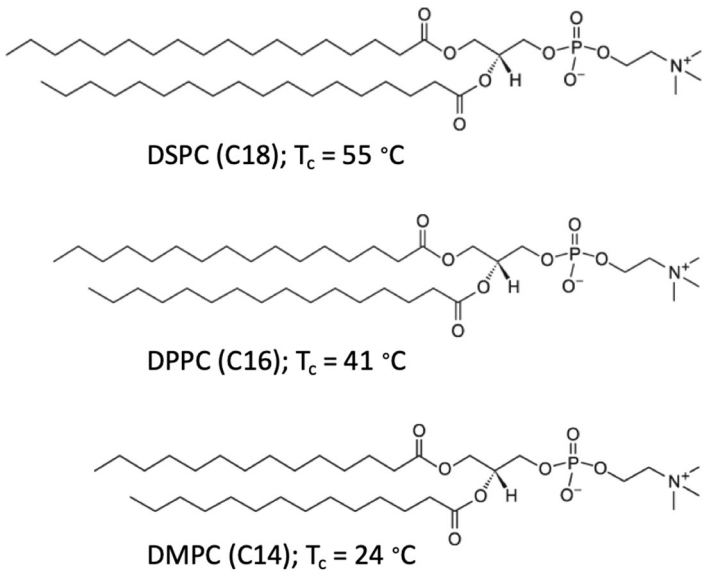

Figure 4.2 Structure of DSPC, DPPC and DMPC with their transition temperature, T_c [7, 8]

Table 4.2 Characteristics of FA-loaded nanoliposomes with various compositions

Lipid composition	Size (d, nm)	PDI	ξ potential (mV)	Encapsulation efficiency, EE (%)	Drug/lipid ratio (mol/mol)	Drug concentration (μg/mL)
DMPC	90.6 ± 0.2	0.058 ± 0.007	-7.2 ± 2.1	91.7 ± 0.3	0.13 ± 0.01	977.0 ± 41.3
DPPC	94.4 ± 1.8	0.094 ± 0.009	-8.2 ± 3.7	90.8 ± 4.1	0.10 ± 0.01	855.4 ± 34.7
DSPC	101.3 ± 2.0	0.085 ± 0.005	-6.4 ± 0.8	88.0 ± 4.8	0.07 ± 0.01	659.3 ± 61.7

The effect of different acyl chain lengths on FA loading and release was evaluated (**Table 4.2**). Particle sizes of nanometer range, narrow polydispersity index (<0.2), and high encapsulation efficiency (about 90%) were obtained for all the three formulations. It was observed that, with increasing chain lengths, the mean particle diameter increased. Additionally, there was a decreasing trend in the drug loading with increasing chain length (DMPC (0.13) > DPPC (0.10) > DSPC (0.07)) for an initial drug/lipid molar ratio of 0.15. This could be because as the chain length increases, inter-chain van der Waals forces increase, rendering less space available for lipophilic FA incorporation in the bilayer. A similar phenomenon has been observed with other hydrophobic drugs [9].

In term of drug release, higher initial drug burst release was observed in DMPC-based nanoliposomes for the first two days (DMPC (385 μg) > DPPC (229 μg)

and DSPC (299 µg). **Figure 4.3B**). DMPC is known to have lower gel-to-liquid phase transition temperature (Tc = 23 °C) [10], suggesting that the membrane lipid component is in fluid liquid crystalline phase under the release study conditions, with the temperature was set to physiological temperature at 37 °C. The fluid state of the DMPC lipid membrane could have contributed to the higher drug leakage. Though the difference in the burst releases between DPPC and DSPC was not statistically significant (**Figure 4.3B**), the lower total drug in DSPC liposomes mentioned previously caused earlier depletion of the FA cargo. Overall, the results suggested that DPPC-based nanoliposomes have the greatest potential to deliver an adequate amount of FA cargo to the targeted site with minimal drug leakage during *in vivo* blood circulation.

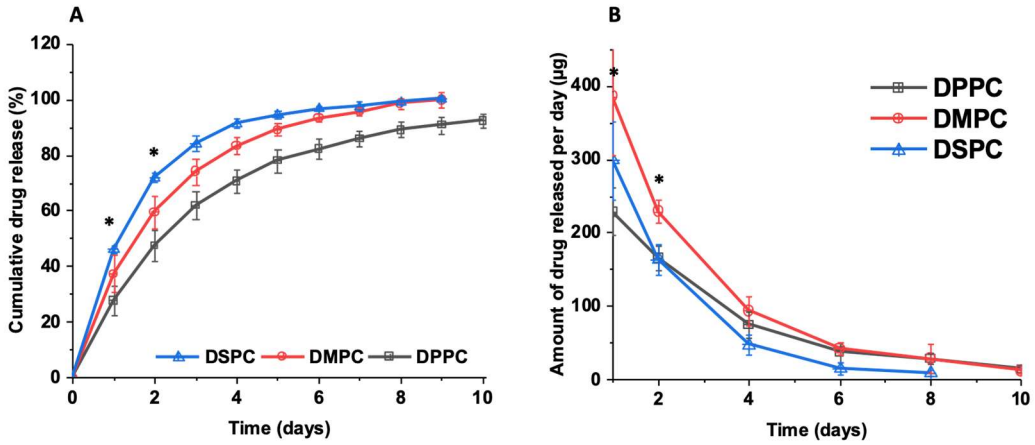

Figure 4.3 *In vitro* dialysis release profiles of FA-loaded nanoliposomes after extrusion. (A) Cumulative drug release profiles of FA-loaded nanoliposomes composed of DPPC, DMPC, and DSPC. (B) *In vitro* FA released per day from 1 mL nanoliposomes composed of DPPC, DMPC, and DSPC. Statistical analysis was done for day 1 and 2; * $p < 0.05$ vs. DPPC; n = 3.

4.2.2 Effect of PEGylation on FA Loading and Release

PEGylation on the liposomal surface was performed to achieve long-circulating stealth nanoliposomes. The zeta potential became increasingly negative with addition of negatively charged DSPE-PEG (**Table 4.3**) due to carbamate linkage used for conjugation of PEG to DSPE, resulting in a net negative charge from the phosphate group of the lipid. Interestingly, the incorporation of DSPE-PEG into DPPC liposomes caused a significant reduction in the mean particle

diameter. This decrease in size after PEGylation may be due to decreased aggregation of the particles (due to negative charge) [11, 12]. In terms of drug loading, the presence of DSPE-PEG did not significantly change the FA encapsulation and loading. Nevertheless, PEGylated liposomes displayed slower release rate compared to conventional liposomes. Similar observations have been reported previously for both lipophilic and hydrophilic drug encapsulation in liposomes [13, 14]. The slower release rate of FA in PEGylated liposomes could be attributed to the partitioning effect resulted from PEGylation [15-17]. Furthermore, studies have indicated that drug transport through PEGylated lipid membranes is impacted due to specific interactions between the PEG polymer layer and the drug and it is dependent on both the PEGylation level and PEG molecular weight [18, 19].

Table 4.3 Characteristics of FA-loaded DPPC nanoliposomes with PEGylation, compared to unPEGylated formulation

Lipid composition	Size (d, nm)	PDI	ζ potential (mV)	Encapsulation efficiency, EE (%)	Drug/lipid ratio (mol/mol)	Drug concentration (μg/mL)
DPPC	94.4 ± 1.8	0.094 ± 0.009	-8.2 ± 3.7	90.8 ± 4.1	0.10 ± 0.01	855.4 ± 34.7
DPPC/DSPE-PEG (2000)	89.5 ± 0.7	0.061 ± 0.004	-29.8 ± 2.1	89.8 ± 2.2	0.11 ± 0.003	938.0 ± 68.9

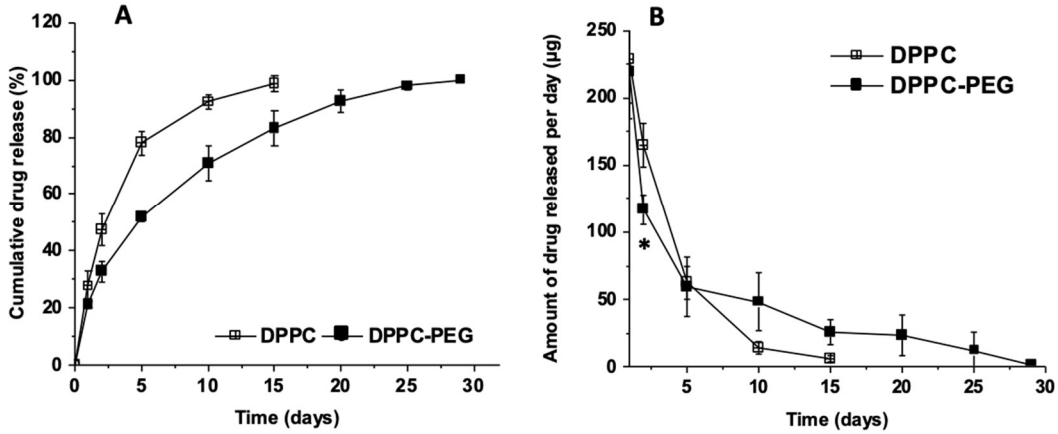

Figure 4.4 *In vitro* dialysis release profiles of FA-loaded nanoliposomes after extrusion. (A) Cumulative drug release profiles of FA-loaded nanoliposomes composed of DPPC and DPPC/DSPE-PEG 2000. (B) *In vitro* FA released per

day from 1 mL nanoliposomes composed of DPPC and DPPC/DSPE-PEG 2000. Statistical analysis was done for day 1 and 2; * $p < 0.05$ vs. DPPC; n = 3

4.2.3 Stability of FA-loaded Nanoliposomes

A relatively high FA loading (D/L ratio of 0.11 ± 0.003) for lipophilic drug-encapsulated liposomes was achieved. Increasing loading of lipophilic drug into the liposomal bilayer is challenging as it has been associated with bilayer destabilization [20, 21]. D/L of other lipophilic drug-loaded liposomes reported previously include that of curcumin (0.07) [22], ibuprofen (0.03 – 0.12) [23], amphotericin B (0.1) [24], paclitaxel (0.15) [25], and aryl-imidazole compound (0.29) [26]. Despite the high loading of FA, the nanoliposomal formulation showed good stability for at least 3 months (**Table 4.4** and **Figure 4.5**).

Table 4.4 Measurement of size, polydispersity index (PDI), and zeta potential of FA-loaded nanoliposomes composed of DPPC and DSPE-PEG 2000 (95:5 molar ratio) during storage at 4 °C

Duration (months)	Size (d.nm)	PDI	ζ potential (mV)
0	89.5 ± 0.7	0.06 ± 0.004	-26.7 ± 1.1
1	89.3 ± 2.7	0.09 ± 0.04	-25.7 ± 5.0
2	89.8 ± 2.1	0.07 ± 0.01	-26.1 ± 1.5
3	88.7 ± 1.8	0.06 ± 0.003	-25.7 ± 2.1

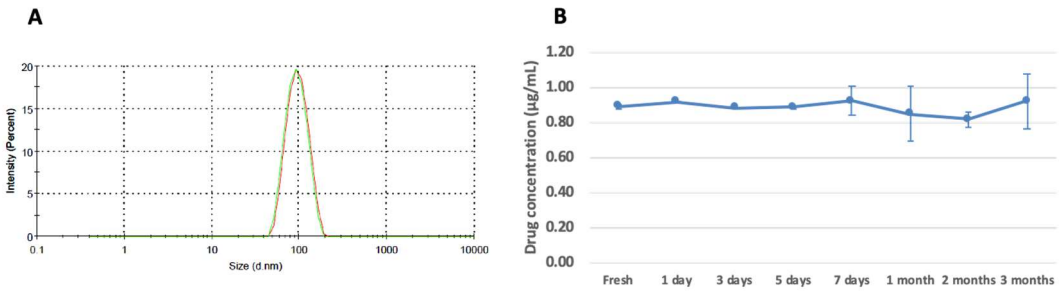

Figure 4.5 Storage stability of FA-loaded nanoliposomes composed of DPPC and DSPE-PEG 2000 (95:5 molar ratio) at 4 °C. (A) Intensity weighted particle size distribution from Malvern Zetasizer. Red: freshly prepared formulation. Green: after 3 months storage at 4 °C. (B) Measurement of drug concentration over time at 4 °C storage.

Nano-sized liposomes with spherical shape were successfully formed with the thin film hydration and extrusion method, and the spherical shape was maintained even at high FA loading and PEGylation (**Figure 4.6**).

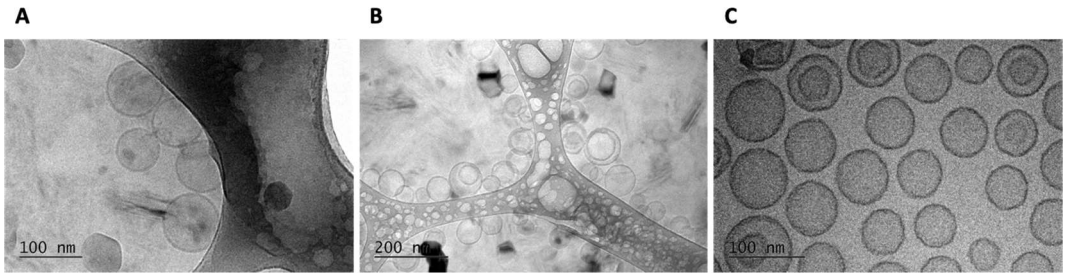

Figure 4.6 Cryo-TEM images of nanoliposomal formulation after extrusion. (A) Blank nanoliposomes composed of DPPC. (B) FA-loaded nanoliposomes composed of DPPC (drug/lipid molar ratio of 0.10 ± 0.01). (C) FA-loaded nanoliposomes composed of DPPC and DSPE-PEG 2000 (95:5 molar ratio) (drug/lipid molar ratio of 0.11 ± 0.003).

The overall characteristics of FA-loaded PEGylated nanoliposomes, notably high drug loading, capability of delivering majority of drug to targeted site with minimal drug leakage in circulation and good storage stability, makes it a potential candidate for anti-inflammatory drug delivery for atherosclerosis treatment

4.3 Summary

Passive nanoliposomes were evaluated in terms of their ability to encapsulate GC, which is a class of drug that has been extensively studied and reported to show exceedingly good potential as a therapeutic agent for atherosclerosis. Two types of GC, Dex and FA, were used in this study, and it was found that the encapsulation efficiency and release were more favourable with FA, which was more lipophilic. This could be due to better partitioning of more lipophilic drug in the bilayer compartment of nanoliposomes. PEGylation was shown to be capable of tuning the release rate of the drug, but was more effective in FA, than Dex. Besides PEGylation, the release rate of lipophilic GC can also be controlled by varying the lipid chain lengths.

Notably, FA-loaded PEGylated nanoliposomes were shown to have high drug loading, high encapsulation efficiency, good storage stability, and low burst release in the first 48 hours. This formulation is, therefore, a potential candidate for atherosclerosis treatment.

References

[1] Poon, M., et al., *Dexamethasone inhibits macrophage accumulation after balloon arterial injury in cholesterol fed rabbits.* Atherosclerosis, 2001. **155**(2): p. 371-80.

[2] Asai, K., et al., *Dexamethasone-Induced Suppression of Aortic Atherosclerosis in Cholesterol-Fed Rabbits - Possible Mechanisms.* Arteriosclerosis and Thrombosis, 1993. **13**(6): p. 892-899.

[3] Hoffmann, R., et al., *Evaluation of a high-dose Dexamethasone-eluting stent.* American Journal of Cardiology, 2004. **94**(2): p. 193-195.

[4] Liu, X.S., et al., *Study of antirestenosis with the Biodivysio dexamethasone eluting starlit (STRIDE): A multicenter trial.* Journal of the American College of Cardiology, 2002. **39**(5): p. 15a-15a.

[5] Bressler, N.M. and H. Bauchner, *Expression of concern: Thakur A, Kadam R, Kompella UB. Trabecular meshwork and lens partitioning of corticosteroids: implications for elevated intraocular pressure and cataracts. Arch Ophthalmol. 2011:129(7):914-920.* JAMA Ophthalmol, 2015. **133**(4): p. 375.

[6] Nguyen, L.T.H., et al., *The Potential of Fluocinolone Acetonide to Mitigate Inflammation and Lipid Accumulation in 2D and 3D Foam Cell Cultures.* Biomed Research International, 2018.

[7] Silvius, J.R., *Thermotropic phase transitions of pure lipids in model membranes and their modifications by membrane proteins.* Lipid-protein interactions, 1982. **2**: p. 239-281.

[8] *Phase Transition Temperatures for Glycerophospholipids*. [cited 2020 5 Feb]; Available from: https://avantilipids.com/wp-content/uploads/2015/11/Phase_Transition_Temps_for_Glycerophospholipids_Table.pdf.

[9] Bhardwaj, U. and D.J. Burgess, *Physicochemical properties of extruded and non-extruded liposomes containing the hydrophobic drug dexamethasone.* Int J Pharm, 2010. **388**(1-2): p. 181-9.

[10] Corporation, N.A. *COATSOME® MC-4040 (DMPC)*. 2005-2019 [cited 2019 6 April]; Available from:

https://www.nofamerica.com/store/index.php?dispatch=products.view&product_id=265.

[11] Kaur, R., et al., *Manipulation of the surface pegylation in combination with reduced vesicle size of cationic liposomal adjuvants modifies their clearance kinetics from the injection site, and the rate and type of T cell response.* Journal of Controlled Release, 2012. **164**(3): p. 331-337.

[12] Tang, J., et al., *Effect of size and pegylation of liposomes and peptide-based synthetic lipoproteins on tumor targeting.* Nanomedicine: Nanotechnology, Biology and Medicine, 2017. **13**(6): p. 1869-1878.

[13] Yuan, J., et al., *Improved Antitumor Efficacy and Pharmacokinetics of Bufalin via PEGylated Liposomes.* Nanoscale Res Lett, 2017. **12**(1): p. 585.

[14] Er, Y., et al., *The encapsulation and release of guanosine from PEGylated liposomes.* J Liposome Res, 2009. **19**(1): p. 29-36.

[15] Silvander, M., P. Hansson, and K. Edwards, *Liposomal surface potential and bilayer packing as affected by PEG-lipid inclusion.* Langmuir, 2000. **16**(8): p. 3696-3702.

[16] Belsito, S., R. Bartucci, and L. Sportelli, *Sterically stabilized liposomes of DPPC/DPPE-PEG:2000. A spin label ESR and spectrophotometric study.* Biophys Chem, 1998. **75**(1): p. 33-43.

[17] Kepczynski, M., et al., *Which physical and structural factors of liposome carriers control their drug-loading efficiency?* Chem Phys Lipids, 2008. **155**(1): p. 7-15.

[18] Er, Y., et al., *The encapsulation and release of guanosine from PEGylated liposomes.* Journal of Liposome Research, 2009. **19**(1): p. 29-36.

[19] Panwar, P., et al., *Preparation, characterization, and in vitro release study of albendazole-encapsulated nanosize liposomes.* International journal of nanomedicine, 2010. **5**: p. 101-108.

[20] Khan, D.R., et al., *Effects of drug hydrophobicity on liposomal stability.* Chemical Biology & Drug Design, 2008. **71**(1): p. 3-7.

[21] Bernsdorff, C., R. Reszka, and R. Winter, *Interaction of the anticancer agent Taxol (TM) (paclitaxel) with phospholipid bilayers.* Journal of Biomedical Materials Research, 1999. **46**(2): p. 141-149.

[22] Pandelidou, M., et al., *Preparation and Characterization of Lyophilised EGG PC Liposomes Incorporating Curcumin and Evaluation of Its Activity Against Colorectal Cancer Cell Lines.* Journal of Nanoscience and Nanotechnology, 2011. **11**(2): p. 1259-1266.

[23] Mohammed, A.R., et al., *Liposome formulation of poorly water soluble drugs: optimisation of drug loading and ESEM analysis of stability.* International Journal of Pharmaceutics, 2004. **285**(1-2): p. 23-34.

[24] Szoka, F.C., D. Milholland, and M. Barza, *Effect of Lipid-Composition and Liposome Size on Toxicity and Invitro Fungicidal Activity of Liposome-Intercalated Amphotericin-B.* Antimicrobial Agents and Chemotherapy, 1987. **31**(3): p. 421-429.

[25] Kan, P., et al., *A Liposomal Formulation Able to Incorporate a High Content of Paclitaxel and Exert Promising Anticancer Effect.* Journal of Drug Delivery, 2011.

[26] Liu, J.B., et al., *Liposome formulation of a novel hydrophobic aryl-imidazole compound for anti-cancer therapy.* Cancer Chemotherapy and Pharmacology, 2006. **58**(3): p. 306-318.

Chapter 5

Folate-targeting Nanoliposomes

In this chapter, folate-targeting liposomes (active liposomes) were formulated and their effect on cellular uptake was studied. Our aim was to develop active targeting nanoliposomes for atherosclerotic foam cells and provide a systematic study on the optimization of ligand concentration and PEG spacer length for enhanced internalization by foam cells. This chapter contains results and discussion of foam cell folate receptor expression level, characteristics of folate-targeting liposomes and the effect of various folate- targeting liposomes on foam cell uptake.

5.1 Cell Surface Folate Receptor (FR) Determination by Folate-FITC

HeLa cells and healthy human foreskin fibroblasts (HFF) were used in this study as the positive and negative controls, respectively. HeLa cells are human cervical carcinoma cell lines that are commonly known for having FR overexpression [1-3]. After 1 hour treatment of folate-FITC on the cells, the amount of FITC measured on foam cells was found to be approximately 9.46 fold higher than that of HFF, and only 1.4 fold lower than that of HeLa. This finding indicated that foam cells expressed high amount of cell surface folate receptors that could be exploited for delivery of therapeutic treatment.

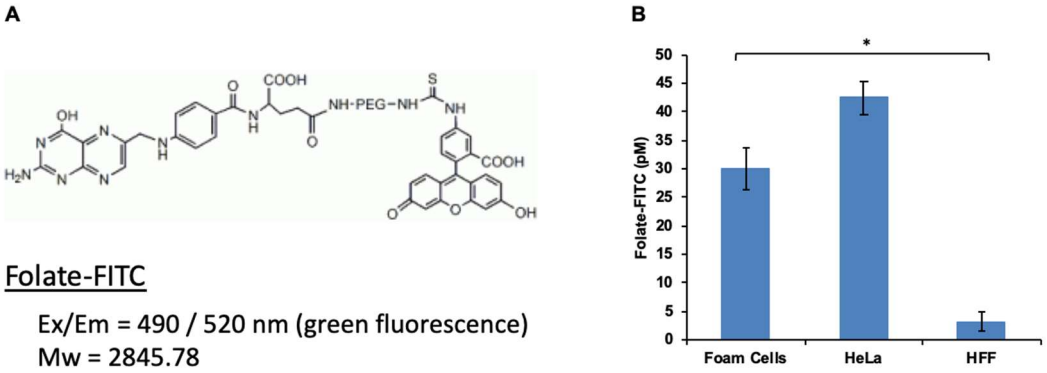

Figure 5.1 (A) Molecular structure of folate-FITC treated to the cells for cell surface folate receptor (FR) measurement. Relevant details such as excitation and emission wavelengths as well as molecular weight are inserted. (B) FR measurement represented by amount of folate-FITC attached on cell surface. HeLa and healthy human foreskin fibroblasts (HFF) were positive and negative control respectively. * $p < 0.05$; $n = 3$

5.2 Characterization of Active Targeting Liposomes

DPPC was chosen as the base of the liposomes due to favorable results in encapsulating FA, an anti-inflammatory drug, as discussed in the previous chapter. Active targeting liposomes were prepared by incorporating DSPE-PEG (2000)-Folate into DPPC liposomes.

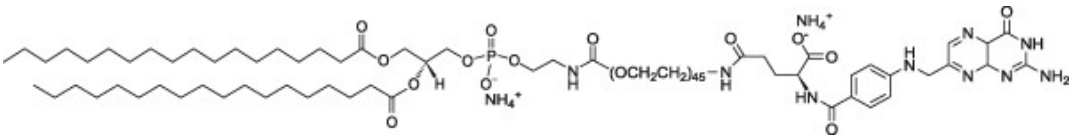

Figure 5.2 Structure of commercially available folate-conjugated lipid (DSPE-PEG (2000)-Folate) [4]

Table 5.1 Characteristics of active targeting liposomes with DSPE-PEG-Folate molecules as targeting ligands incorporated in DPPC-based liposomes

PEG spacer size	Intended folate concentration (mol%)	Intended number of folate molecules per liposomes	Final folate concentration (mol%)	Final number of folate molecules per liposomes	Insertion efficiency (%)	Size (d.nm)	PDI	ζ potential (mV)
PEG 2000	0%	-	-	-	-	105.1 ± 2.3	0.077 ± 0.002	-6.94 ± 1.40
	0.3%	240	0.32% ± 0.03%	256 ± 41	105.1% ± 10.2%	100.1 ± 3.5	0.073 ± 0.010	-11.7 ± 10.2
	0.5%	400	0.46% ± 0.02%	391 ± 18	92.7% ± 4.6%	102.2 ± 0.5	0.077 ± 0.014	-19.0 ± 0.4
	0.7%	560	0.56% ± 0.04%	476 ± 16	80.5% ± 5.4%	102.3 ± 2.0	0.079 ± 0.008	-21.1 ± 3.8
	0.9%	720	0.72% ± 0.04%	627 ± 32	79.6% ± 4.5%	104.5 ± 2.9	0.111 ± 0.055	-20.2 ± 7.3
PEG 5000	0.3%	249	0.30% ± 0.03%	247 ± 23	99.1% ± 9.3%	101.8 ± 1.3	0.063 ± 0.008	-15.9 ± 1.3
	0.5%	425	0.41% ± 0.02%	346 ± 17	81.4% ± 4.0%	103.0 ± 0.7	0.081 ± 0.022	-17.9 ± 1.5
	0.7%	608	0.58% ± 0.03%	501 ± 27	82.5% ± 4.5%	104.0 ± 1.3	0.073 ± 0.001	-20.9 ± 2.6
	0.9%	775	0.79% ± 0.05%	681 ± 41	87.9% ± 5.4%	103.6 ± 0.7	0.088 ± 0.009	-18.0 ± 0.8

Insertion efficiencies of at least 80% were obtained for all formulations (**Table 5.1**). Folate incorporation was efficient (>90%) at lower ligand numbers (240 – 400 folates per liposome for PEG 2000 spacer; 249 folates per liposome for PEG 5000 spacer) and was moderately efficient (≈ 80%) at higher ligand numbers (560 -720 folates per liposome for PEG 2000 spacer; 425 – 775 folates per liposome for PEG 5000 spacer). Similar trends have been observed elsewhere [5]. Particle sizes of nanometer range (≈ 100 nm) and narrow polydispersity index (<0.2) were obtained for all formulations. The inclusion of folate ligands did not significantly affect the particle size. The zeta potential of the liposomes became negative with incorporation of DSPE-PEG-Folate due to negative charges at the phosphate group on the lipid head and carboxyl group on folate. The active targeting liposome formulations were stable in storage for at least 3 months (**Table 5.2** and **Figure 5.3**)

Table 5.2 Measurement of size, polydispersity index (PDI), and zeta potential of active targeting nanoliposomes composed of DPPC/DSPE-PEG 2000-Folate (99.1: 0.9 molar ratio) during storage at room temperature and 4 °C

	Room Temperature (~25 °C)			4 °C		
Duration	**Size (d.nm)**	**PDI**	**ζ potential (mV)**	**Size (d.nm)**	**PDI**	**ζ potential (mV)**
Fresh	106.0 ± 0.5	0.058 ± 0.009	-23.8 ± 1.2	106.0 ± 0.5	0.058 ± 0.009	-23.8 ± 1.2
1 day	105.9 ± 1.0	0.077 ± 0.009	-27.8 ± 1.1	106.6 ± 0.3	0.063 ± 0.008	-22.9 ± 2.1
2 days	108.0 ± 1.0	0.090 ± 0.022	-27.2 ± 0.4	107.3 ± 1.1	0.076 ± 0.011	-23.1 ± 0.5
1 week	107.1 ± 0.4)	0.095 ± 0.023	-28.6 ± 0.5	107.8 ± 0.8	0.089 ± 0.012	-27.4 ± 0.9
2 weeks	107.2 ± 0.8	0.093 ± 0.015	-24.9 ± 1.6	108.8 ± 1.3	0.103 ± 0.014	-26.8 ± 1.4
1 month	108.4 ± 0.8	0.074 ± 0.013	-27.8 ± 4.3	109.6 ± 1.5	0.112 ± 0.012	-29.3 ± 0.7
3 months	107.1 ± 1.2	0.095 ± 0.014	-25.4 ± 2.2	108.9 ± 1.2	0.137 ± 0.012	-27.4 ± 1.2

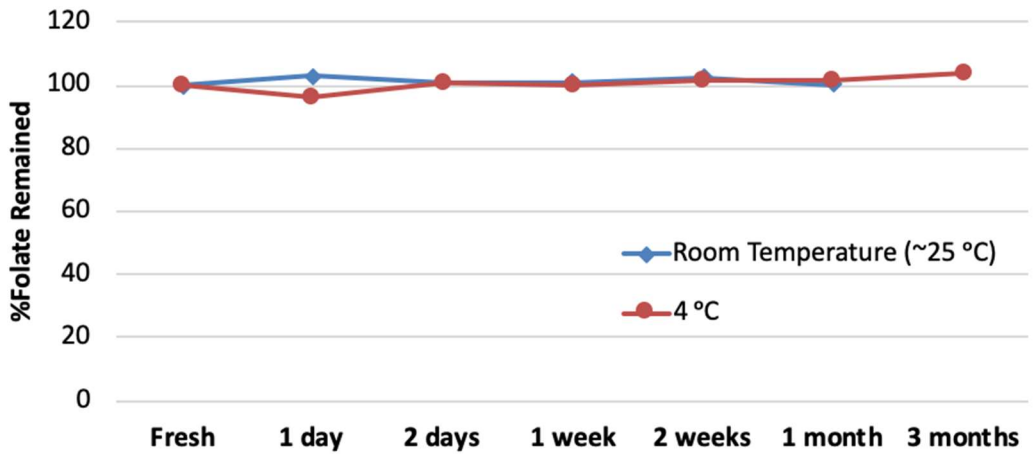

Figure 5.3 Measurement of folate molecule concentration in the active targeting liposome formulation composed of DPPC/DSPE-PEG 2000-Folate (99.1: 0.9 molar ratio) during storage at room temperature and 4 °C

5.3 Cell Uptake Study and Cell Viability Study

As cell integrity affects cellular uptake, cell viability study was conducted prior to the cell uptake study to determine the particle concentration that is safe for the cells. XCELLigence was used to measure foam cell proliferation and viability upon treatment with liposomes. **Figure 5.4** shows foam cell proliferation as represented by cell index on the y-axis, with treatment of various liposomal concentrations over duration of 24 hours.

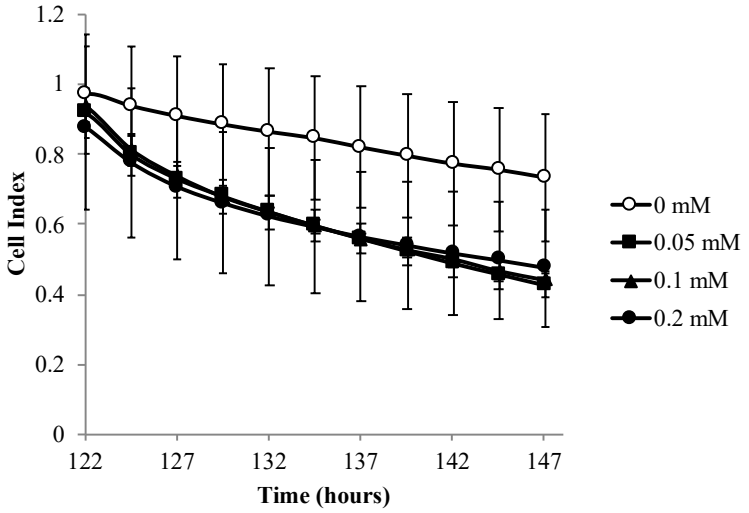

Figure 5.4 xCELLigence cell viability and proliferation assay of foam cells in response to nanoliposomes (DPPC/DPPE-Rhodamine/DSPE-PEG 2000-Folate 99/0.1/0.9 molar ratio) of various concentrations. THP-1 cells were seeded and differentiated into macrophages (with PMA for 3 days) and foam cells (with oxidized LDL for 2 days) in xCELLigence E-plates. Current impedance due to cell proliferation (cell index) was monitored real-time.

It can be observed in **Figure 5.4** that there is a downward trend in cell index even without particle treatment. This is probably due to foam cells being inherently unhealthy. Additionally, there was a slight drop between control (0 mM) and treated cells (0.05 – 0.2 mM) but this difference was insignificant. From this observation, particle concentration of 0.2 mM was selected for subsequent cell uptake studies so that more pronounced treatment effect can be observed.

To evaluate the effect of PEG spacer length and density of folate ligand on FR targeting level, active targeting liposomes of various ligand concentrations (0.3 – 0.9 mol%) for both 2000 and 5000 PEG spacers were prepared (**Figure 5.5A**) and foam cell uptake was examined by flow cytometry. Based on literature, effective folate targeting occurred below 1 mol% [5-7]. Higher molar fraction of folate-PEG-lipid might cause folate molecules to multimerize, forming dimers, trimers, or tubular quartets, causing incapability to bind to FR, which can only bind to one molecule of folic acid [6, 7]. For PEG 2000 spacer length, optimum

cell uptake was observed at 0.5 mol% (**Figure 5.5B**). Interestingly, enhanced cell uptake was not observed with PEG 5000 spacer. A plausible explanation for this unexpected observation could be related to the conformation of the PEG spacer. It is well established that at low molar fraction, long PEG polymers fold into mushroom-like globular structures in water [8]. This could bury the conjugated ligand within the PEG coating, hindering the ligand-receptor pairing. Another possible explanation could be the increased likelihood for folate-PEG 5000 molecules to multimerize owing to longer PEG spacer length, leading to ineffective binding to FR on the cells. For better understanding on the feasibility of this occurrence, we performed a theoretical calculation (**Appendix**). As the folate molecule is affixed to the extremity of the PEG, its average position from liposome surface can be represented as $R_e = aN^{0.64}$, which is equivalent to its Flory radius R_F, the average dimension of PEG coil in water [7, 9]. In the formula, a is the size of the ethylene glycol monomer (3.5 Å) , and N is the degree of polymerization (45 and 113 for PEG 2000 and PEG 5000 respectively) [7]. Thus, the R_e for PEG 2000 and PEG 5000 are around 40 Å and 72.1 Å respectively. These correspond to surface area coverage of about 50.27 nm^2 and 163.31 nm^2 for PEG 2000 and PEG 5000 respectively. As our active targeting formulations were prepared by pre-insertion method, we assume there are folate-PEG molecules on both the inner and outer leaflets of the liposomes. Assuming liposomes of 100 nm in size and bilayer thickness of 5 nm, the surface areas are about 2.54×10^4 nm^2 and about 3.14×10^4 nm^2 for inner and outer leaflet respectively. Thus, the numbers of folate-PEG 2000 molecules required to cover the entire liposomal surface are approximately 507 and 625 molecules for inner and outer leaflets respectively. These sum up to a total of 1132 ligand molecules (~ 1.4 mol%). Performing a similar calculation for folate-PEG 5000, the numbers of ligands are 156 and 193 molecules for inner and outer leaflets respectively, adding up to a total of 349 molecules (~ 0.4 mol%), which is close to the lower end of the range of folate concentrations used in our study. This means that at folate concentration of around 0.4 mol% or greater, the folate molecule at the extremity of the PEG 5000 spacer could interact with its neighboring folate molecule, assuming the PEG was coiled in average dimension in solution. Thereby, the theoretical calculation suggests that there is a great likelihood for folate molecules with PEG 5000 spacer to interact with the

neighboring folate molecules with the range of folate concentrations used in our study, leading to lack of cell uptake enhancement.

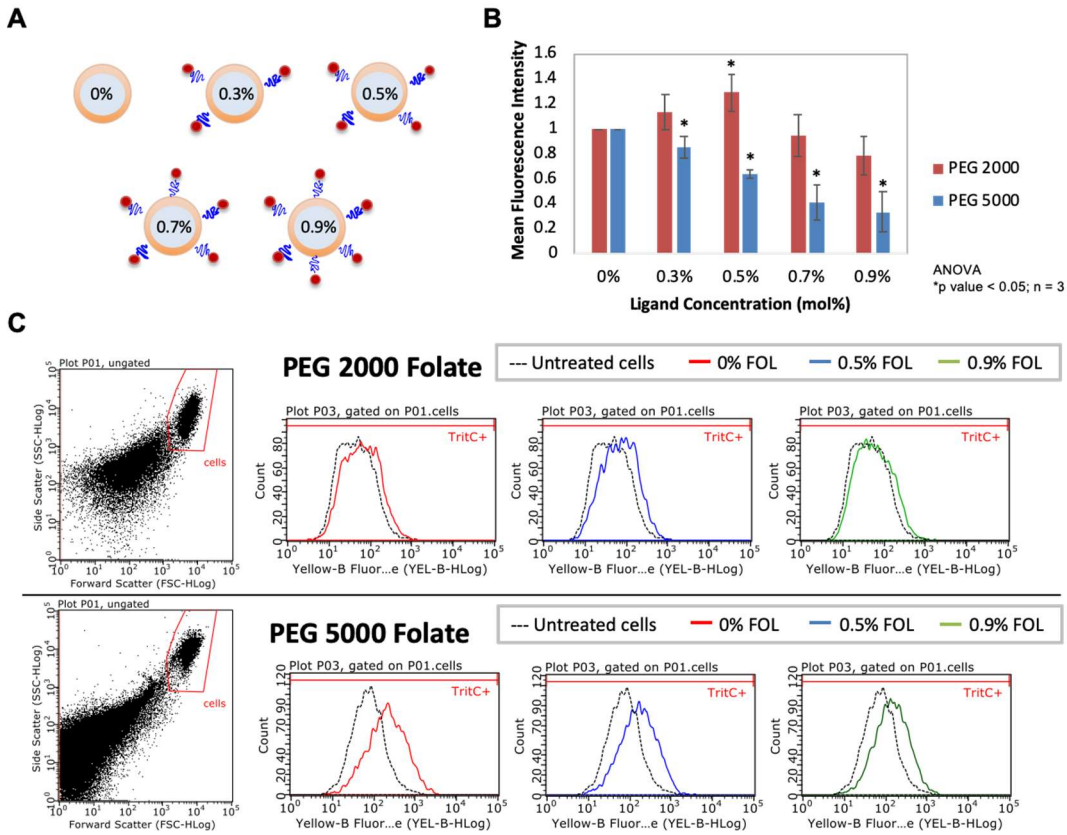

Figure 5.5 (A) Illustration of nanoliposomes with various ligand concentration. (B) Normalized cellular uptake as the mean fluorescence intensity (MFI) of rhodamine-positive cells after subtraction of untreated cells autofluorescence MFI and normalized to MFI of bare liposomes (0% ligand concentration). (C) Dot plot from flow cytometry with gating of cells shown and logarithmic flow cytometry histograms for liposomes with various folate (FOL) content. Histograms for PEG 2000 and PEG 5000 spacer are shown.

To ensure that the increase in cell uptake was not due to breaching of cell integrity, an MTT assay was performed with PEG 2000 (0.5% FOL) at the same concentration as that used for the cell uptake study (0.2 mM lipid concentration, 2 x 10^{-12} mol lipid/cell). The formulation did not show any cytotoxic effect against foam cells (**Figure 5.6**)

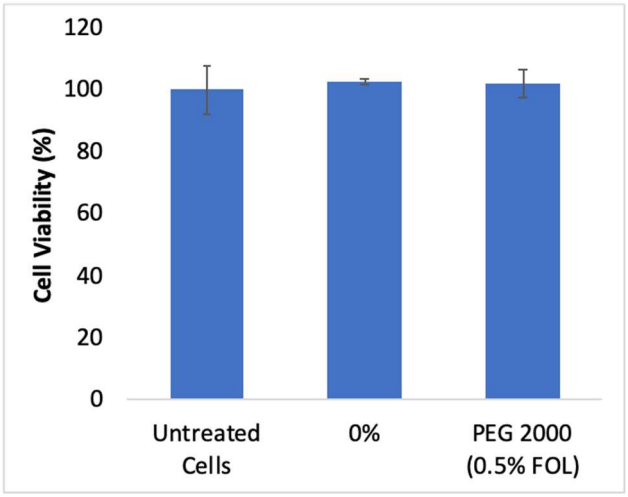

Figure 5.6 MTT assay measuring foam cell viability after treatment with bare DPPC liposomes and DPPC liposomes with DSPE-PEG 2000-Folate (0.5 mol%) labelled as 0% and PEG 2000 (0.5% FOL) respectively. Percentage of cell viability was normalized to the value of foam cells without liposome treatment labelled as untreated cells.

5.4 Summary

Our study demonstrated that human THP-1 monocyte-derived foam cells express high level of folate receptors that could be targeted for delivery of therapeutic treatment. Folate-targeting liposomes could be prepared with high folate insertion efficiency. The effects of PEG spacer length and surface density of folate molecules on foam cell uptake were evaluated. PEG 2000 (0.5% FOL) showed the most enhanced cellular uptake and was not cytotoxic to foam cells.

References

[1] Liu, H., et al., *Synthesis of Luminescent Carbon Dots with Ultrahigh Quantum Yield and Inherent Folate Receptor-Positive Cancer Cell Targetability.* Sci Rep, 2018. **8**(1): p. 1086.

[2] Gabrielson, N.P. and D.W. Pack, *Efficient polyethylenimine-mediated gene delivery proceeds via a caveolar pathway in HeLa cells.* J Control Release, 2009. **136**(1): p. 54-61.

[3] Yanchao, S., Wen Shi, Wei Chen, Xiaohua Li, Huimin Ma, *Fluorescent carbon nanodots conjugated with folic acid for distinguishing folate-receptor-positive cancer cells from normal cells.* Journal of Materials Chemistry, 2012(25): p. 12568-12573

[4] 2020 [cited 2020 5 Feb]; Available from: https://avantilipids.com.

[5] Saul, J.M., et al., *Controlled targeting of liposomal doxorubicin via the folate receptor in vitro.* J Control Release, 2003. **92**(1-2): p. 49-67.

[6] Yamada, A., et al., *Design of folate-linked liposomal doxorubicin to its antitumor effect in mice.* Clin Cancer Res, 2008. **14**(24): p. 8161-8.

[7] Reddy, J.A., et al., *Folate-targeted, cationic liposome-mediated gene transfer into disseminated peritoneal tumors.* Gene Ther, 2002. **9**(22): p. 1542-50.

[8] Barenholz, Y., *Liposome application: problems and prospects.* Current Opinion in Colloid & Interface Science, 2001. **6**(1): p. 66-77.

[9] Jeppesen, C., et al., *Impact of polymer tether length on multiple ligand-receptor bond formation.* Science, 2001. **293**(5529): p. 465-8.

Chapter 6

The Effect of PEG Surface Density on Folate-mediated Foam Cell Targeting

In this chapter, PEGylation was added to active targeting nanoliposomes in an effort to incorporate prolonged blood circulation effect. Our aim was to examine the effect of PEG-to-ligand ratio on the targeting efficacy of folate-decorated nanoliposomes and provide an answer to our hypothesis that targeting effect of folate-targeting nanoliposomes would progressively decrease and eventually be lost as PEG-to-ligand ratio is increased. In this chapter, folate-free PEG of various lengths (PEG 750, 2000 and 5000) were incorporated into active liposomes at various PEG-to-ligand ratio and their uptake by foam cells were examined in the presence of high level of human serum.

6.1 Determination of Liposome Concentration and Serum Incubation Time for Cell Uptake Study

When liposomes are introduced into the bloodstream, they are immediately surrounded by plasma proteins. Blood plasma contains approximately 3700 identified proteins, with total serum protein typically around 60 – 80 g/L [1]. When in close proximity and thermodynamically favorable conditions, serum proteins will attach to the liposomal surface, forming a coating that could change the physicochemical properties of the liposomal surface as well as prevent exposure of targeting ligands, leading to a decrease in the cellular uptake [1-3]. Considering this aspect, we determined to evaluate the targeting efficiency of the active targeting liposomes in the presence of high serum level. Liposomes were pre-incubated in 80% human serum, the concentration level commonly used in literature [3-5], before treating them to foam cells. Liposomes (DPPC/DPPE-Rhodamine/DSPE-PEG 2000-Folate 99.4/0.1/0.5 molar ratio) of various concentrations (0.05 – 0.8 µmol/mL) were prepared and pre-incubated in serum for various duration (30, 60, and 90 minutes).

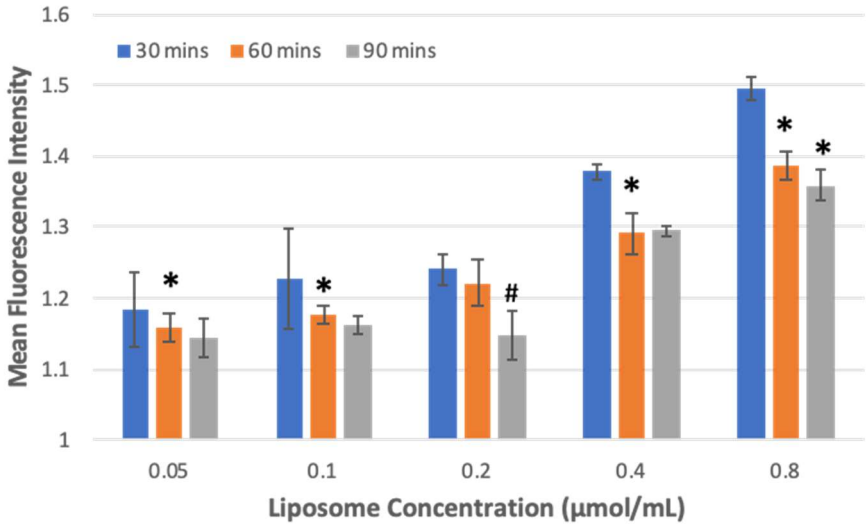

Figure 6.1 Normalized cellular uptake as mean fluorescence intensity (MFI) of rhodamine-positive cells divided by MFI of cellular autofluorescence. The effect of particle-serum incubation time on cellular uptake was compared for various liposome concentration. * p-value <0.05 vs. 30 mins; # p-value < 0.05 vs. 60 mins.

We found that there was no significant difference in uptake from 0.05 to 0.2 μmol/mL liposome concentration (**Figure 6.1**). From 0.4 to 0.8 μmol/mL, the cell uptake increased with increasing particle concentration. This finding suggests that the cell uptake inhibition effect exerted by the serum binding prevailed at low particle concentration up to 0.2 μmol/mL but was attenuated at higher particle concentration perhaps due to inadequate serum binding on the particles. Particle concentration of 0.2 μmol/mL was selected for subsequent studies as it was the highest particle concentration with adequate serum binding. The highest particle concentration was preferred as it had a more appreciable cellular uptake effect. Additionally, this concentration was the same as that used in previous cell uptake study in chapter 5 and was found to be non-cytotoxic (**Figure 5.3** and **Figure 5.5**).

As can be observed in **Figure 6.1**, the cell uptake inhibition effect from serum was time-dependent as well. The effect was more pronounced at higher incubation time, suggesting increasing serum binding with increasing incubation time. From this result, 90 minutes serum incubation time was selected for subsequent studies as it has more pronounced serum inhibition effect compared to 30 and 60 minutes, signifying more adequate serum binding on liposome surface.

6.2 Foam Cell Uptake as Function of PEG Length and Content

Although PEG is present on the targeting ligand molecule as the spacer, folate-decorated liposomes were reported to exhibit poor circulation time *in vivo* [6, 7]. Thus, inclusion of additional folate-free PEG appears to be crucial in the design of folate-targeted liposomal delivery system. However, folate-free PEG exerts steric hindrance that could interfere with the folate ligand-receptor binding and uptake by cells expressing a high level of FRs [8]. Therefore, optimizing the density and length of PEGylation with respect to the liposomal surface ligand is critical. Nevertheless, few studies have been reported with regards to optimization of these parameters, and to our knowledge, there has not been any study that reported optimization of these factors with foam cells in the presence of a high level of serum.

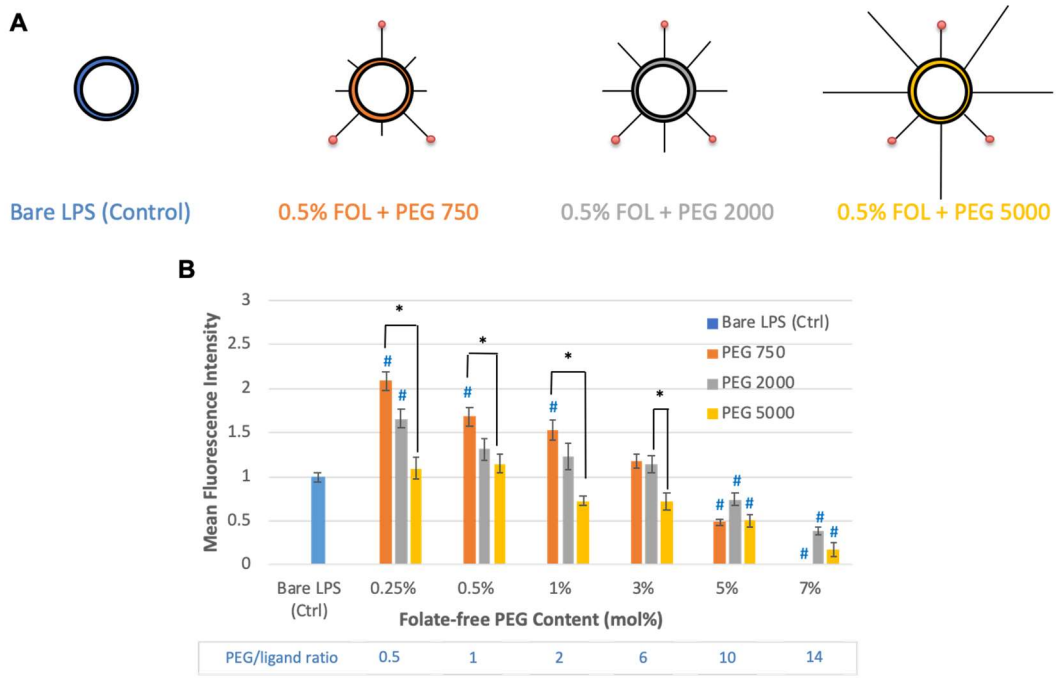

Figure 6.2 Normalized cell uptake as the mean fluorescence intensity (MFI) of rhodamine-positive cells after subtraction of untreated cells autofluorescence MFI and normalized to MFI of bare liposomes. * p-value <0.05 among the 3 PEG sizes of the same concentration; # p-value < 0.05 vs. bare LPS (Ctrl). LPS = liposomes. Ctrl = control.

As shown in the schematic diagram (**Figure 6.2**), liposomes of various PEG lengths (PEG 750, 2000, 5000) and concentrations (0.25 – 7 mol%) were formulated with folate ligand concentration fixed at 0.5 mol%. Each sample and control (bare liposomes) were pre-incubated in 80% human serum for 90 minutes prior to cell treatment. As shown in **Figure 6.2B,** foam cell uptake was dependent on both PEG length and content. The longer the PEG length and the higher the PEG content, the lower the cell uptake. For PEG 750, enhanced cellular uptake from folate functionalization was observed for PEG content from 0.25% up to 1% (PEG/ligand ratio from 0.5 up to 2) (**Figure 6.2B**). At PEG 750 content of 3 mol% (PEG/ligand ratio 6), there was no difference between targeted and non-targeted liposomes (**Figure 6.2B**). As PEG content was further increased to 5% (PEG/ligand ratio 10), the uptake became less than that of bare liposome for all liposome formulations. For PEG 2000, the active targeting effect was only observed at 0.25 mol% (PEG/ligand ratio 0.5). From 0.5% - 3% (PEG/ligand ratio 1 – 6), there was no significant cellular uptake enhancement

compared to non-targeted liposomes. For PEG 5000, no cellular uptake enhancement was observed (**Figure 6.2B**). This result demonstrated that, firstly, the active targeting effect is present with PEG 750 (0.25 – 1 mol%) and PEG 2000 (0.25 mol%) liposomal formulations even in the presence of 80% serum. Secondly, the highest targeting efficiency was achieved at low PEG density with the configuration of longer folate spacer length and shorter folate-free PEG. This finding agrees with our hypothesis that the targeting effect of folate-targeting nanoliposomes will progressively decrease and eventually be lost as PEG-to-ligand ratio is increased. We found that the value of PEG-to-ligand ratio at which the targeting effect is lost, is dependent on the PEG length (>2 for PEG 750; >0.5 for PEG 2000; <0.5 for PEG 5000). Our calculation showed that the PEG was predominantly in mushroom conformation, except for PEG 5000 from 3 mol% onwards were in brush conformation [9]. Clearly the brush configuration did not present any cell uptake enhancement. Typically, liposome morphology is adversely affected above 7 mol% (forming micelles instead of vesicles) [10], and thus we did not try higher PEG concentration.

The cell uptake was observable using confocal microscopy (**Figure 6.3**) although the uptake amount was not quantifiable. We noted observable cell uptake of liposomes containing 5 mol% PEG 2000 (**Figure 6.3**), which is the typical PEG length and content used in commercial long-circulating liposomes [11]. Despite less superior uptake compared to the bare liposome control used in this study (**Figure 6.2B**), we did not compare this formulation to nontargeted PEGylated liposomes, which is the limitation of this study. PEGylated liposomes are expected to exhibit lower cellular interaction compared to bare liposomes due to steric hindrance exerted by PEG on the cells [12].

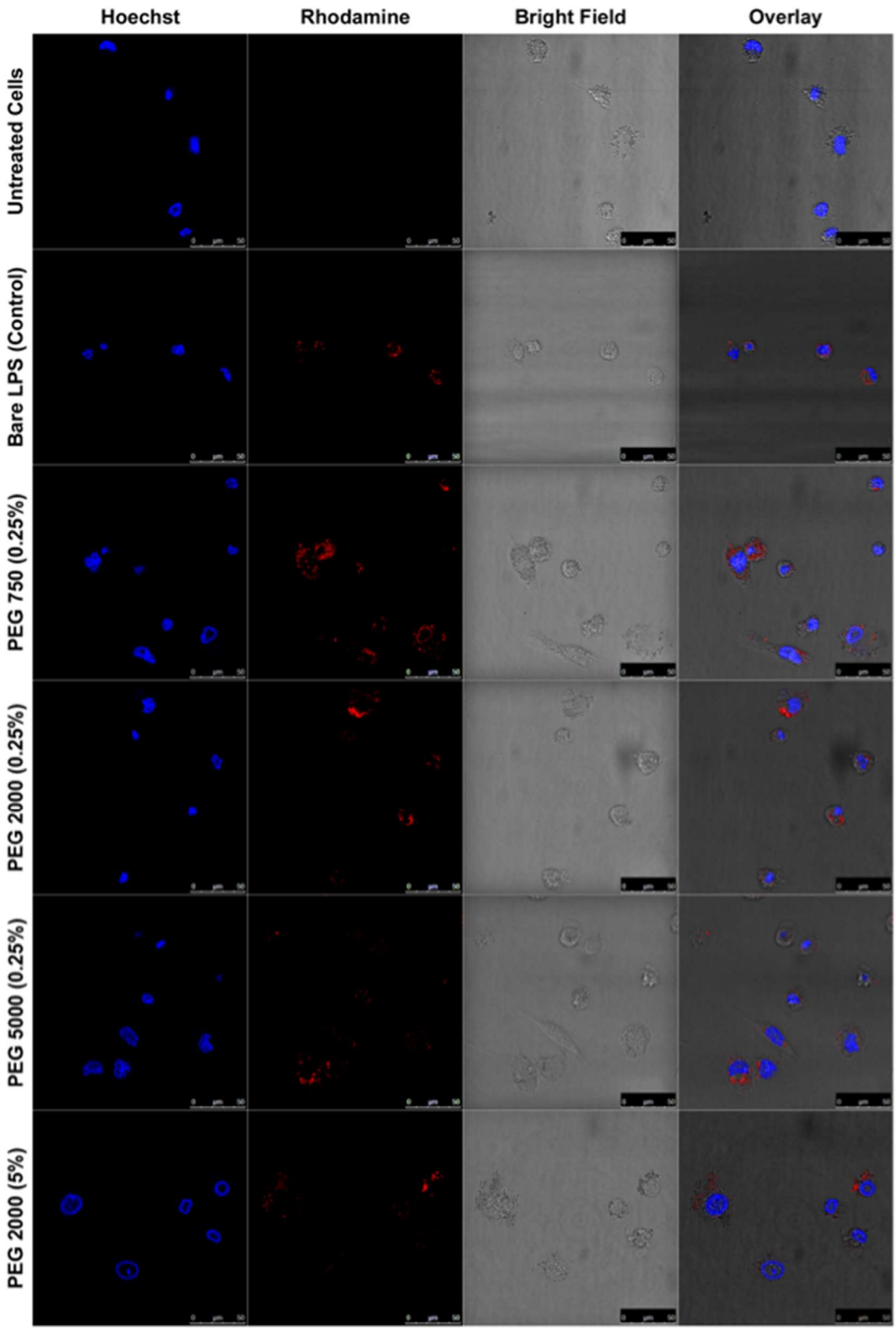

Figure 6.3 Evaluation of cellular uptake using confocal microscopy. Nuclei were visualized by staining with Hoechst 33342.

Folate-decorated liposomes have been reported to show poor circulation time *in vivo* [6, 7]. Even with addition of folate-free PEG, the nanoparticles tend to

accumulate in liver at higher amount than that of conventional passive stealth liposomes [6, 7]. This could be due to the expression of folate receptors on Kupffer cells, the resident macrophages in liver [13]. Whether or not folate ligand promotes opsonization is still unknown. Despite high liver accumulation, folate liposomes have been shown to accumulate in the diseased area either at higher level or similar amount to that of passive stealth liposomes with less off-target accumulation outside of liver [6, 14]. This suggests that active targeting have better performance than passive targeting. However, improvement in blood circulation time of active liposomes would provide considerable benefit, as it would enhance the amount of drug-loaded nanoparticles available in the blood to access the diseased site.

6.3 Cytotoxicity

To ensure that cellular uptake was not caused by cell death, an MTT assay was conducted with foam cells treated with the same treatment condition as that used for the cell uptake study. No cytotoxic effect was observed (**Figure 6.4**)

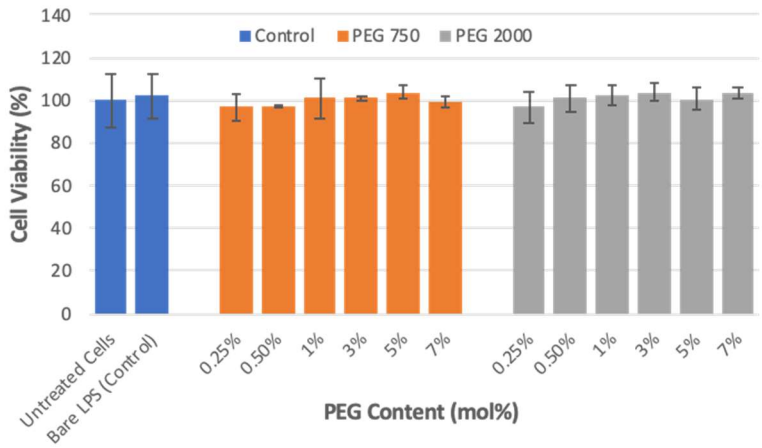

Figure 6.4 MTT assay measuring foam cell viability after treatment with active targeting DPPC liposomes containing combination of 0.5 mol% DSPE-PEG 2000-Folate and DSPE-PEG of various concentrations. Treatment was done after incubation of liposomes in 80% human serum for 90 minutes at 37 °C. Percentage of cell viability was normalized to the value of foam cells without liposome treatment, labelled as untreated cells

6.4 Summary

The effects of PEG length and surface density on foam cell uptake were evaluated in the presence of high serum level. We found that the highest targeting effect was achieved at low PEG density with the configuration of longer folate spacer length and shorter folate-free PEG. The active targeting effect was present even in 80% serum with PEG 750 (0.25 – 1 mol%) and PEG 2000 (0.25 mol%). As PEG/ligand ratio was increased, a decreasing trend in cellular uptake was observed. This finding is in agreement with our hypothesis that the targeting effect of folate-targeting nanoliposomes will progressively decrease and eventually be lost as PEG-to-ligand ratio is increased. However, the value of PEG-to-ligand ratio at which the targeting effect was lost depended on PEG length (>2 for PEG 750; >0.5 for PEG 2000; <0.5 for PEG 5000).

References

[1] Caracciolo, G., *Liposome-protein corona in a physiological environment: challenges and opportunities for targeted delivery of nanomedicines.* Nanomedicine, 2015. **11**(3): p. 543-57.

[2] Reddy, J.A., et al., *Folate-targeted, cationic liposome-mediated gene transfer into disseminated peritoneal tumors.* Gene Ther, 2002. **9**(22): p. 1542-50.

[3] Johnstone, S.A., et al., *Surface-associated serum proteins inhibit the uptake of phosphatidylserine and poly(ethylene glycol) liposomes by mouse macrophages.* Biochim Biophys Acta, 2001. **1513**(1): p. 25-37.

[4] Chonn, A., S.C. Semple, and P.R. Cullis, *Separation of large unilamellar liposomes from blood components by a spin column procedure: towards identifying plasma proteins which mediate liposome clearance in vivo.* Biochim Biophys Acta, 1991. **1070**(1): p. 215-22.

[5] Harvie, P., et al., *Comparative pharmacokinetics, distributions in tissue, and interactions with blood proteins of conventional and sterically stabilized liposomes containing 2',3'-dideoxyinosine.* Antimicrob Agents Chemother, 1996. **40**(1): p. 225-9.

[6] Gabizon, A., et al., *In vivo fate of folate-targeted polyethylene-glycol liposomes in tumor-bearing mice.* Clin Cancer Res, 2003. **9**(17): p. 6551-9.

[7] Yamada, A., et al., *Design of folate-linked liposomal doxorubicin to its antitumor effect in mice.* Clin Cancer Res, 2008. **14**(24): p. 8161-8.

[8] Gabizon, A., et al., *Targeting folate receptor with folate linked to extremities of poly(ethylene glycol)-grafted liposomes: in vitro studies.* Bioconjug Chem, 1999. **10**(2): p. 289-98.

[9] de Gennes, P.G., *Polymers at an interface; a simplified view.* Advances in Colloid and Interface Science, 1987. **27**(3-4): p. 189-209.

[10] Pappalardo, M.M., D.; Grasso, D.; La Rosa, C., *Phase behaviour of polymer-grafted DPPC membranes for drug delivery systems design.* Journal of Thermal Analysis and Calorimetry, 2005. **80**(2): p. 413-418.

[11] Chang, H.I. and M.K. Yeh, *Clinical development of liposome-based drugs: formulation, characterization, and therapeutic efficacy.* Int J Nanomedicine, 2012. **7**: p. 49-60.

[12] Fang, Y., et al., *Cleavable PEGylation: a strategy for overcoming the "PEG dilemma" in efficient drug delivery.* Drug Deliv, 2017. **24**(sup1): p. 22-32.

[13] Samaniego, R., et al., *Macrophage uptake and accumulation of folates are polarization-dependent in vitro and in vivo and are regulated by activin A.* J Leukoc Biol, 2014. **95**(5): p. 797-808.

[14] Poh, S., et al., *Selective liposome targeting of folate receptor positive immune cells in inflammatory diseases.* Nanomedicine, 2018. **14**(3): p. 1033-1043.

Chapter 7

Discussion and Future Work

In this chapter, the summary of the idea and work done in this thesis are provided. The first section draws together the threads of studies done in this thesis and discuss the impacts of the experimental findings. Additionally, the extent of fulfilment of hypothesis raised in chapter 1 is described. In the second section, possible future opportunities are discussed.

7.1 Discussion and Conclusion

Intravenous delivery of therapeutic agents is not an easy task. It is estimated that only 1 out of 100,000 molecules of agents could reach the intended site [1]. A delivery system for intravenous delivery is generally required to be biocompatible, stable in *in vivo* condition, able to accumulate in the pathological site, able to achieve sustained release to maintain desirable therapeutic level for prolonged period of time, able to prevent premature pharmacological action of the drug until it reaches the pathological site and able to prevent premature degradation of drug [1]. These properties have been reported before in liposomes [2-4]. Additionally, liposomes appear to have inherent anti-atherogenic property based on their ability to accept cholesterol from atherosclerotic vessel wall.

Therefore, we started the PhD work with development of anti-inflammatory drug-loaded liposomes (Chapter 4). A classical way to tune liposomal drug loading and release is by controlling the rigidity of the liposomal membrane through selection of lipid chain lengths. The use of cholesterol for membrane rigidity control was avoided to maximize the cholesterol efflux capacity of liposomes [5]. Besides, cholesterol has been shown to reduce partitioning of small molecules into liposomal bilayer [6]. The decrease in loading efficiency of FA drug with incorporation of cholesterol was observed on our side (data not shown). From the findings, we selected DPPC for its favorable drug loading and release characteristics compared to other lipids. Subsequently, as an effort to enhance liposomal stability in *in vivo* condition, PEGylation was incorporated on liposomal surface. Drug loading, release and particle stability remained favorable after PEGylation. In this chapter, we demonstrated a liposomal formulation with high drug loading that exhibited sustained drug release with low burst, indicating capability of delivering majority of drug to targeted site with minimal drug leakage in circulation, and good storage stability. These characteristics make this formulation a potential candidate for novel anti-inflammatory atherosclerosis nanotherapy.

After obtaining favorable results with nontargeted liposomes (passive liposomes), we worked on furnishing the liposome with active targeting

capability (Chapter 5). For a drug delivery system to efficiently deliver its therapeutic payload, it should not only localize in the extracellular fluid of pathological site, but also gaining intracellular access into the targeted cells. Folate targeting was an attractive opportunity because of its strong ligand-receptor pairing affinity, ability to retain its receptor-binding and endocytosis property even when covalently linked to PEG, and its selective expression on foam cells. In this chapter, we formulated folate-targeting liposomes and optimized the mole fraction and PEG spacer length of the folate ligands. Folate targeting is traditionally utilized for antitumor therapy [7-9] and has not been well-explored for atherosclerosis therapeutic delivery. This study demonstrated the feasibility and highlighted the opportunity of exploiting foam cell folate receptor for delivery of therapeutic treatment.

The active liposomes developed in chapter 5 should be further furnished with folate-free PEG to achieve prolonged blood circulation time *in vivo.* However, the optimal content of PEG and surface configuration of the folates and PEG combination have not been established. Studies have shown that PEG molecules exert steric barrier, hindering particle-cell interaction [10]. At high PEG density, the extent of nanoparticle surface coverage will be more extensive. Thus, we hypothesized that targeting effect of folate-targeting nanoliposomes will progressively decrease and eventually be lost as PEG-to-ligand ratio is increased. It was also interesting to see the effect of various PEG and folate surface configuration on cell uptake. In addition, to mimic *in vivo* condition to a larger extent, we pre-incubated liposomes in serum. Serum proteins are known to bind to liposome surface *in vivo*, potentially changing its surface properties [11]. The findings in chapter 6 confirmed our hypothesis that targeting effect of folate-targeting nanoliposomes will progressively decrease and eventually be lost as PEG-to-ligand ratio is increased. However, we found that the value of PEG-to-ligand ratio at which the targeting effect is lost, is dependent on the PEG length (>2 for PEG 750; >0.5 for PEG 2000; <0.5 for PEG 5000). The results demonstrated that the active targeting effect was present even in 80% serum with PEG 750 (0.25 – 1 mol%) and PEG 2000 (0.25 mol%). The formulations developed in this chapter could potentially enhance therapeutic efficacy of liposomal anti-inflammatory nanotherapy.

The novel anti-inflammatory therapy developed in this PhD work could be envisioned for treatment after an acute clinical event or as adjunct therapy in combination with stents.

7.2 Future Work

The studies presented in this thesis are preliminary and more studies will have to be done to obtain a good nanotherapy formulation.

(i) Pharmacokinetics of liposomal formulations have to be investigated to obtain circulation time of various potential formulations. It is expected that passive stealth liposomes exhibit longer circulation time than active liposomes. However, active liposomes might have higher accumulation of particles at the plaque. The outcome of this study will eventually assist us to select several potential formulations for subsequent efficacy study.

(ii) Biodistribution of liposomal formulations *in vivo*. Radiolabeled passive and active liposomes can be prepared and intravenously administered to two groups of apolipoprotein E-knockout ($Apoe^{-/-}$) mice, the first of which had been fed with normal chow and the second group with high cholesterol diet for 12 – 14 weeks. After 24 hours liposome administration, tissue of interest such as aorta can be excised and the amount of radiation per gram of tissue can be quantified and compared between passive and active liposomes. The finding from this study will provide information about the targeting efficacy of active liposomes, whether or not there is increased accumulation of active liposomes in the plaque compared to passive liposomes.

(iii) Therapeutic efficacy of FA-loaded liposomes. This can be examined by analyzing mean plaque area and the number of immunostained plaque macrophages after treatment histologically as well as using flow cytometry. The most efficacious formulation will have the lowest number of plaque macrophages and smallest mean plaque area.

(iv) Investigation of the release of drug from liposomes in blood serum. There could be some interaction between blood serum and the liposomes that disrupts the integrity of the liposomes and causes leakage of cargo.

(v) The fate and stability of liposomes in the plaque can be monitored under MRI by using magnetic nanoparticle-loaded liposomes.

It would also be interesting to perform following studies:

(vi) Foam cell uptake mechanism can be studied by the use of several endocytosis inhibitors.

(vii) Serum binding studies can be performed to investigate the amount and type of serum proteins bound on various liposomes with different surface functionalization.

(viii) The conformation of PEG on the liposome surface can be investigated with small angle X-ray scattering technique

(ix) The location of drug in the bilayer can be investigated by using hydrophobic fluorescent probes of increasing chain length and spectroscopic methods. Commonly used methods reported in the literature to evaluate drug location within liposomes include derivative spectroscopy, fluorescence quenching [12-14] (using membrane-soluble probes such as 2-AS to 12-AS [15]), fluorescence anisotropy [16] (DPH [15], ANS and pyrene as hydrophobic probes [17]), fluorescent resonant energy transfer (FRET), fluorescent polarization and NMR (^{1}H-NMR, ^{2}H-NMR and ^{31}P-NMR).

(x) Binding of drug to liposomes can be studied by isothermal calorimetry technique (ITC). The thermodynamic signatures given by ITC can be subsequently compared to other drug-liposome systems.

(xi) Binding of other GC can be studied by ITC to provide an insight of how changes in molecular structure could affect the drug loading and release from liposomes.

References

[1] Murday, J.S., et al., *Translational nanomedicine: status assessment and opportunities.* Nanomedicine, 2009. **5**(3): p. 251-73.

[2] Barenholz, Y., *Doxil(R)--the first FDA-approved nano-drug: lessons learned.* J Control Release, 2012. **160**(2): p. 117-34.

[3] Hann, I.M. and H.G. Prentice, *Lipid-based amphotericin B: a review of the last 10 years of use.* Int J Antimicrob Agents, 2001. **17**(3): p. 161-9.

[4] Passero, F.C., Jr., et al., *The safety and efficacy of Onivyde (irinotecan liposome injection) for the treatment of metastatic pancreatic cancer following gemcitabine-based therapy.* Expert Rev Anticancer Ther, 2016. **16**(7): p. 697-703.

[5] Lobatto, M.E., et al., *Perspectives and opportunities for nanomedicine in the management of atherosclerosis.* Nat Rev Drug Discov, 2011. **10**(11): p. 835-52.

[6] Kepczynski, M., et al., *Which physical and structural factors of liposome carriers control their drug-loading efficiency?* Chem Phys Lipids, 2008. **155**(1): p. 7-15.

[7] Yamada, A., et al., *Design of folate-linked liposomal doxorubicin to its antitumor effect in mice.* Clin Cancer Res, 2008. **14**(24): p. 8161-8.

[8] Gabizon, A., et al., *In vivo fate of folate-targeted polyethylene-glycol liposomes in tumor-bearing mice.* Clin Cancer Res, 2003. **9**(17): p. 6551-9.

[9] Saul, J.M., et al., *Controlled targeting of liposomal doxorubicin via the folate receptor in vitro.* J Control Release, 2003. **92**(1-2): p. 49-67.

[10] Gabizon, A., et al., *Targeting folate receptor with folate linked to extremities of poly(ethylene glycol)-grafted liposomes: in vitro studies.* Bioconjug Chem, 1999. **10**(2): p. 289-98.

[11] Caracciolo, G., *Liposome-protein corona in a physiological environment: challenges and opportunities for targeted delivery of nanomedicines.* Nanomedicine, 2015. **11**(3): p. 543-57.

[12] Neves, P., et al., *Influence of structural factors on the enhanced activity of moxifloxacin: a fluorescence and EPR spectroscopic study.* Anal Bioanal Chem, 2007. **387**(4): p. 1543-52.

[13] Ferreira, H., et al., *Interaction of clonixin with EPC liposomes used as membrane models.* J Pharm Sci, 2005. **94**(6): p. 1277-87.

[14] Lucio, M., et al., *Use of liposomes to evaluate the role of membrane interactions on antioxidant activity.* Anal Chim Acta, 2007. **597**(1): p. 163-70.

[15] Rodrigues, C., et al., *Interaction of rifampicin and isoniazid with large unilamellar liposomes: spectroscopic location studies.* Biochim Biophys Acta, 2003. **1620**(1-3): p. 151-9.

[16] Kunwar, A., et al., *Transport of liposomal and albumin loaded curcumin to living cells: an absorption and fluorescence spectroscopic study.* Biochim Biophys Acta, 2006. **1760**(10): p. 1513-20.

[17] Giraud, M.N., et al., *Interaction of indomethacin and naproxen with gastric surface-active phospholipids: a possible mechanism for the gastric toxicity of nonsteroidal anti-inflammatory drugs (NSAIDs).* Biochem Pharmacol, 1999. **57**(3): p. 247-54.

APPENDIX

Chapter 3 & 5 – Supplementary Information

Calculation of folate numbers per liposomes

Assuming liposomes are unilamellar, the number of lipid molecules in a unilamellar liposome can be calculated with following formula:

$$N_{tot} = [4\pi(d/2)^2 + 4\pi((d/2) - h)^2] / a$$

where d is the diameter of the liposome, h is the thickness of the bilayer and a is the lipid head group area.

Assuming h = 5 nm and a = 0.71 nm^2 for phosphatidylcholine, the formula can be simplified into:

$$N_{tot} = 17.69 \times [(d/2)^2 + ((d/2) - 5)^2].$$

Subsequently, the number of liposome particles per liter can be calculated by using following equation:

$$N_{lipo} = (M_{lipid} \times N_a)/N_{tot}$$

where M_{lipid} is the molar concentration of lipid, N_a is the Avogadro number (6.023×10^{23}), and N_{tot} is total number of lipids per liposome

Finally, folate numbers per liposomes can be calculated as:

number of folate molecules per liter / number of liposome particles per liter

Number of folate molecules per liter can be quantified using UV absorbance.

Theoretical calculation of PEG surface coverage

If folate molecule is affixed to the extremity of PEG, its average position from liposomal surface can be represented as:

$$R_e = aN^{0.64}$$

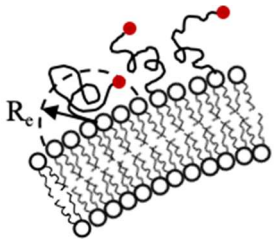

Figure 8.1 Schematic illustration of PEG-ligand on lipid bilayer membrane. The average position of ligand at the distal end of PEG is represented by $R_e = aN^{0.64}$ [1].

Assuming a liposome of 100 nm in size and bilayer thickness of 5 nm, the dimensions can be illustrated as follows:

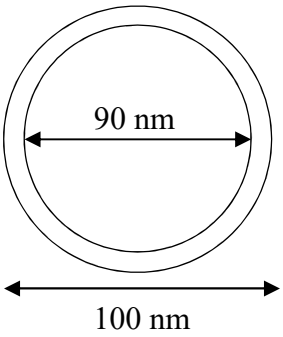

Surface area of inner leaflet = 4 π (90 nm/2)^2 = 25 446.9 nm^2 = 2.54 x 10^4 nm^2
Total lipid molecules at inner leaflet = surface area of inner leaflet / area of a single lipid head = (25 446.9 / 0.71) nm^2 = 35 840.70 molecules

Surface area of outer leaflet = 4 π (100 nm/2)^2 = 31 415.93 nm^2 = 3.14 x 10^4 nm^2
Total lipid molecules at outer leaflet = surface area of outer leaflet / area of a single lipid head = (31 415.93 / 0.71) nm^2 = 44 247.79 molecules

Total lipid molecules = 35 840.70 + 44 247.79 = 80 088.49 molecules
Folate with PEG 2000 spacer
The average length of PEG 2000 spacer in aqueous solution is R_e = (3.5 Å) $(45)^{0.64}$ = 40 Å
Liposome surface area covered by the PEG 2000 spacer of length $R_e = \pi R_e^2 = \pi$ (40 Å)^2
= 50.27 nm^2

Number of PEG 2000-Folate molecules required to cover the entire liposomal surface

= (2.54 x 10^4 /50.27) nm^2 = 507 molecules (inner leaflet)

= (3.14 x 10^4 /50.27) nm^2 = 625 molecules (outer leaflet)

Total PEG 2000-Folate = 507 + 625 = 1132 molecules

PEG 2000-Folate concentration (mol%) = (1132 / 80 088.49) x 100% = 1.4 mol%

At PEG 2000-Folate concentration of 1.4 mol % and above, the folate molecule can interact with the neighboring folate

Folate with PEG 5000 spacer

The average length of PEG 5000 spacer in aqueous solution is R_e = (3.5 Å) $(113)^{0.64}$ = 72.1 Å

Liposome surface area covered by the PEG 5000 spacer of length $R_e = \pi R_e^2 = \pi$ (72.1 Å)^2 = 163.31 nm^2

Number of PEG 5000-Folate molecules required to cover the entire liposomal surface

= (2.54 x 10^4 /163.31) nm^2 = 156 molecules (inner leaflet)

= (3.14 x 10^4 /163.31) nm^2 = 193 molecules (outer leaflet)

Total PEG 5000-Folate = 156 + 193 = 349 molecules

PEG 5000-Folate concentration (mol%) = (349 / 80 088.49) x 100% = 0.4 mol%

At PEG 5000-Folate concentration of 0.4 mol % and above, the folate molecule can interact with the neighboring folate

References

[1] Jeppesen, C., et al., *Impact of polymer tether length on multiple ligand-receptor bond formation.* Science, 2001. **293**(5529): p. 465-8.